DC-DC Converters -
Dynamic Model Design and
Experimental Verification

Bengt Johansson

Abstract

To obtain high performance control of a dc-dc converter, a good model of the converter is needed. The load usually affects the dynamics and one way to take this into consideration is to regard the load as a part of the converter. The load is often the most variable part of this system. If the load current and the output voltage are measured there are good possibilities to obtain a good model of the load on-line. Adaptive control can then be applied to improve the control.

In peak current-mode control, the output voltage and the inductor current are measured and utilized for control. In the author's licentiate thesis, analytic models were derived for the case where the load current is also measured and utilized for control. The control-to-output transfer function, the output impedance, and the audio susceptibility were derived for the buck, boost, and buck-boost converters operated in continuous conduction mode in the case of resistive load. The use of load current can be seen as gain scheduling in the case where the load is a resistor. Gain scheduling can be considered a special case of adaptive control. The majority of the results in the licentiate thesis were validated by comparing the frequency responses predicted by the analytic models and switched large-signal simulation models.

In this thesis, additional results are presented for the buck converter. Experimental results obtained by means of a network analyzer verify the derived control-to-output transfer function and the audio susceptibility but not the output impedance at low frequencies. In the experimental buck converter there are stray resistances in the inductor, transistor, and diode but these stray resistances were not considered in the licentiate thesis. A new transfer function for the output impedance is derived where these stray resistances are considered and it is in good agreement with the experimental result also at low frequencies.

If the current to the output capacitor is measured in addition to the output voltage and the inductor current, the load current can be calculated as

the difference between the inductor and capacitor currents in the case of the buck converter. Hence, the measurement of the load current can be replaced by measurement of the capacitor current. If this possibility is utilized and the capacitor current is measured by means of a current transformer, a low-frequency resonance is introduced in the frequency responses according to experimental results. The reason for this resonance is due to the high-pass-filter characteristics of the current transformer. A new analytic model is derived which predicts the resonance.

Acknowledgements

Notation

Frequently used signals and parameters are presented with name and description in the list below. Signals and parameters that only appear in one of the chapters are not included in the list. The names of signals consist of lower-case letters. However, exceptions are made for the subscript part of the names. The names of the signals are also used to denote their dc values but capital letters are used in this case. However, the letters in the subscript part are not changed. The dc value names are not included in the list.

Name	Description
C	Capacitance of the capacitor
d	Duty cycle
d'	$d' = 1 - d$
i_c	Current reference
i_{cap}	Capacitor current
i_e	External ramp used for slope compensation
i_{inj}	Current injected into the output stage
i_L	Inductor current
i_{load}	Load current
k_f	Input voltage feedforward gain (see Section 2.3)
k_r	Output voltage feedforward gain (see Section 2.3)
L	Inductance of the inductor
m_1	Slope of the inductor current while the transistor is on
$-m_2$	Slope of the inductor current while the transistor is off
m_c	Relative slope of the external ramp, $m_c = 1 + M_e/M_1$
M_e	Slope of the external ramp
R	Resistance of the load resistor
R_a	Average stray resistance, $R_a = DR_{on} + D'R_{off}$

R_c	Equivalent Series Resistance (ESR) of the capacitor
R_d	Resistance in the diode while it conducts
R_i	Gain of inductor-current sensor
R_L	Resistance in the inductor
R_{off}	Stray resistance while the transistor is off, $R_{off} = R_L + R_d$
R_{on}	Stray resistance while the transistor is on, $R_{on} = R_L + R_t$
R_t	Resistance in the transistor while it is on
T_s	Switching period
v_g	Input voltage
v_o	Output voltage
v_{ref}	Voltage reference
δ	Control signal of the transistor driver
ω_n	Half the switching frequency, $\omega_n = \pi/T_s$

Signals are often divided into a dc part and an ac part. The ac part is denoted by using the hat-symbol (^). As mentioned earlier, the dc part is denoted by using capital letters. To explicitly denote that a signal is a function of time, the variable t is added to the name, i.e. $signalname(t)$. The sampled version of a continuous-time signal is denoted by replacing the variable t with n. The Laplace transform of a continuous-time signal is denoted by replacing the variable t with s. The Z-transform of a discrete-time signal is denoted by replacing the variable n with z.

The notation is to some extent chosen such that it is compatible with the one used by Ridley (1991).

Contents

Chapter 1 Introduction

This thesis is concerned with the modeling and control of dc-dc converters with current-mode control. Special focus is placed on using load current measurements for control.

In the licentiate thesis, Johansson (2003), a number of models for buck, boost and buck-boost converters were developed and analyzed in detail. Later experiments verified the accuracy of some of the models and revealed certain inconsistencies in other models. Therefore the experiments have motivated further refinements of the models. This thesis emphasizes the buck converter models.

In this chapter, the background of the problem is described, the motivation for the work is presented and the contributions of the thesis are outlined.

1.1   Background

DC-DC Converters

Figure 1.1 shows a dc-dc converter as a black box. It converts a dc input voltage, $v_g(t)$, to a dc output voltage, $v_o(t)$, with a magnitude other than the input voltage (Erickson and Maksimovic, 2000, Section 1.1). The converter often includes one (or several) transistor(s) in order to control the output voltage, using the control signal $\delta(t)$.

It is desirable that the conversion be made with low losses in the converter. Therefore, the transistor is not operated in its linear interval. Instead, it is operated as a switch and the control signal is binary. While the transistor is on, the voltage across it is low which means that the power loss in the transistor is low. While the transistor is off, the current through it is low
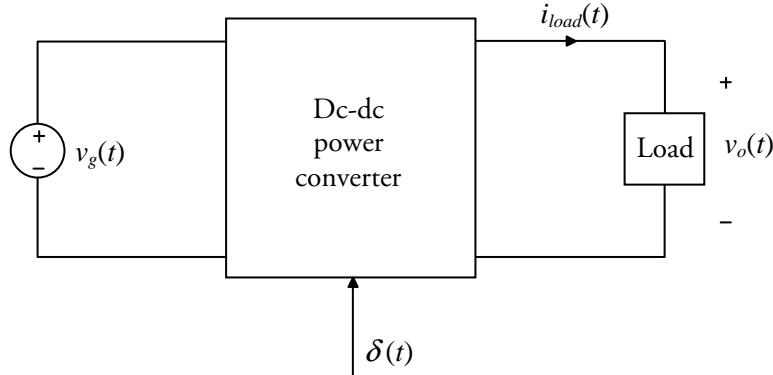
Figure 1.1: A dc-dc converter.

and the power loss is also low. To obtain low losses, resistors are avoided in the converters. Capacitors and inductors are used instead since ideally they have no losses.

The electrical components can be combined and connected to each other in different ways, called topologies, each one having different properties. The buck, boost, and buck-boost converters are three basic converter topologies. The buck converter has an output voltage that is lower than the input voltage. The boost converter has an output voltage that is higher than the input voltage (in steady state). The buck-boost converter is able to have an output voltage magnitude that is higher or lower than the input voltage magnitude.

Figure 1.2 shows the buck converter with two controllers. Here it is assumed that all components are ideal. The load consists of a resistor with resistance R. The converter has a low-pass output filter consisting of an inductor with inductance L and a capacitor with capacitance C. While the transistor is on, the inductor current, $i_L(t)$, increases since the input voltage is higher than the output voltage in the buck converter. As the transistor is turned off, the diode must start to conduct since the inductor current cannot stop flow instantaneously. The voltage across the diode is zero when it is conducting and the inductor current will decrease. Figure 1.3 shows the waveforms of the control signal and the inductor current. The converter is usually designed so that the magnitude of the ripple in the output voltage becomes small. If the ripple is insignificant, the inductor current increases and decreases linearly as shown in Figure 1.3. The voltage across the diode is equal
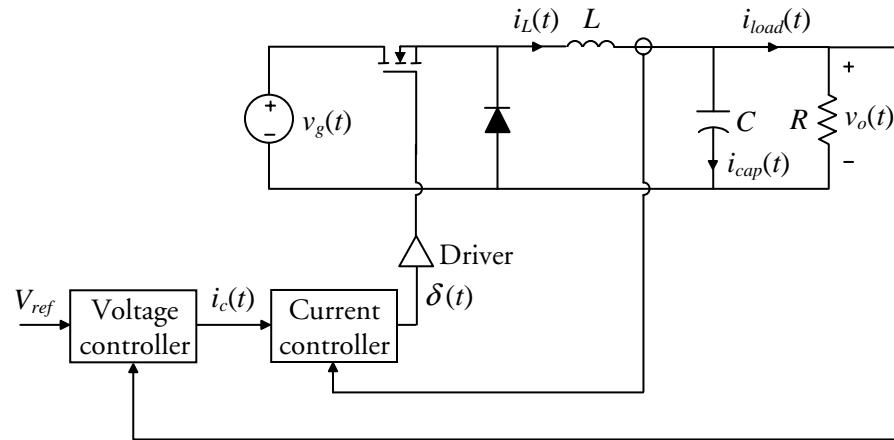
Figure 1.2: The buck converter with a current controller and a voltage controller.
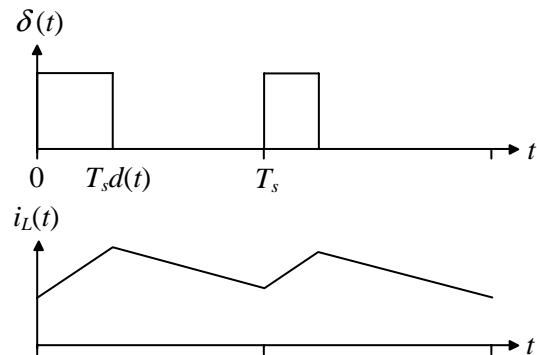
Figure 1.3: The waveforms of the control signal and the inductor current.

to the input voltage or equal to zero. The output filter of the converter filters this voltage waveform and the magnitude of the ripple in the output voltage depends on the filter design. If the inductor current becomes zero before the transistor is turned on, it will remain at zero until the transistor is turned on since the diode can only conduct in one direction. If the converter is operated so that the inductor current is zero during some part of the switching period,

it is said to be operated in discontinuous conduction mode. Otherwise, it is operated in continuous conduction mode.

The switching period, T_s, of the converter is determined by the control signal $\delta(t)$, as shown in Figure 1.3. In this figure, the switching period is held constant. The average output voltage is controlled by changing the width of the pulses. In Figure 1.3, the falling edge is controlled i.e. when the transistor should turn off. The duty cycle, $d(t)$, is a real value in the interval 0 to 1 and it is equal to the ratio of the width of a pulse to the switching period. The control signal $\delta(t)$ can be obtained from $d(t)$ by using a pulse width modulator. The duty cycle can be seen as a discrete-time signal.

State-Space Averaging

The converter acts as a time-invariant system while the transistor is on. While the transistor is off the converter acts as another time-invariant system and if the inductor current reaches zero, the converter acts as yet another time-invariant system. If the transistor is controlled as described previously, the converter can be described as switching between different time-invariant systems during the switching period. Consequently, the converter can be modeled as a time-variant system. State-space averaging (Middlebrook and Cuk, 1976) is one method to approximate this time-variant system with a linear continuous-time time-invariant system. This method uses the state-space description of each time-invariant system as a starting point. These state-space descriptions are then averaged with respect to their duration in the switching period. The averaged model is nonlinear and time-invariant and has the duty cycle, $d(t)$, as the control signal instead of $\delta(t)$. This model is finally linearized at the operating point to obtain a small-signal model. From the model we will extract three major transfer functions:

- The control-to-output transfer function describes how a change in the control signal affects the output voltage.
- The output impedance describes how a change in the load current affects the output voltage.
- The audio susceptibility describes how a change in the input voltage affects the output voltage.

Current-Mode Control

Figure 1.2 shows the buck converter controlled by two control loops. The inductor current is fed back to the current controller in the inner loop and the output voltage is fed back to the voltage controller in the outer loop. This control method is called current-mode control. (The name current controller is used instead of current modulator in this thesis, see Section 2.3.) Assume that the outer loop is not present. The system is then a closed loop system since the inductor current is fed back. If the outer loop is added, a new closed loop is obtained. The control signal from the outer loop acts as the reference signal for the current controller. The three transfer functions mentioned above will in general be different for the new closed loop system.

The current controller controls the inductor current. This can be made in different ways. One way is to control the peak value of the inductor current in each switching period. Ridley (1991) and Tan and Middlebrook (1995) have presented two models for current-mode control. (The voltage controller is actually excluded.) The main difference between the two models is the modeling of the current loop gain. Al-Mothafar and Hammad (1999) found that also the audio susceptibilities predicted by the two models are different.

The average value of the inductor current can be controlled instead of the peak value. This control method is usually called average current-mode control.

The output voltage is fed back to the voltage controller so that the output voltage is kept near the voltage reference signal V_{ref} (see Figure 1.2). The voltage controller controls the reference signal of the current controller, $i_c(t)$. An alternative is to let the voltage controller control the duty cycle directly. This means that the measurement of the inductor current and the current controller are not needed. This control method is called voltage-mode control.

1.2   Motivation for the Work

Many aspects must be considered in the case where a converter is to be designed. One such aspect is keeping the output voltage in the specified voltage interval. Here are some examples of changes that can decrease the variation of the output voltage:

- Change the properties of some of the components in the converter, e.g. increase the capacitance of the capacitor.
- Change the converter topology.
- Change to a more advanced controller.
- Increase the number of signals that are measured and used by the controller.

Each one of these changes has one or several disadvantages such as:

- Higher cost.
- Increased weight and volume.
- Lower reliability.
- Lower efficiency (see Poon, Tse, and Liu (1999)).

Therefore, the change or changes that are most suitable depend to a large extent on the converter specification at hand.

Converters can be improved as better components are developed and more knowledge becomes available. This motivates research in the areas of components, converter topologies and controllers for example.

To obtain high performance control of a system, a good model of the system is needed. A model of a system can be derived by using the laws of physics and/or by using measurements of the system, i.e. system identification (Ljung, 1999). When the system is changed during the time it is in use, it is an advantage to apply system identification that can be used on-line for updating the model. The adjusted model is then used to adjust the parameters of the controller, which is the essence of adaptive control (Åström and Wittenmark, 1995). An adaptive controller can perform better than a non-adaptive controller, which must be designed for the worst case.

One difficulty with adaptive control is making the identification such that the model adjusts sufficiently fast during a system change without making the identification sensitive to measurement noise. If the adjustment is slow, the controller must be designed to be cautious. This means that there will be no significant improvement compared to a non-adaptive controller.

The adjustment can, in general, be made faster if the number of parameters to be estimated in a system is fewer. One way to achieve this is to fix the parameters whose values are known with great precision and vary only slightly. Another way is to measure a larger number of signals in the process and the reason for this is explained as follows. A way to decrease the number of parameters to be estimated is to simply identify a part of the system. To

identify this subsystem, its input and output signals must be measured. If a larger number of signals in the process are measured, it may be possible to divide the process into different smaller parts. Note that the time for the sampling and computation are not considered in this discussion.

The load usually affects the dynamics and one way to take this into consideration is to regard the load as a part of the converter. If a measurement of the load current, $i_{load}(t)$, (see Figure 1.2) is introduced, it is possible to consider the load as one part to be identified. The output voltage is then regarded as the input signal and the load current as the output signal of this part. If adaptive control is to be introduced, a suitable first step may be to only identify the load. Often this is the most variable part of the converter. This first step may be sufficient to obtain a controller that meets the performance specifications. As a second step, identification of the rest of the converter may further improve control. Computational time is one price to pay. This second step may be more expensive than other solutions to improve the performance of the closed loop system. This discussion motivates the research in identification of the load.

As mentioned above, the output voltage and the load current should be measured to obtain fast load identification. There are several papers that suggest that the load current should be measured and utilized for control of the converter and they show what properties are obtained. Two of these papers are mentioned here. In these two papers, the output voltage and the inductor current are assumed to be measured besides the load current.

Redl and Sokal (1986) show that the transient in the output voltage due to a step change in the load can be much reduced. They call the use of the measured load current feedforward. For a definition of feedforward, see Åström and Hägglund (1995, Section 7.3). Redl and Sokal also show that the control-to-output transfer function does not change when this feedforward is introduced.

The dc gain of the control-to-output transfer function normally depends on the load. Hiti and Borojevic (1993) use the measured load current to make the control-to-output transfer function invariant for different loads at dc for the boost converter. Hiti and Borojevic thus show that the control-to-output transfer function changes when the use of measured load current is introduced. The control Hiti and Borojevic use turns out to be exactly the same as the one Redl and Sokal propose for the boost converter.

To summarize, Redl and Sokal show that the control-to-output transfer function <u>does not change</u> when the use of measured load current is introduced while Hiti and Borojevic show that it <u>does change</u>. It thus seems

to be a contradiction. Since the output voltage and the load current are assumed to be measured in the two papers, the analysis may be connected to identification of the load in some way. Therefore, it is motivated to investigate this possible connection and contradiction before the work with identification of the load starts.

1.3   Literature Review

The number of references was limited in the previous sections to make the descriptions clear. In this section, an extended review of works related to this thesis is made. Some models for (uncontrolled) dc-dc converters are first reviewed. Models for current-mode control are then considered. Next, some works related to the effect loads have on the dynamics of the converters are reviewed. Finally, several works where the measured load current is used for control are reviewed.

Models for DC-DC Converters without Controllers

There are several methods that can be used to obtain a linear continuous-time time-invariant model of a dc-dc converter. State-space averaging (Middlebrook and Cuk (1976) and Mitchell (1988)), circuit averaging (Wester and Middlebrook (1973) and Vorperian (1990)), and the current-injected approach (Clique and Fossard (1977) and Kislovski, Redl and Sokal (1991)) are some of them. If these methods are applied to a converter that is operated in continuous conduction mode, the resulting models are accurate both at low and high frequencies. (The frequencies are here related to the interval dc to half the switching frequency, i.e. high frequencies are lower than half the switching frequency.) However, if these methods are applied to a converter that is operated in discontinuous conduction mode, the resulting models are only accurate at low frequencies. Sun et al. (2001) present a modified method to obtain models for converters operated in discontinuous conduction mode that are accurate both at low and high frequencies.

Tymerski (1991, 1994) uses time-varying system theory to derive models for the frequency function and these models are claimed to be exact for all frequencies, i.e. also higher than half the switching frequency. The control-to-output frequency function is derived in the cases where the converter is operated in continuous conduction mode or discontinuous conduction mode. The models are more complicated than the previously mentioned models.

When the control-to-output frequency function of a converter is used to design a controller, the frequency interval dc to half the switching frequency is the most interesting. The previously mentioned models may therefore be sufficient when designing a controller.

Models for Current-Mode Control

A large number of continuous-time models for current-mode control have been presented during the years. Some of these models are intended to be accurate also at high frequencies. The models presented by Ridley (1991), Tan and Middlebrook (1995), and Tymerski and Li (1993) are designed to be accurate from dc to half the switching frequency. Tymerski and Li (1993) present a state-space model while the Ridley and Tan models uses the PWM switch model (Vorperian, 1990). Tymerski (1994) derives a model for the frequency function (from control signal to output voltage) and it is claimed to be exact for all frequencies.

The main difference between the Ridley and Tan models is the modeling of the current loop gain. The current loop gain can be measured by using a digital modulator (Cho and Lee, 1984) or an analog technique (Tan and Middlebrook, 1995) but the results are not the same. The current loop gain according to the Ridley model predicts the measurement result obtained by use of a digital modulator while the Tan model predicts the result obtained when the analog technique is used. The analog technique is preferred according to Tan and Middlebrook (1995). However, Lo and King (1999) claim that the analog technique is not correct for measuring the current loop gain and that a digital modulator should be used instead. A digital modulator can add a significant delay to the pulse width modulator. Mayer and King (2001) present a model for the current loop gain that includes the effects of delay in the pulse width modulator. If the delay is set to zero in this model, the predicted current loop gain is the same as the one predicted by the Ridley model.

Remark The Ridley model includes feedforward gains. Ridley (1991) presents an approximate expression for the current loop gain for the buck converter and the feedforward gains are ignored in the derivation of this expression. This makes the approximation error significant at low frequencies if the converter operates close to discontinuous conduction mode (Ridley, 1990b). If the feedforward gains are not ignored, the following approximate expression is obtained:

$$T_i(s) = \frac{1}{m_c D' \Delta(s)} \left(\frac{L}{RT_s}(1 + sCR)H_e(s) - 0.5 \right). \qquad (1.1)$$

The term -0.5 is added compared to the expression presented by Ridley. Hence, (1.1) is not that much more complicated. The approximation error of (1.1) is insignificant, even when the converter operates close to discontinuous conduction mode. Note that the sensitivity to stray resistances in the inductor, transistor, and diode for the three major transfer functions are decreased when the current loop is closed since the inductor current is controlled. However, this is not the case for the current loop gain which has the same sensitivity as the open loop transfer functions.

Effect of Load on Converter Dynamics

The load usually affects the dynamics of the converter. In Section 1.2, the load was considered to be a part of the converter. An alternative is to exclude the load from the converter and use the Thevenin equivalent circuit as a model of the output of the converter.

One way to ensure reasonable stability margins is to define an impedance specification of the load. Feng et al. (2002) discuss forbidden regions for the impedance ratio Z_o / Z_i where Z_o is the output impedance of the converter (without load) and Z_i is the impedance of the load. Sudhoff et al. (2000) present a forbidden region that is smaller than all previously presented forbidden regions and, hence, the conservativeness is reduced.

Choi et al. (2002) present a method to design the outer (voltage) controller in current-mode control in the case where the load dynamics are unknown. The design is made such that the controlled unloaded converter has suitable stability margins and low output impedance of resistive characteristics. In the design, a constant current sink is actually assumed to be connected to the output to be able to obtain a desired operation point. Hence, the converter is only unloaded in the small-signal sense.

Varga and Losic (1992) try to derive a control technique such that the output impedance is zero. However, there is a shortcoming in their "proof" of the stability of the inner closed loop system. The loop gain of this system is as follows (Equation 9):

$$LG_i(s) = \frac{Z'_{ekv}(s)}{Z'_{ekv}(s) + Z''_{ekv}(s)}.$$ (1.2)

They claim that the system is stable since the magnitude of $LG_i(s)$ is less than unity. However, since $Z'_{ekv}(s)$ and $Z''_{ekv}(s)$ are complex numbers, $\left|LG_i(j\omega)\right|$ may be greater than unity for some ω. The control technique utilizes positive feedback of the inductor current.

Some of the works presented in the next subsection also analyzes how the load affects the dynamics of the converter.

Using Load Current for Control

Several works where the measured load current is used for control are reviewed in this subsection.

As mentioned in Section 1.2, Redl and Sokal (1986) show how the measured load current should be used to reduce the transient in the output voltage when a step change in the load occurs. They only consider the case where current-mode control is used. Schoneman and Mitchell (1989) analyze the proposed use of load current further in the case of the buck converter. However, there is a shortcoming in their work (see Section 2.7). Kislovski, Redl and Sokal (1991, Section 11.4) present a control technique which tries to equalize the output and input power of the converter. To do this, the load current, output voltage, input current, and input voltage must be measured.

Suntio et al. (2003) derive a general small-signal model for the case where the measured load current is used for control. They use an unterminated two-port model of the converter as a starting point. The output port of this model consists of the Thevenin equivalent circuit.

As mentioned in Section 1.2, Hiti and Borojevic (1993) use the measured load current to modify the current-mode control for the boost converter such that the dc gain becomes independent of the load. This control technique is extended by Hiti and Boroyevich (1994) such that the parameters in the outer (voltage) controller are adapted to different load current and output voltage levels.

Varga and Losic (1989) extend voltage mode control of the buck converter by including an inner loop where the measured load current is utilized such that the output impedance is zero. They do not investigate the stability of the closed load current loop. A preliminary investigation made by the author of this thesis shows that the magnitude of the load current loop

gain theoretically is lower than unity if the load is a (positive) resistance. For other types of loads the closed load current loop may not be stable. One disadvantage with the control technique is that the derivative of the load current must be used. This is not necessary in the control technique proposed by Redl and Sokal (1986) which uses current-mode control as a starting point.

Kanemaru et al. (2001) also extend voltage mode control of the buck converter. The control technique utilizes the load current which is measured by means of a current transformer. A current transformer has high-pass-filter characteristics and by choosing a current transformer with a low magnetizing inductance, the corner frequency of the current sensor is high. In this case, the output of the current sensor is approximately proportional to the derivative of the load current. Hence, the control technique is similar to the one presented by Varga and Losic (1989). However, the corner frequency of the current sensor and the amplification of the output signal of the current sensor are chosen such that the output voltage squared error is minimized.

Carrasco et al. (1995) design a fuzzy-logic controller for the buck converter. The controller utilizes measurements of the output voltage and the load current.

Zhang et al. (2004) present a novel control scheme for voltage regulator modules where measurements of the output voltage and the load current are utilized for control. Voltage regulator modules are used as power supplies for microprocessors.

As mentioned previously, Redl and Sokal (1986) extend current-mode control by utilizing also measurements of the load current. Schoneman and Mitchell (1989) show that, in the case of the buck converter, equivalent control can be obtained if the current to the output capacitor is measured instead of the inductor and load currents. Hence, only the output voltage and the capacitor current must be measured. Ioannidis et al. (1998) present a novel control design approach for average current-mode controlled buck converters. Furthermore, they propose that the capacitor current is measured instead of the inductor current since several advantages can be gained. They show that the output impedance is significantly reduced and that the dynamics of the converter remain almost unchanged with load variations. They also show that the effect of stray resistance in the inductor on the closed-loop transfer functions is minor. They show that the stray resistance in the inductor introduces a zero in the output impedance transfer function at a low frequency. Ioannidis and Manias (1999) also utilize measured capacitor current instead of inductor current in the controller.

1.4   Main Contributions

This thesis is a continuation of the licentiate thesis, Johansson (2003). Therefore, the main contributions of the licentiate thesis are first presented and then the main contributions of this thesis are presented. The practical importance of some of the contributions is discussed.

The Licentiate Thesis

The main contributions of the licentiate thesis are presented in this subsection.

Some of the properties that can be obtained using measured load current for control are analyzed. The analysis is only made for the case where current-mode control is used. An accurate model is used in the case where the load is a linear resistor.

1. The analysis confirms that low output impedance can be obtained.

2. The analysis shows that in the case where the load is a current source, i.e. the load current is independent of the output voltage, the following properties are obtained:
   - The use of measured load current for control is feedforward.
   - The control-to-output transfer function does not change when this feedforward is introduced. (If it had changed, it would not have been a feedforward.)

3. The analysis shows that in the case where the load is a linear resistor, the following properties are obtained:
   - The control-to-output transfer function can change when the measured load current is introduced for control.
   - The converter can become unstable when the measured load current is introduced for control.
   - The control-to-output transfer function can be almost invariant for different linear resistive loads if the measured load current is used for control. This is especially the case for the buck converter.
   - The use of measured load current for control is not feedforward. It can instead be seen as gain scheduling, which can be considered a special case of adaptive control (Åström and Wittenmark, 1995, Chapter 9).

It is also shown that the two published models for current-mode control, Ridley (1991) and Tan and Middlebrook (1995), give accurate expressions for the control-to-output transfer function and the output impedance but not for the audio susceptibility. A novel model for the audio susceptibility is presented and it is used to improve the Ridley and Tan models. The novel model is in some cases inaccurate at low frequencies but the improvements are made in such a way that this shortcoming is not transferred to the improved models. The improved models are accurate.

Accurate (continuous-time) expressions for the control-to-output transfer function, the output impedance, and the audio susceptibility are derived for dc-dc converters that meet the following specifications:

- The converter topology is buck, boost or buck-boost.
- The converter is operated in continuous conduction mode.
- Current-mode control with constant switching frequency and peak-current command is used.
- The load is a linear resistor.

This Thesis

The main contributions of this thesis are presented in this subsection.

After the licentiate thesis was published, experiments were made to verify some of the presented models. These experiments verified the accuracy of some of the models and revealed some inconsistencies in some other models. Therefore the experiments have motivated further refinements of the models. Redl and Sokal (1986) propose control laws for the buck, boost and buck-boost converters. In the licentiate thesis, these control laws were considered as important special cases. The proposed control law for the buck converter is very simple to implement and may therefore be the most interesting to use in practice. Therefore, this thesis is emphasizing models for the buck converter. The main contributions of this thesis are:

1. If the frequency functions predicted by the transfer functions derived in the licentiate thesis are compared with experimental results obtained by means of a network analyzer, it is found that there is a large difference in one case. The transfer function for the output impedance does not predict the experimental results at low frequencies in the case where the measured load current is utilized for control. The reason for the difference is that the stray resistances in the inductor, transistor, and diode are not

considered in the licentiate thesis. A new transfer function for the output impedance is derived where these stray resistances are considered.

2. Experimental results are presented for the case where the load is a resistor and these results verify the frequency functions predicted by the control-to-output transfer function, the transfer function for the audio susceptibility, and the new transfer function for the output impedance.

3. Redl and Sokal (1986) suggest that the load current is not measured directly. Instead, the current to the output capacitor, $i_{cap}(t)$, is measured and the load current can then be calculated as the difference between the inductor current and capacitor current (see Figure 1.2). In the experiments mentioned in item 1 and 2 above, the capacitor current is measured by means of a current shunt. This solution has several drawbacks such as increased magnitude of the ripple in the output voltage and decreased efficiency. Redl and Sokal (1986) suggest that a current transformer is used to measure the capacitor current. However, the current transformer has high-pass-filter characteristics and these introduce a resonance in the buck converter at a low frequency. A new model is derived for the case where a current transformer is used to measure the capacitor current. Experimental results are presented also for this case and they verify the frequency functions predicted by the new model.

Practical Importance of the New Models

The licentiate thesis and this thesis increase the understanding of the properties of the converters and how to derive models. Furthermore, the following new transfer functions are presented:

1. The novel model for audio susceptibility for current-mode control.
2. The three major transfer functions in the case where the load current is measured (with a current shunt) and utilized for control.
3. The same transfer functions as in item 2 except that the load current is measured (indirectly) by means of a current transformer.

It is verified both by simulations and experiments that these transfer functions are accurate (the experimental verification is only made for the buck converter).

The novel model in item 1 above is mainly of academic interest since the errors in the predictions of the audio susceptibility in the Ridley and Tan models often are small and only appear at high frequencies.

The transfer functions in item 2 above may be more interesting to use in practice since the changes of the current through the load resistor are accounted for. This is not made in Schoneman and Mitchell (1989) (see Section 2.7). However, in case of the buck converter the current through the load resistor mainly affects the properties of the converter at low frequencies. This means that the design of the (outer) voltage controller does not change so much if the new model is used instead since the gain of the controller usually is very high at low frequencies.

The most interesting transfer functions to use in practice are probably the ones in item 3 above which can be used in the case where the capacitor current is measured with a current transformer. The reason for this is that the resonance changes the phase curve significantly. The resonance frequency increases if the corner frequency of the current transformer increases (see Section 5.4). Therefore, the higher the corner frequency of the current transformer, the more the design of the voltage controller is affected.

The output impedance transfer functions in items 2 and 3 above are improved by considering the stray resistances in the inductor, transistor, and diode in the modeling. This improves the prediction of the output impedance at low frequencies. This improvement may not be so important in practice since the voltage controller usually makes the output impedance low at low frequencies. An exception may be the design of voltage regulator modules where it is suitable to obtain an output impedance which is constant for all frequencies (Zhang et al., 2004). (The definition of output impedance is in this case the impedance in the Thevenin equivalent circuit.)

One may ask if in practice it is important to use models which include high frequency extensions. In the case of the buck converter it may be important since the crossover frequency can be designed to be high, e.g. one tenth of the switching frequency. According to the small-signal models for the boost and buck-boost converters, these converters are not minimum-phase systems. Therefore, the crossover frequency must usually be designed to be rather low. Consequently, the high-frequency properties of the boost and buck-boost converters may not be so important to consider in practice when designing the voltage controllers.

1.5   Outline of the Thesis

In Chapter 2, a brief review of the licentiate thesis is presented. The new transfer function for the output impedance is derived in Chapter 3. The frequency functions predicted by some of the transfer functions presented in Chapter 2 and Chapter 3 are compared with experimental results in Chapter 4. The case where a current transformer is used to measure the capacitor current is analyzed in Chapter 5. A summary and future work are presented in Chapter 6.

1.6   Publications

The author has published the following conference papers:

1. Johansson, B. and Lenells, M. (2000), Possibilities of obtaining small-signal models of DC-to-DC power converters by means of system identification, *IEEE International Telecommunications Energy Conference*, pp. 65-75, Phoenix, Arizona, USA, 2000.
2. Johansson, B. (2002a), Analysis of DC-DC converters with current-mode control and resistive load when using load current measurements for control, *IEEE Power Electronics Specialists Conference*, vol. 1, pp. 165-172, Cairns, Australia, 2002.
3. Johansson, B. (2002b), A comparison and an improvement of two continuous-time models for current-mode control, *IEEE International Telecommunications Energy Conference*, pp. 552-559, Montreal, Canada, 2002.

Paper 1 is neither included in the licentiate thesis nor in this thesis. Papers 2 and 3 contain parts of the licentiate thesis. Errata for the three papers are presented in Chapter 9 of the licentiate thesis.

Chapter 2 Models for Buck Converters – A Summary of the Licentiate Thesis

The next chapters are partly based on the results presented in the licentiate thesis by Johansson (2003). Therefore, it is suitable to first make a summary of the licentiate thesis and this is made in this chapter. However, since only the buck converter is considered in the next chapters, few results for the boost and buck-boost converters are presented here.

2.1   Chapter Survey

In Section 2.2, the operation of the buck converter is described. The method of state-space averaging is explained. The model obtained by applying this method to the buck converter is presented and compared with results from simulations of a switched model.

Current-mode control is explained in Section 2.3. The Ridley and Tan models are reviewed and compared. The models obtained by applying these models to the buck converter are presented and compared with simulation results. The results of the comparison are explained.

The novel model for the audio susceptibility is presented in Section 2.4. The expression obtained by applying this model to the buck converter is presented and compared with the corresponding ones in Section 2.3.

In Section 2.5, the Ridley and Tan models are improved by using the results in Section 2.4.

In Section 2.6, some approximations of the models for current-mode control presented in the previous sections are showed.

Some properties that can be obtained when using load current measurements to control the converter are analyzed in Section 2.7. The results of this analysis are compared with simulation results.

A summary and concluding remarks are presented in Section 2.8.

2.2   State-Space Averaging

The converter can be described as switching between different time-invariant systems during each switching period and is subsequently a time-variant system. There are several methods that approximate this time-variant system with a linear continuous-time time-invariant system. State-space averaging (Middlebrook and Cuk, 1976) is used here.

The outline of this section is as follows. The circuit and operation of the buck converter are first presented. The method of state-space averaging is then explained. The control-to-output transfer function, the output impedance, and the audio susceptibility can be obtained by applying this method to the buck converter and the results are presented. Finally, a switched simulation model of the buck converter is presented. It is shown how the frequency functions of the converter are obtained from this simulation model. The frequency functions are presented and compared with the three transfer functions for the buck converter.

Operation of the Buck Converter

The circuit and operation of the buck converter are presented in this subsection. Numerous notations are introduced.

The components of a converter are not ideal and some of these non-idealities can be considered in a model. Only one non-ideality is considered in the licentiate thesis. The capacitor is modeled as an ideal capacitor in series with an ideal resistor with resistance R_c. The resistance R_c is called the Equivalent Series Resistance (ESR) of the capacitor.

Figure 2.1 shows the circuit of the buck converter where the ESR of the capacitor is included. The waveforms of the signals in the circuit are as shown in Figure 2.2 and they are obtained from a simulation. Steady state is reached and, therefore, the control signal, $\delta(t)$, consists of pulses with constant width. The time intervals where the control signal $\delta(t)$ is high are called t_{on} and the once where $\delta(t)$ is low are called t_{off}. The switching period, T_s, is
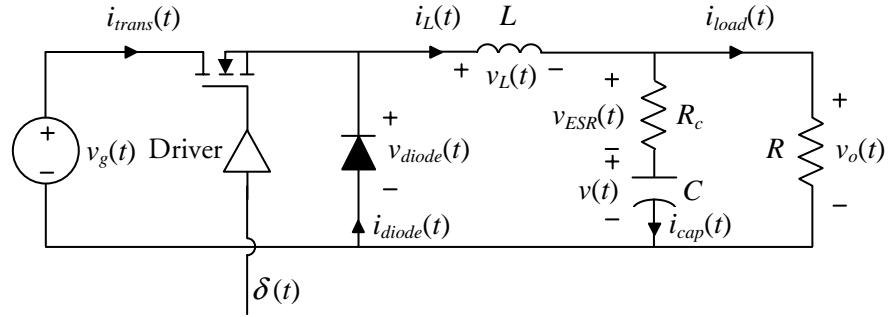
Figure 2.1: The circuit of the buck converter.

the time between two successive positive flanks of $\delta(t)$ and hence equal to the sum of t_{on} and t_{off}. The ratio of t_{on} to T_s is called the duty cycle or the duty ratio and it is denoted by $d(t)$. The duty cycle is constant in steady state and equal to D (the dc value of $d(t)$). During t_{on} the transistor operates in the on state and during t_{off} the transistor operates in the off state. The voltage across the diode, $v_{diode}(t)$, is equal to the input voltage, $v_g(t)$, during t_{on} and equal to zero during t_{off}. The input voltage is held constant at V_g during the simulation. The diode voltage is filtered by the *L-C* low-pass output filter. The corner frequency of this filter is chosen to be much lower than the switching frequency to obtain small magnitude of the ripple in the output voltage, $v_o(t)$. Consequently, the output voltage is approximately equal to the mean value of the diode voltage and lower than $v_g(t)$.

The voltage across the inductor, $v_L(t)$, is equal to the difference between $v_{diode}(t)$ and $v_o(t)$. During each time interval, the slope of $i_L(t)$ is almost constant since $v_L(t)$ is almost constant. The inductor current is equal to the transistor current, $i_{trans}(t)$, during t_{on} and equal to the diode current, $i_{diode}(t)$, during t_{off}. The capacitor current, $i_{cap}(t)$, is equal to the difference between $i_L(t)$ and the load current, $i_{load}(t)$. The mean value of $i_{cap}(t)$ is zero in steady state. The magnitude of the ripple in $v_o(t)$ is larger than the magnitude of the ripple in the voltage across the (ideal) capacitor, $v(t)$, due to the capacitor's ESR.

Table 2.1 shows the parameter values used in the simulation. These are also used by Ridley (1991). The switching frequency, f_s, is equal to 50 kHz (the inverse of T_s).
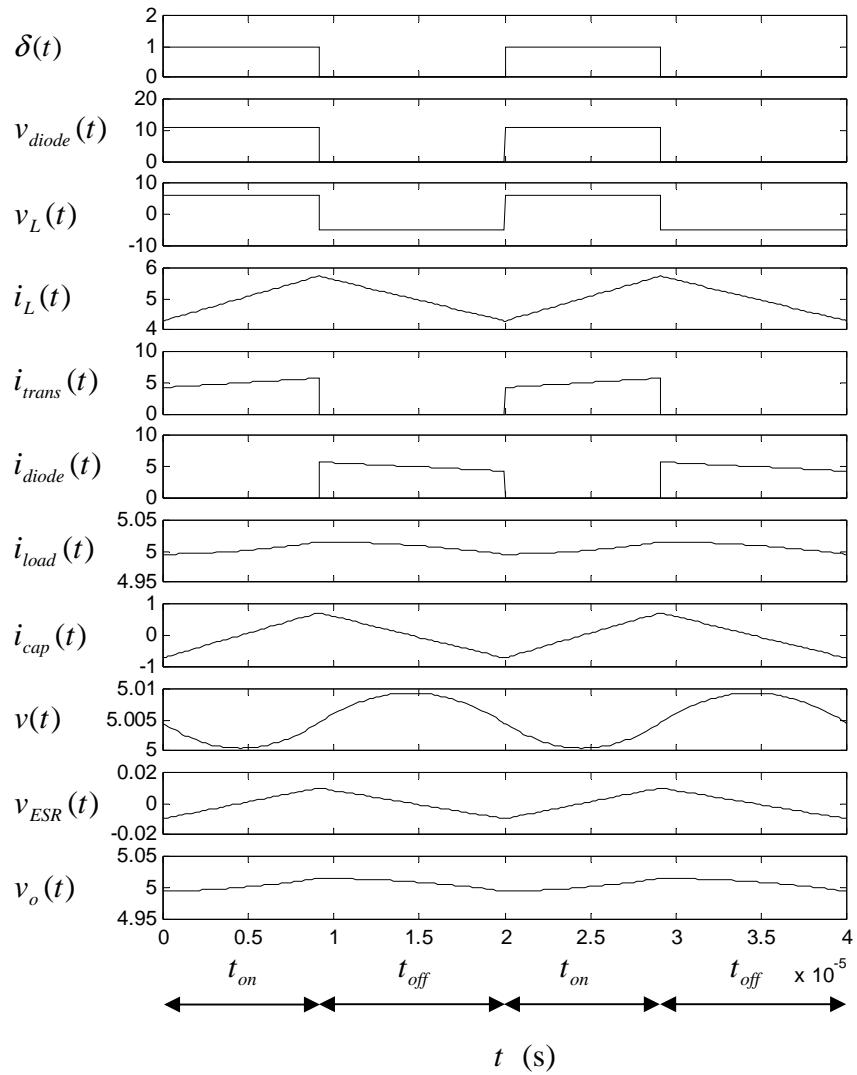
Figure 2.2: The waveforms of the signals in steady state for a buck converter. The unit of the voltages is Volt and the unit of the currents is Ampere.

Table 2.1: The parameter values used in the simulation of the buck converter.

| Parameter	Value
L	37.5 μH
C	400 μF
R_c	14 mΩ
R	1 Ω
V_g	11 V
D	0.455
T_s	20 μs
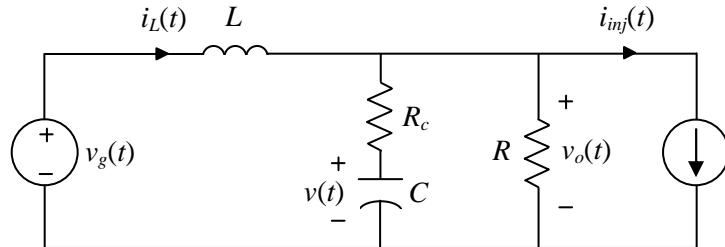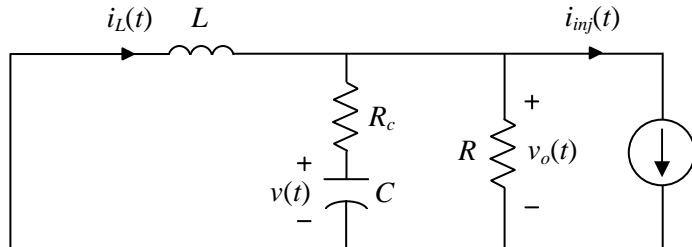
The Method of State-Space Averaging

In this subsection, the method of state-space averaging is explained. The control-to-output transfer function, the output impedance, and the audio susceptibility can be obtained by applying this method to the converters and the results are presented.

The converter can be described as switching between different time-invariant systems and is subsequently a time-variant system. The state-space descriptions of the different time-invariant systems are used as a starting point in the method of state-space averaging. Consider the buck converter in Figure 2.1. While the transistor is on, the voltage across the diode is equal to the input voltage. The circuit in Figure 2.3 can therefore be used as a model of the buck converter during t_{on}. In the figure, a current source is added. It injects the current $i_{inj}(t)$ into the output stage of the converter. This current is an input signal and is needed to determine the output impedance. While the transistor is off, the voltage across the diode is equal to zero and the circuit in Figure 2.4 can be used as a model.

Assume that the state-space descriptions of the circuits in Figure 2.3 and Figure 2.4 are

$$
\begin{cases}
\dfrac{d\mathbf{x}(t)}{dt} = \mathbf{A}_1\mathbf{x}(t) + \mathbf{B}_1\mathbf{u}(t) \\
\mathbf{y}(t) = \mathbf{C}_1\mathbf{x}(t) + \mathbf{E}_1\mathbf{u}(t)
\end{cases}
\tag{2.1}
$$

Figure 2.3: The circuit of the buck converter during t_{on}.

Figure 2.4: The circuit of the buck converter during t_{off}.

and

$$
\begin{cases}
\dfrac{d\mathbf{x}(t)}{dt} = \mathbf{A}_2\mathbf{x}(t) + \mathbf{B}_2\mathbf{u}(t) \\
\mathbf{y}(t) = \mathbf{C}_2\mathbf{x}(t) + \mathbf{E}_2\mathbf{u}(t)
\end{cases}
\tag{2.2}
$$

respectively, where

$$
\mathbf{x}(t) = \begin{bmatrix} i_L(t) \\ v(t) \end{bmatrix},
\tag{2.3}
$$

$$
\mathbf{u}(t) = \begin{bmatrix} v_g(t) \\ i_{inj}(t) \end{bmatrix},
\tag{2.4}
$$

$$\mathbf{y}(t) = v_o(t). \tag{2.5}$$

(2.1) and (2.2) are two different linear time-invariant systems. In state-space averaging, these two systems are first averaged with respect to their duration in the switching period:

$$\begin{cases} \dfrac{d\mathbf{x}(t)}{dt} = \left(d(t)\mathbf{A_1} + (1 - d(t))\mathbf{A_2}\right)\mathbf{x}(t) + \left(d(t)\mathbf{B_1} + (1 - d(t))\mathbf{B_2}\right)\mathbf{u}(t) \\ \mathbf{y}(t) = \left(d(t)\mathbf{C_1} + (1 - d(t))\mathbf{C_2}\right)\mathbf{x}(t) + \left(d(t)\mathbf{E_1} + (1 - d(t))\mathbf{E_2}\right)\mathbf{u}(t) \end{cases} \tag{2.6}$$

(2.6) is an approximation of the time-variant system and new variable names should formally have been used. To limit the number of variable names, this is not made. The duty cycle, $d(t)$, is an additional input signal in (2.6). A new input vector is therefore defined:

$$\mathbf{u'}(t) = \begin{bmatrix} \mathbf{u}(t) \\ d(t) \end{bmatrix}. \tag{2.7}$$

This is not made in traditional presentations of state-space averaging, where the control signal $d(t)$ is kept separate from the disturbance signals $v_g(t)$ and $i_{inj}(t)$. However, in system theory, all control signals and disturbance signals are put in an input vector.

Since the duty cycle can be considered to be a discrete-time signal with sampling interval T_s, one cannot expect the system in (2.6) to be valid for frequencies higher than half the switching frequency.

The second step in state-space averaging is linearization of the nonlinear time-invariant system in (2.6). The deviations from an operating point are defined as follows:

$$\mathbf{x}(t) = \mathbf{X} + \hat{\mathbf{x}}(t), \tag{2.8}$$

$$\mathbf{u'}(t) = \mathbf{U'} + \hat{\mathbf{u}}'(t), \tag{2.9}$$

$$\mathbf{y}(t) = \mathbf{Y} + \hat{\mathbf{y}}(t). \tag{2.10}$$

Capital letters denote the operating-point (dc, steady-state) values and the hat-symbol (^) denotes perturbation (ac) signals. The result of the linearization is a linearized (ac, small-signal) system:

$$\begin{cases} \dfrac{d\hat{\mathbf{x}}(t)}{dt} = \mathbf{A'}\hat{\mathbf{x}}(t) + \mathbf{B'}\hat{\mathbf{u}}'(t) \\ \hat{\mathbf{y}}(t) = \mathbf{C'}\hat{\mathbf{x}}(t) + \mathbf{E'}\hat{\mathbf{u}}'(t) \end{cases}. \tag{2.11}$$

Besides the ac model (2.11), a dc model can be obtained from (2.6) by setting $\hat{\mathbf{x}}(t)$, $\hat{\mathbf{u}}'(t)$, $\hat{\mathbf{y}}(t)$, and $d\mathbf{x}(t)/dt$ to zero.

If the Laplace transform of (2.11) is calculated, several transfer functions can be extracted. By applying state-space averaging to the three treated converters the following results are obtained for the three major transfer functions. The control-to-output transfer function, the output impedance, and the audio susceptibility for the buck converter are

$$\frac{\hat{v}_o(s)}{\hat{d}(s)} = \frac{RV_g\left(1 + sR_cC\right)}{R + s\left(L + RR_cC\right) + s^2\left(R + R_c\right)LC}, \tag{2.12}$$

$$Z_{out}(s) = -\frac{\hat{v}_o(s)}{\hat{i}_{inj}(s)} = \frac{sRL\left(1 + sR_cC\right)}{R + s\left(L + RR_cC\right) + s^2\left(R + R_c\right)LC}, \tag{2.13}$$

$$\frac{\hat{v}_o(s)}{\hat{v}_g(s)} = \frac{RD\left(1 + sR_cC\right)}{R + s\left(L + RR_cC\right) + s^2\left(R + R_c\right)LC}. \tag{2.14}$$

To be spared from introducing new variable names, the Laplace transform of a signal is denoted by the same name as the signal, e.g. $L\{v_o(t)\} = v_o(s)$, even if this is not a formally correct notation. The operating-point value of $d(t)$ is denoted D and

$$D' = 1 - D. \tag{2.15}$$

Note that the denominators in the three transfer functions (2.12)-(2.14) are the same. Therefore, the positions of the two poles are the same for the three transfer functions. This is also the case for the zero caused by the ESR of output capacitor. The transfer function for the output impedance has an

additional zero at the origin. This means that the output impedance tends to zero as the frequency tends to zero.

For the boost converter, the control-to-output transfer function, the output impedance, and the audio susceptibility are found in Johansson (2003, Section 2.6, Equations 2.142-2.144). The corresponding results for the buck-boost converter are found in Johansson (2003, Section 2.9, Equations 2.186-2.188).

Simulation Model and Results

In this subsection, a switched simulation model of the buck converter is presented. It is shown how the frequency functions of the converter are obtained from this simulation model. The frequency functions are presented and compared with the three transfer functions for the buck converter.

We simulate a buck converter by using the software MATLAB/SIMULINK including Power System Blockset. Figure 2.5 shows the complete simulation model. The buck converter is a subsystem. Its simulation model is shown in Figure 2.6 and it has three input signals and three output signals. The input signals *vg*, *iinj*, and *delta* are the input voltage, injected current, and control signal, respectively. *iinj* is multiplied by -1 to obtain a direction of the injected current that agrees with the one defined in Figure 2.3. The input signal *delta* controls the transistor. A controllable switch emulates the diode. The inverse of *delta* is used to control this switch since the diode should conduct when the transistor in not conducting. To be able to start a simulation, a dummy resistor is included in the model. The resistance of this resistor is set to 1 MΩ and its effect on the simulation result is negligible. The output signals *vo*, *iload*, and *iL* are "measurements" of the output voltage, load current, and inductor current, respectively.

The input and output signals of the converter are connected as shown in Figure 2.5, to obtain the frequency functions of the converter. The input voltage, *vg*, is the sum of its dc value, *Vg*, and its ac value *vghat*. The injected current, *iinj*, and the duty cycle, *d*, are implemented in a corresponding way. The dc value of *iinj*, i.e. *Iinj*, is equal to zero in all the simulations. Only one signal generator at the time is activated.

The pulse width modulation (PWM) makes use of a saw-tooth signal, e.g. the one shown in Figure 2.7. The period of the signal is equal to T_s, i.e. the switching period. When the signal *sawtooth* becomes greater than the duty cycle, *d*, the SR-latch is reset. A relay block is used to generate a reset signal
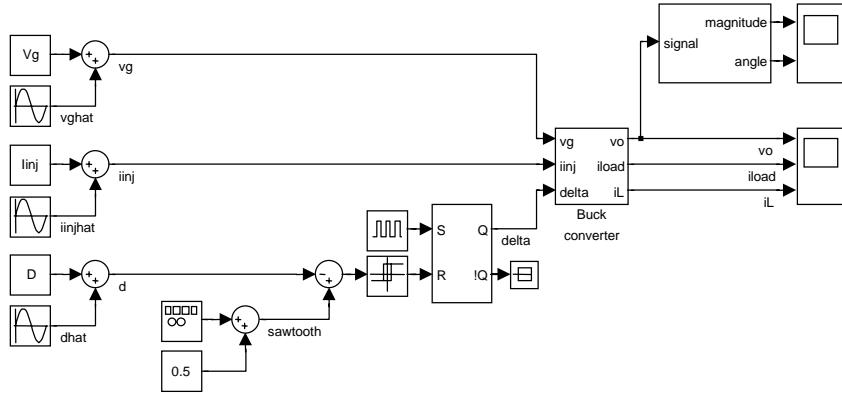
Figure 2.5: The complete simulation model.
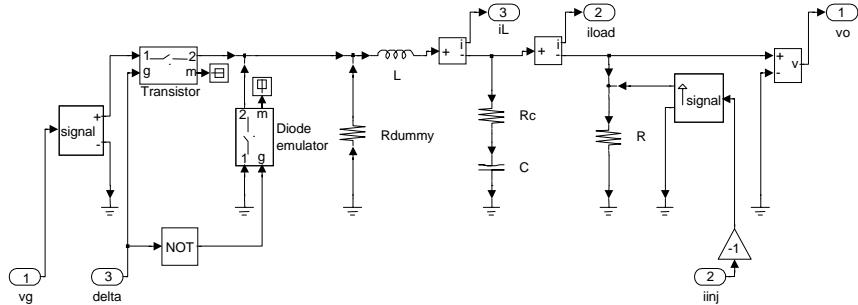
Figure 2.6: The buck converter subsystem.

that is either 0 or 1. A pulse generator sets the SR-latch. The set signal is synchronized with the *sawtooth* signal so that the SR-latch is set each time the *sawtooth* signal goes from 1 to 0. The output signal of the SR-latch, *delta*, is a pulse train and the width of each pulse is determined by the duty cycle signal *d*.

Consider the output signal *vo* of the converter which represents the output voltage. This signal has a Fourier component with a frequency equal to the frequency of the signal from the active signal generator. There exist other Fourier components in the output voltage (Erickson and Maksimovic,
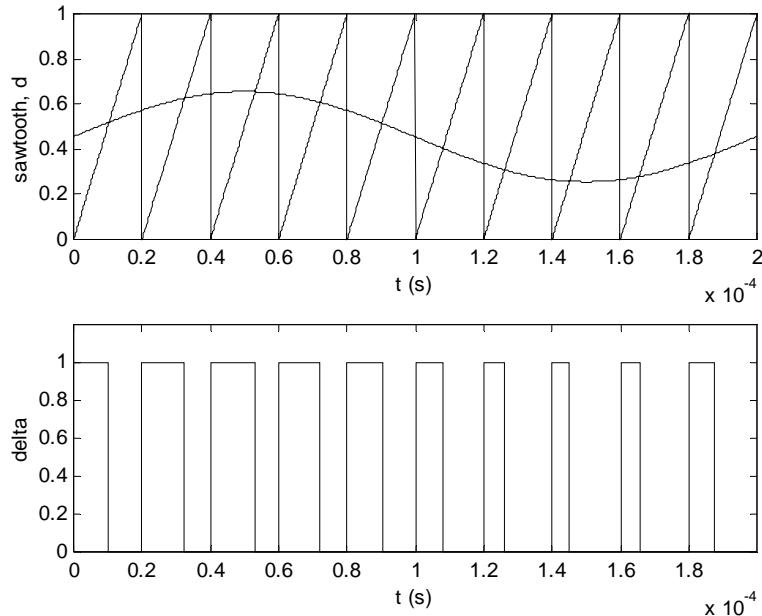
Figure 2.7: The waveforms of the signals in a pulse-width modulator.

2000, Section 7.1). The output of a linear system such as (2.12), (2.13), or (2.14) only consists of one Fourier component if the input is a sinusoidal. The frequency of this component is the same as the frequency of the input sinusoidal. To be able to compare the simulation results with the linearized model, only the Fourier component in the output voltage with a frequency equal to the frequency of the signal from the active signal generator is considered. A network analyzer also just considers this Fourier component (Erickson and Maksimovic, 2000, Section 8.5).

To evaluate a frequency function at a specific frequency, the active signal generator is set to generate a sinusoidal with this frequency. The specific frequency is also set in the Fourier analysis block.

The result of the Fourier analysis is the magnitude and the phase of the component. The analysis is repeated during the simulation and the results are viewed by using the oscilloscope block. At the start of each simulation, the result of the Fourier analysis changes considerably since the inductor current
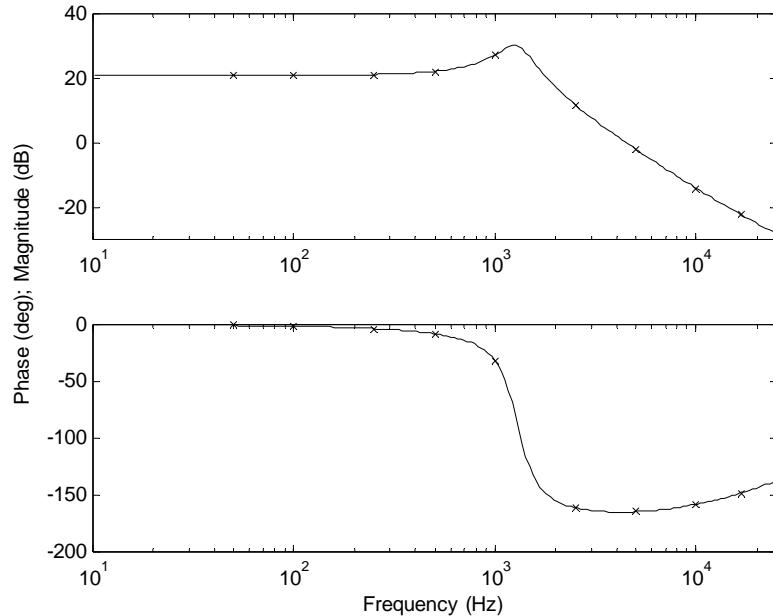
Figure 2.8: The control-to-output transfer function of a buck converter. Solid
line: the analytic model. X: the simulation results.

and the capacitor voltage are far from the final dc values. The simulation is
stopped when the changes in the result of the Fourier analysis is negligible.

The frequency function at a specific frequency can be expressed as its
magnitude and its phase. The magnitude is equal to the ratio of the
magnitude of the output voltage, obtained from the Fourier analysis, to the
magnitude of the signal from the active signal generator. The phase is equal to
the phase of the output voltage, obtained from the Fourier analysis, since the
phase of the signal from the active signal generator is zero.

A simulation is conducted for each one of the frequencies that is
evaluated. This procedure is repeated three times since there are three
different signal generators.

The frequency functions predicted by the linearized model of the buck
converter are now compared with simulation results. The parameter values
shown in Table 2.1 are used in the linearized model and the simulation
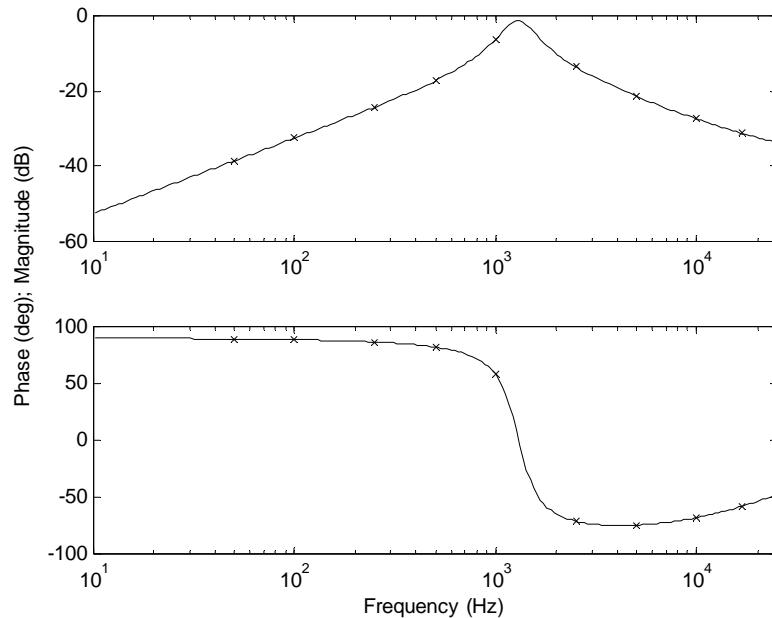
Figure 2.9: The output impedance of a buck converter. Solid line: the analytic model. X: the simulation results.

model. Figure 2.8, Figure 2.9, and Figure 2.10 show the Bode plot for the control-to-output transfer function (2.12), output impedance (2.13), and audio susceptibility (2.14), respectively. Simulation results are also shown. The figures show that the predicted frequency functions agree closely with the simulation results. Note that the frequency axes are limited to half the switching frequency (25 kHz).

For the boost and buck-boost converters the conclusion is the same, i.e. the predicted frequency functions agree closely with the simulation results.

2.3   Current-Mode Control

In this section we consider models for converters with current-mode control. The two models presented by Ridley (1991) and Tan and Middlebrook (1995) are compared with simulation results.
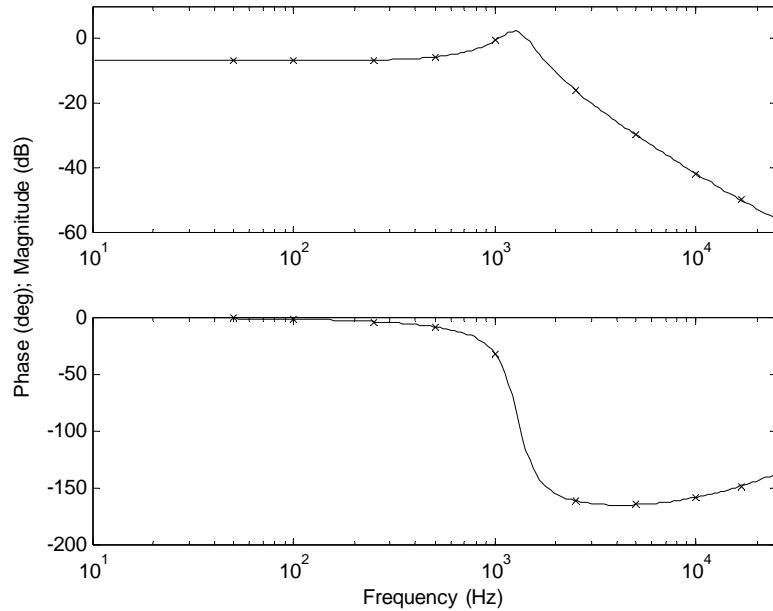
Figure 2.10: The audio susceptibility of a buck converter. Solid line: the analytic model. X: the simulation results.

Current-mode control is also called current programmed control and current-injected control. Descriptions of current-mode control can be found in e.g. Kislovski, Redl and Sokal (1991, Chapter 5), Erickson and Maksimovic (2000, Chapter 12), and Mitchell (1988, Chapter 6).

The outline of this section is as follows. The operation of current-mode control is first explained. The Ridley and Tan models are then reviewed and compared. The control-to-output transfer function, the output impedance, and the audio susceptibility can be obtained by applying these two models to the buck converter with current-mode control and the results are presented. The simulation model is extended and simulation results are compared with the presented transfer functions. The results of the comparison are also explained.
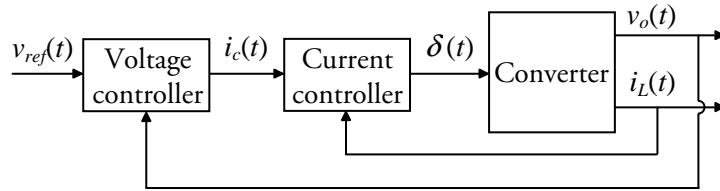
Figure 2.11: Current-mode control.
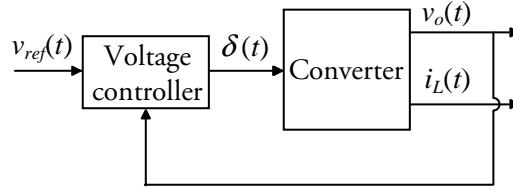
Figure 2.12: Voltage-mode control.

Operation of Current-Mode Control

The operation and implementation of current-mode control are discussed in this subsection.

In current-mode control, two control loops are used (Redl and Sokal, 1986). See Figure 2.11. The inner loop is fast and controls the inductor current, $i_L(t)$. The outer loop is slower and controls the output voltage, $v_o(t)$. The inductor current is fed back via the current controller in the inner loop while the output voltage is fed back via the voltage controller in the outer loop. The voltage controller has the reference signal $v_{ref}(t)$. The voltage controller tries to get $v_o(t)$ equal to $v_{ref}(t)$ by changing its control signal, $i_c(t)$. This signal is subsequently used as the reference signal for the current controller. The current controller aims at getting $i_L(t)$ equal to $i_c(t)$ (in a sense) by changing its control signal, $\delta(t)$, which is the input (control) signal of the converter. Thus, current-mode control is an application of cascade control (Goodwin, Graebe and Salgado, 2001, Section 10.7).
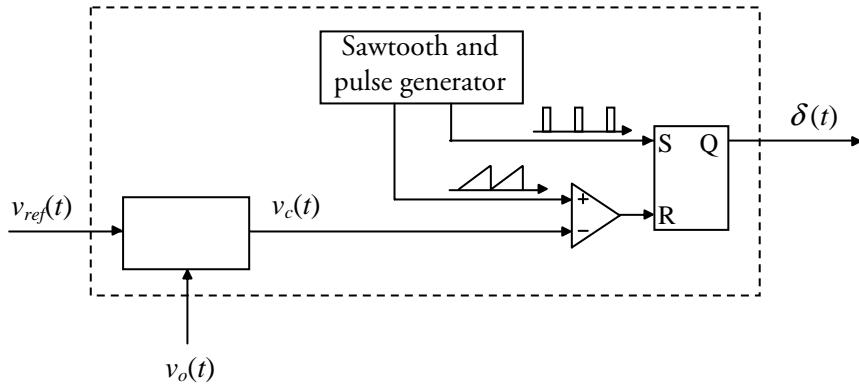
Figure 2.13: A voltage controller in voltage-mode control.
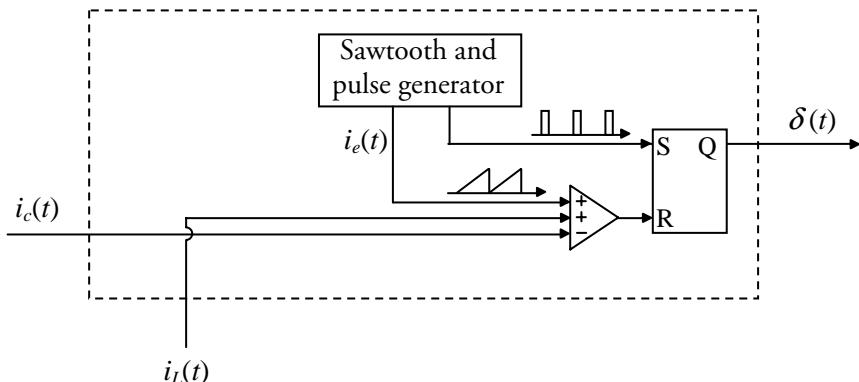
Figure 2.14: A current controller in current-mode control.

In the case of current-mode control, the control signal of the voltage controller is analog and the control signal of the current controller is digital (binary).

In the case of voltage-mode control, see Figure 2.12, the control signal of the voltage controller is digital using $\delta(t)$. There is no current controller and the inductor current does not need to be measured. A voltage controller is shown in Figure 2.13. The first (left) part is usually a voltage-error amplifier and its output signal, $v_c(t)$, is analog. The second (right) part of the controller is a pulse width modulator (compare this modulator with the

circuit shown in Figure 2.5). The duty cycle, $d(t)$, depends linearly on the control signal $v_c(t)$. Voltage-mode control is also called duty ratio control.

A typical current controller in current-mode control is implemented as shown in Figure 2.14. The peak inductor current is controlled and the control method is therefore called peak current-mode control. This is the most common type of current-mode control and the word "peak" is often left out. If the controllers in Figure 2.14 and Figure 2.13 are compared, the current controller seems to consist only of a modulator. Kislovski, Redl and Sokal (1991, Chapter 5) use the name current modulator instead of current controller. Average current-mode control is another type of current-mode control (Kislovski, Redl and Sokal, 1991, Chapter 5). The first part of the current controller in average current-mode control is a current-error amplifier. It may in this case not be suitable to call the current controller a current modulator since one may consider it consists of more than a modulator (compare this current controller with the voltage controller in voltage-mode control). The name current controller may therefore be seen as more general and it is used here. The modulator is seen as a (large or small) part of the current controller.

The operation of the current controller in (peak) current-mode control shown in Figure 2.14 will now be explained. For a moment assume that the saw-tooth signal, $i_e(t)$, is not present. The period of the signal from the pulse generator is equal to T_s and the signal sets the SR-latch. Each time this occurs, the transistor is turned on and the inductor current, $i_L(t)$, starts to increase as shown in Figure 2.15. When $i_L(t)$ becomes greater than the signal $i_c(t)$, the SR-latch is reset and $i_L(t)$ then decreases until a new set pulse is generated. This is the same function as the pulse width modulator in Figure 2.5 and Figure 2.13 except the inductor current, $i_L(t)$, replaces the saw-tooth signal. Compare the waveforms shown in Figure 2.15 and Figure 2.7. The signal $i_c(t)$ is the reference signal of the current controller. The current controller tries to get $i_L(t)$ equal to $i_c(t)$ in the sense that it is the peak value of $i_L(t)$ that is of interest. In average current-mode control, it is the average value of $i_L(t)$ that is of interest. The current controller in (peak) current-mode control is fast since it manages to get the peak value of $i_L(t)$ equal to $i_c(t)$ directly. The inner closed loop system in (peak) current-mode control can therefore be seen as a current source.

To be compatible with the definitions made by Ridley (1991), the saw-tooth signal, $i_e(t)$, is from now on called the external ramp.

The feedback of $i_L(t)$ can cause instability (Erickson and Maksimovic,
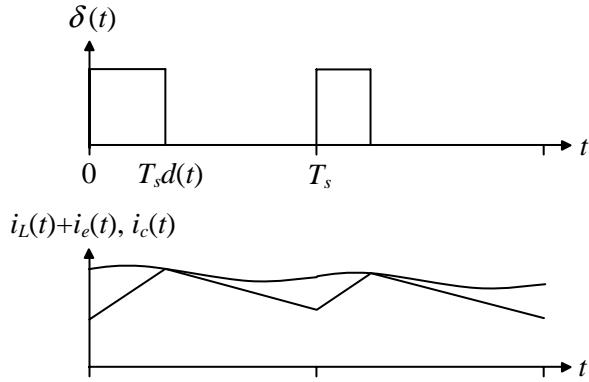
Figure 2.15: The waveforms of the signals in a current controller in (peak) current-mode control.

2000, Section 12.1). The control of the inductor current is unstable if the steady-state duty cycle, D, is greater than 0.5. It is unstable in the sense that the duty cycle, $d(t)$, never reaches a constant level even if $i_c(t)$ is constant. However, it is stable in the sense that the peak value of $i_L(t)$ is equal to $i_c(t)$.

It is possible to obtain stability also in the case where D is greater than 0.5 if slope compensation is utilized. With slope compensation, $i_c(t)$ is compared with the sum of $i_L(t)$ and an external ramp, $i_e(t)$. The slope of the sum is greater than the slope of $i_L(t)$ alone. The characteristic value α is now defined as

$$\alpha = \frac{M_2 - M_e}{M_1 + M_e}, \tag{2.16}$$

where M_e is the slope of $i_e(t)$, M_1 is the slope of $i_L(t)$ while the transistor is on and $-M_2$ is the slope of $i_L(t)$ while the transistor is off. None of M_e, M_1, and M_2 is negative with these definitions. M_e must be chosen such that $|\alpha| < 1$ to obtain stability.

The Ridley and Tan Models Applied to the Buck Converter

In this subsection, the two models presented by Ridley (1991) and Tan and Middlebrook (1995) are reviewed and compared. The control-to-output

transfer function, the output impedance, and the audio susceptibility can be obtained by applying these two models to the buck converter with current-mode control and the results are presented.

A large number of continuous-time models for current-mode control have been presented during the years. The Ridley and Tan models are designed to be accurate from dc to half the switching frequency. They differ mainly in the modeling of the current loop gain.

When an accurate model of current-mode control has been needed, the one presented by Ridley (1991) often has been chosen. An example of this is Lo and King (1999), where the choice was between the Ridley and Tan models. In Lo and King (1999), the Tan model is considered suspect and some other authors have also expressed this opinion.

The Ridley and Tan models include high-frequency extensions to be accurate up to half the switching frequency. These high-frequency extensions are based on an accurate control-to-current transfer function. We will first make a brief review of how this transfer function is obtained.

In Figure 2.15, $i_e(t)$ is added to $i_L(t)$ but the same function is obtained if $i_e(t)$ is subtracted from $i_c(t)$ and this is used in Figure 2.16(a). Figure 2.16(a) shows the waveforms of the signals $i_c(t)$, $i_c(t) - i_e(t)$, and two different versions of the inductor current. The first version (solid line) shows the inductor current waveform in steady state, i.e. in the case where there are no perturbations of $i_c(t)$. The second version (dashed line) shows the inductor current waveform in the case where there is a step perturbation in $i_c(t)$ as shown in Figure 2.16(a). The transistor is assumed to turn on at the points $t = nT_s$, where n is an integer. The transistor will then turn off at the points $t = (n + D)T_s$ in steady state. It is assumed that the changes in the input voltage and the output voltage are negligible so that the slopes of the inductor current can be considered constant.

The perturbations of $i_c(t)$ and $i_L(t)$ are shown in Figure 2.16(b) and Figure 2.16(c), respectively. An approximation of $\hat{i}_L(t)$ is shown in Figure 2.16(d). If we search for a linearized model, the use of the waveform in Figure 2.16(d) instead of the waveform in Figure 2.16(c) does not cause an error since the relative error in the integral of $\hat{i}_L(t)$ then is infinitely small.

The signal $i_c(t)$ affects the waveform of the inductor current. If the changes in $i_c(t)$ are small, the value of $i_c(t)$ is important only in a small surrounding of the points $t = (n + D)T_s$. If the changes of $i_c(t)$ in these surroundings are slow, only a sampled version of $i_c(t)$ (or $\hat{i}_c(t)$) is needed in order to obtain an accurate model. A sampled version of $\hat{i}_c(t)$ is shown in
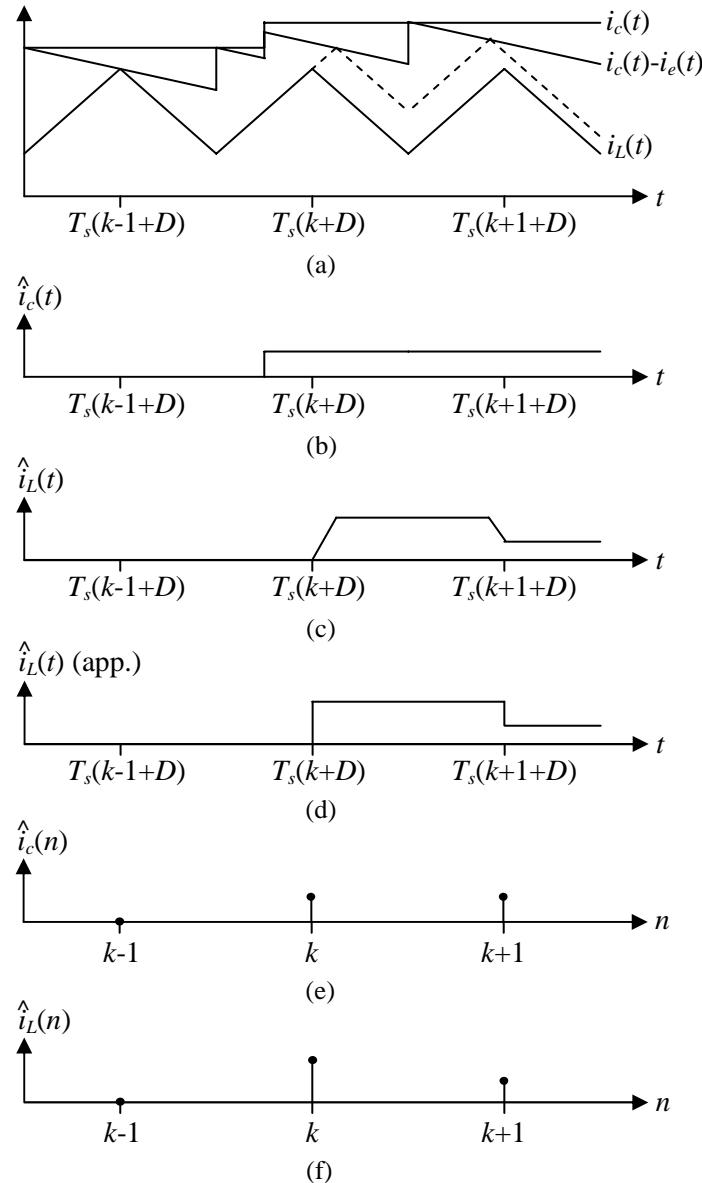
Figure 2.16: Different versions of the currents in a current controller.

Figure 2.16(e) and it is denoted $\hat{i}_c(n)$. To be spared from introducing new variable names, the sampled (discrete-time) version of a continuous-time signal is denoted by the same name as the continuous-time signal, which is not a formally correct notation.

A sampled version of the approximate $\hat{i}_L(t)$ is shown in Figure 2.16(f) and it is denoted $\hat{i}_L(n)$. An expression that describes how $\hat{i}_L(n)$ depends on $\hat{i}_c(n)$ can be derived. The Z-transform of this expression gives a discrete-time transfer function. By considering that the approximate perturbed inductor current shown in Figure 2.16(d) is reconstructed from $\hat{i}_L(n)$ by using a zero-order-hold circuit the following accurate continuous-time control-to-current transfer function is obtained:

$$F_h(s) = \frac{\hat{i}_L(s)}{\hat{i}_c(s)} = \frac{1}{T_s} \frac{(1+\alpha)e^{sT_s}}{e^{sT_s}+\alpha} \frac{\left(1-e^{-sT_s}\right)}{s}, \qquad (2.17)$$

where α is defined in (2.16). Once again, note that the derivation of (2.17) is made with the assumption that the changes in the input and output voltage are negligible.

Both the Ridley and Tan models are unified models, i.e. they can be applied to different types of converter topologies. The block diagram in Figure 2.17 is used to compare the Ridley and Tan models. Both are small-signal models and, therefore, the linearized model of the converter is included in Figure 2.17.

The model of the current controller consists of six blocks. The R_i block will be explained later in this subsection. $F_m(s)$ is the transfer function of the modulator. Changes in the input and output voltages affect the control and these effects are modeled with the feedforward gains k_f and k_r. Note that the input and output voltages are not fed forward in Figure 2.11. The reason why they are needed in Figure 2.17 is that there are Fourier components missing in the signal $L^{-1}\{\hat{i}_L(s)\}$ compared to the signal $i_L(t)$ in Figure 2.11 (see Section 2.2). It is not just the dc component that is missing. The input and output voltages affect the slopes of the inductor current in each switching period, which is an important factor in the current controller. The use of $\hat{v}_g(s)$ and $\hat{v}_o(s)$ in the small-signal model of the current controller therefore complements $\hat{i}_L(s)$ so that the waveform of $i_L(t)$ is better known. The feedforward gains are in the Ridley and Tan models calculated in a way that makes the amplification of the closed loop system correct at dc. In the next
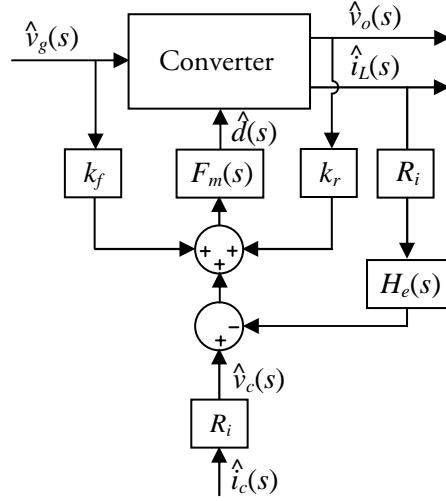
Figure 2.17: A small-signal model of the current controller and the converter.

subsection, it will be shown that this way introduces a modeling error at high frequencies.

$H_e(s)$ is used to include the high-frequency extension in the Ridley model and it is calculated to be

$$H_e(s) = \frac{sT_s}{e^{sT_s} - 1}. \tag{2.18}$$

The Ridley model utilizes an approximation of (2.18). The approximation:

$$e^{-sT_s} \approx \frac{1 + \dfrac{s}{\omega_n Q_z} + \dfrac{s^2}{\omega_n^2}}{1 - \dfrac{s}{\omega_n Q_z} + \dfrac{s^2}{\omega_n^2}}, \tag{2.19}$$

where

$$Q_z = \frac{-2}{\pi}, \tag{2.20}$$

$$\omega_n = \frac{\pi}{T_s}, \tag{2.21}$$

is used both by Ridley and Tan to replace the exponential functions. The approximation error of (2.19) is zero at dc and half the switching frequency, ω_n.

The approximate $H_e(s)$ and $F_h(s)$ are

$$H_e(s) = 1 + \frac{s}{\omega_n Q_z} + \frac{s^2}{\omega_n^2}, \tag{2.22}$$

$$F_h(s) = \frac{\hat{i}_L(s)}{\hat{i}_c(s)} = \frac{1}{1 + \frac{s}{\omega_n Q} + \frac{s^2}{\omega_n^2}}, \tag{2.23}$$

where

$$Q = \frac{1}{\pi(m_c D' - 0.5)}, \tag{2.24}$$

$$m_c = 1 + \frac{M_e}{M_1}. \tag{2.25}$$

The high-frequency extension in the Tan model is obtained by including a pole in $F_m(s)$. Tan and Middlebrook (1995) present the following model for the buck converter:

$$F_m(s) = \frac{1}{\left(M_e + \frac{(D'-D)V_g}{2L}\right)T_s\left(1 + \frac{s}{\omega_p}\right)}, \tag{2.26}$$

$$k_f = -\frac{DD'T_s}{2L}, \tag{2.27}$$

$$k_r = 0, \tag{2.28}$$

$$H_e(s) = 1, \tag{2.29}$$

$$R_i = 1\,\Omega, \tag{2.30}$$

$$\omega_p = \frac{\omega_n}{Q}. \tag{2.31}$$

In a practical current-mode controller, the inductor current is measured and transformed to a voltage signal. Voltage signals also represent the control signal and the external ramp signal. Ridley models this by including a gain, R_i, in the inductor current feedback loop. Tan does not model this and R_i is therefore set to 1 in (2.30). The following variables are used in the Ridley model:

$$\hat{v}_c(s) = R_i \hat{i}_c(s), \tag{2.32}$$

$$S_n = R_i M_1, \tag{2.33}$$

$$S_f = R_i M_2, \tag{2.34}$$

$$S_e = R_i M_e. \tag{2.35}$$

Ridley (1990a) presents the following model for the buck converter:

$$F_m(s) = F_m = \frac{1}{(S_n + S_e)T_s} = \frac{1}{m_c S_n T_s}, \tag{2.36}$$

$$k_f = -\frac{D T_s R_i}{L}\left(1 - \frac{D}{2}\right), \tag{2.37}$$

$$k_r = \frac{T_s R_i}{2L}, \tag{2.38}$$

$$H_e(s) = 1 + \frac{s}{\omega_n Q_z} + \frac{s^2}{\omega_n^2}.$$ (2.39)

By applying the Ridley model to the buck converter the following results are obtained for the three major transfer functions:

$$\frac{\hat{v}_o(s)}{\hat{i}_c(s)} = \frac{\hat{v}_o(s)}{\hat{v}_c(s)/R_i} = \frac{R(1 + sR_c C)}{den(s)},$$ (2.40)

$$Z_{out}(s) = \frac{R(1 + sR_c C)F_h^{-1}(s)}{den(s)},$$ (2.41)

$$\frac{\hat{v}_o(s)}{\hat{v}_g(s)} = \frac{\dfrac{RT_s}{L} D\left(m_c D' - \left(1 - \dfrac{D}{2}\right)\right)(1 + sR_c C)}{den(s)},$$ (2.42)

where

$$den(s) = (1 + s(R + R_c)C)F_h^{-1}(s) + \frac{RT_s}{L}(m_c D' - 0.5)(1 + sR_c C),$$ (2.43)

and $F_h(s)$ is defined in (2.23).

By applying the Tan model to the buck converter the following results are obtained for the three major transfer functions:

$$\frac{\hat{v}_o(s)}{\hat{i}_c(s)} = \frac{R(1 + sR_c C)}{den(s)},$$ (2.44)

$$Z_{out}(s) = \frac{R(1 + sR_c C)F_h^{-1}(s)}{den(s)},$$ (2.45)

$$\frac{\hat{v}_o(s)}{\hat{v}_g(s)} = \frac{\dfrac{RT_s}{L}D\left(m_c D'-\left(1-\dfrac{D}{2}\right)+\dfrac{s}{\pi\omega_n}\right)(1+sR_cC)}{den(s)}, \qquad (2.46)$$

where

$$den(s) =$$

$$(1+s(R+R_c)C)F_h^{-1}(s)+\frac{RT_s}{L}\left(m_c D'-0.5\left(1-s\frac{2}{\pi\omega_n}\right)\right)(1+sR_cC), \qquad (2.47)$$

and $F_h(s)$ is defined in (2.23).

The denominator in the Tan model, (2.47), is almost the same as the one in the Ridley model, (2.43). The difference is often insignificant for converters that are used in practice. The control-to-output transfer functions predicted by the Ridley and Tan models are therefore approximately the same since the numerators in (2.40) and (2.44) are exactly the same. The same is true for the output impedances since the numerators in (2.41) and (2.45) are exactly the same. However, the numerator in (2.42) and (2.46) are not the same. The audio susceptibility predicted by the Tan model includes an extra zero compared to the Ridley model.

If the three transfer functions obtained from the Ridley model, (2.40)-(2.42), are compared with the transfer functions for the open loop system, (2.12)-(2.14), it is found that there are three poles instead of two poles. Furthermore, the ESR zero remains but the zero at the origin for the output impedance is replaced by two zeros determined by $1/F_h(s)$. This means that the output impedance does not tend to zero as the frequency tends to zero.

The control-to-output transfer function, the output impedance, and the audio susceptibility obtained by applying the Ridley model to the boost converters are found in Johansson (2003, Section 3.6, Equations 3.92-3.94). The corresponding results for the buck-boost converter are found in Johansson (2003, Section 3.7, Equations 3.110-3.112).
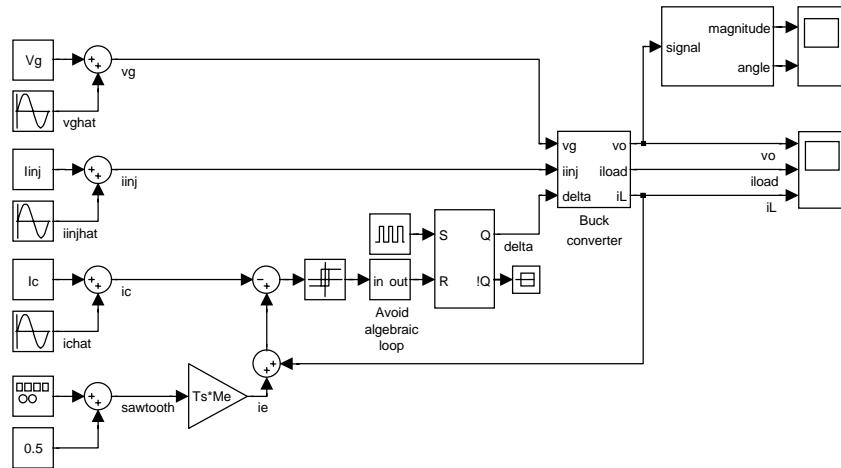
Figure 2.18: The simulation model for current-mode control (without the voltage controller).

A Comparison of the Two Models and the Simulation Results.

In this subsection, a simulation model of a buck converter with current-mode control is presented. The transfer functions obtained by means of the Ridley and Tan models are compared with simulation results. The results of the comparison are also explained.

Figure 2.18 shows the simulation model. The inductor current iL is fed back and added to the external compensation signal ie and the sum is compared to reference signal ic. The signal ie is obtained by multiplying the signal *sawtooth* with $T_s M_e$. The slope of *sawtooth* is equal to $1/T_s$ so the slope of ie is equal to M_e. The reference signal, ic, is the sum of its dc value, Ic, and its ac value *ichat*.

If the output of the relay block is connected directly to the reset input of the SR-latch, the simulation program report an existence of an algebraic loop. To avoid the algebraic loop, the special designed subsystem is inserted between the relay and the SR-latch.

The transfer functions obtained by means of the Ridley and Tan models
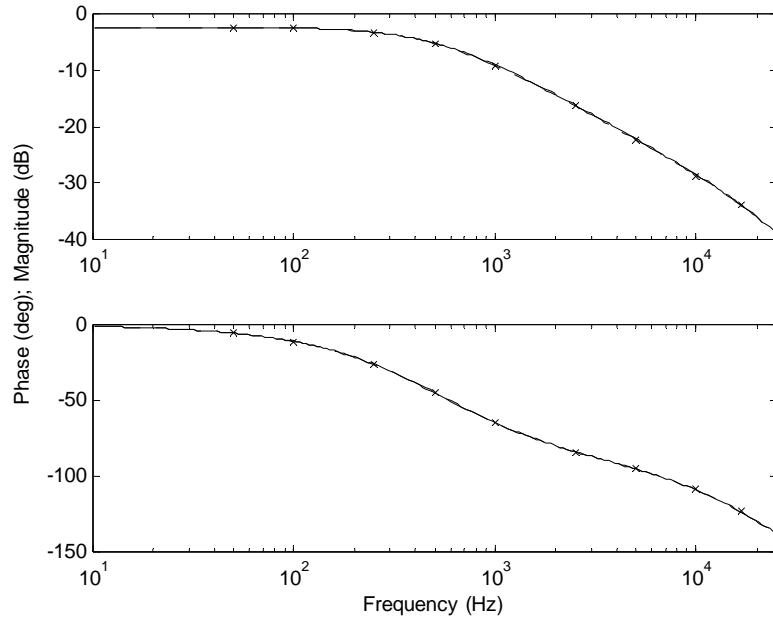
Figure 2.19: The control-to-output transfer function of a buck converter with a current controller. X: the simulation results. Solid line: the Ridley model. Dashed line: the Tan model. Note that the two lines almost coincide.

are now compared with simulation results. The parameters used in the simulation model presented in Section 2.2 are also used here. R_i is set to 1 Ω. Ic is adjusted manually so that the average value of the output voltage, V_o, is equal to 5 V ($D = 0.455$). M_e is calculated by using (2.25) and the first equality in (3.108) (with $R_{on} = 0$):

$$M_e = \frac{V_g - V_o}{L}(m_c - 1),\qquad(2.48)$$

where m_c is chosen to be 2.

Figure 2.19 shows the Bode plots for the control-to-output transfer functions in (2.40) and (2.44) together with the simulation results. From the
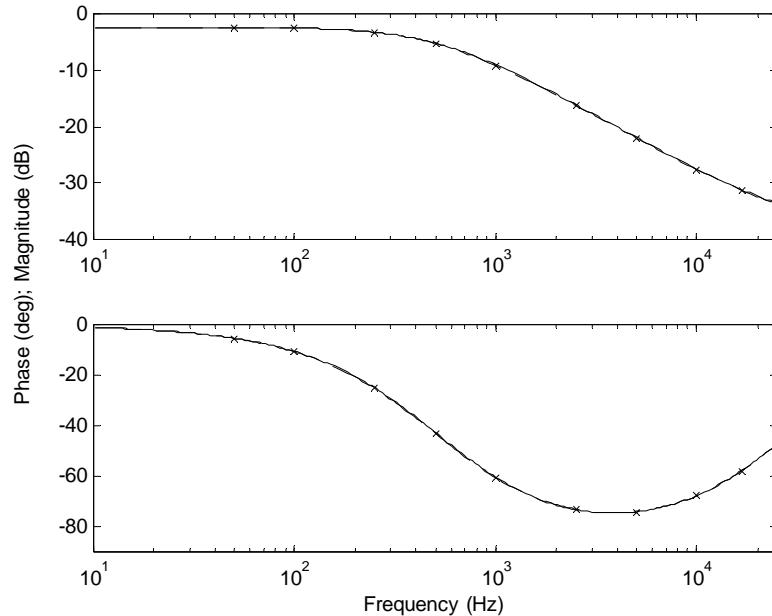
Figure 2.20: The output impedance of a buck converter with a current controller. X: the simulation results. Solid line: the Ridley model. Dashed line: the Tan model. Note that the two lines almost coincide.

figure it is seen that the control-to-output transfer functions predicted by the Ridley and Tan models are almost the same and they agree closely with the simulation results.

Figure 2.20 shows the Bode plots for the output impedances in (2.41) and (2.45) together with the simulation results. From the figure it is seen that the output impedances predicted by the Ridley and Tan models are almost the same and they agree closely with the simulation results.

Figure 2.21 shows the Bode plots for the audio susceptibilities in (2.42) and (2.46) together with the simulation results. From the figure it is seen that the audio susceptibilities predicted by the Ridley and Tan models are <u>not</u> the same and <u>neither</u> agrees closely with the simulation results at high frequencies. The Tan model has the largest deviation from the simulation
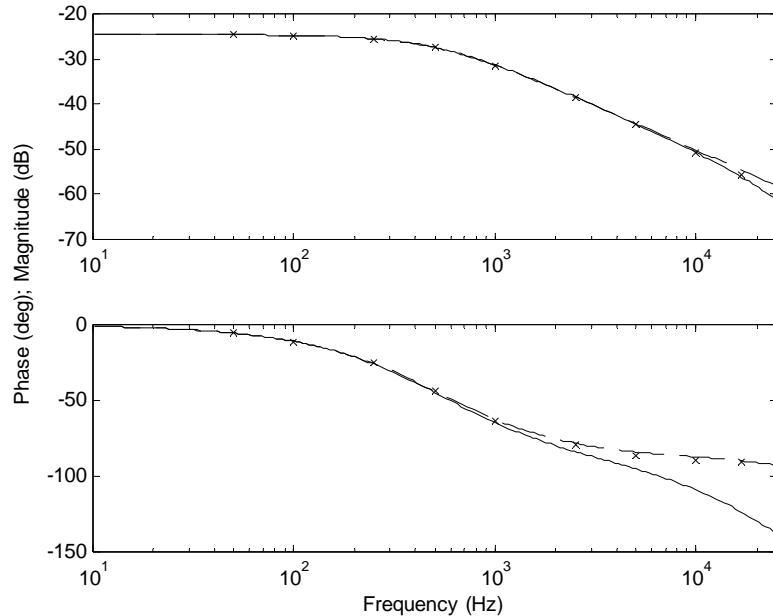
Figure 2.21: The audio susceptibility of a buck converter with a current
            controller. X: the simulation results. Solid line: the Ridley
            model. Dashed line: the Tan model.

results in the magnitude while the Ridley model has the largest deviation
from the simulation results in the phase shift.

The results of the comparison are now explained. The control-to-current
transfer function (2.17) is derived under the assumption that there are no
changes in the input and output voltages. To cope with changes in these
voltages, the feedforward gains k_f and k_r are included in the Ridley and
Tan models. The feedforward gains are calculated in a way that makes the
amplification of the closed loop system correct at dc. At high frequencies, the
perturbation of the voltage across the inductor cannot be considered constant
during a switching period. However, the amplitude of the changes in the
output voltage is low at high frequencies due to the output capacitor. This
explains why the control-to-output transfer functions and the output
impedances predicted by the Ridley and Tan models are so accurate. In the
case where the audio susceptibility is considered, also the input voltage

changes. Since the input voltage is the input signal in this case, its amplitude is assumed to be unity. The perturbation of the voltage across the inductor is therefore not small at high frequencies and the errors in the Ridley and Tan models are significant.

If the transfer functions obtained by applying the Ridley model to the boost and buck-boost converters are compared with simulation results, the conclusion is the same as the one for the buck converter, i.e. the predictions agree closely with the simulation results except at high frequencies in the case of audio susceptibility.

2.4   A Novel Model

Models for converters with current-mode control were considered in Section 2.3. We showed that the way the changes in the input and output voltages are treated in the Ridley and Tan models introduces a modeling error at high frequencies. We also showed that this modeling error is significant for the audio susceptibility. To obtain an accurate model for the audio susceptibility, the changes in the input and output voltages must be treated in a more refined way. In this section, a novel model for the audio susceptibility is presented and compared with simulation results. This model will be utilized in Section 2.5 to improve the Ridley and Tan models.

The outline of this section is as follows. First, the derivation of the novel model is presented briefly. The audio susceptibility obtained by applying the novel model to the buck converter is then presented. It is also compared with simulation results and the Ridley and Tan models.

A Novel Model for the Audio Susceptibility

In this subsection, the derivation of the novel model is presented briefly.

The audio susceptibility describes how a perturbation in the input voltage affects the output voltage. Figure 2.22 shows the converter and the current controller. In the case where the audio susceptibility is considered, the reference signal, $i_c(t)$, is constant and the input voltage, $v_g(t)$, is perturbed. A perturbation in $v_g(t)$ causes a perturbation in the output voltage and the inductor current. It also causes a perturbation in the duty cycle of $\delta(t)$ since the inductor current is fed back to the current controller. The perturbation in the duty cycle of $\delta(t)$ contributes to the perturbation in the output voltage
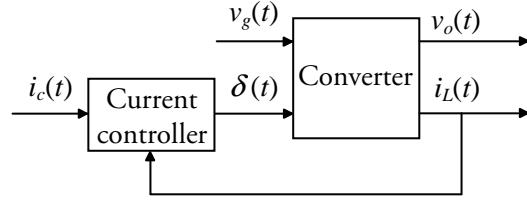
Figure 2.22: The converter and the current controller.

and the inductor current. Since the rule of superposition holds for the linearized converter, the Laplace transform of the perturbed output voltage is

$$\hat{v}_o(s) = \left(\frac{\hat{v}_o(s)}{\hat{v}_g(s)} \right)_{ol} \hat{v}_g(s) + \frac{\hat{v}_o(s)}{\hat{d}(s)} \hat{d}(s). \qquad (2.49)$$

The subscript ol will be used for the converter transfer functions, i.e. for the open loop system, except for the control-to-output transfer function. Note that fractions in (2.49) must be regarded as transfer functions and $\hat{d}(s)$ and $\hat{v}_g(s)$ cannot be canceled. If $\hat{d}(s)$ were known, $\hat{v}_o(s)$ could be calculated with (2.49). A model for $\hat{d}(z)$ (the Z-transform of the sampled version of $\hat{d}(t)$) will first be derived.

The voltage across the inductor depends on the input and output voltages and the topology of the converter according to Table 2.2, see Ridley (1990b, Table 4.2). The positive voltage across the inductor as the transistor is on is called $v_{on}(t)$ while the positive voltage across the inductor as the transistor is off is called $v_{off}(t)$. Both these voltages are here defined to be equal to the expressions in Table 2.2 for all t, i.e. the expressions for $v_{on}(t)$ is valid also when the transistor is off and the expressions for $v_{off}(t)$ is valid also when the transistor is on.

Table 2.2: The positive voltage across the inductor.

	Buck	Boost	Buck-Boost
$v_{on}(t)$	$v_g(t) - v_o(t)$	$v_g(t)$	$v_g(t)$
$v_{off}(t)$	$v_o(t)$	$v_o(t) - v_g(t)$	$v_o(t)$
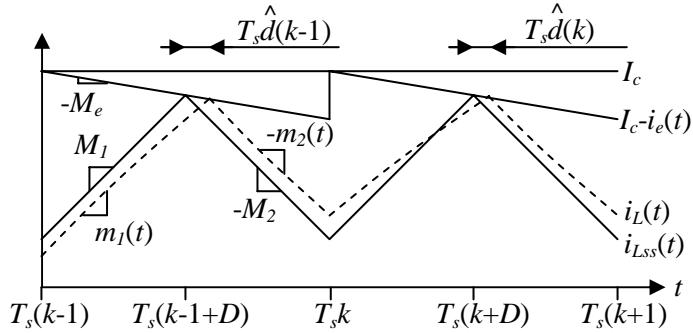
Figure 2.23: The waveforms in steady state and in the case where the input and output voltages change.

The slopes of the inductor current are calculated by

$$m_1(t) = M_1 + \hat{m}_1(t) = \frac{1}{L}\left(V_{on} + \hat{v}_{on}(t)\right) = \frac{1}{L}v_{on}(t), \qquad (2.50)$$

$$m_2(t) = M_2 + \hat{m}_2(t) = \frac{1}{L}\left(V_{off} + \hat{v}_{off}(t)\right) = \frac{1}{L}v_{off}(t). \qquad (2.51)$$

$m_1(t)$ is the positive slope of the inductor current while the transistor is on. The negative slope of the inductor current as the transistor is off corresponds to $-m_2(t)$.

When the audio susceptibility is considered, $i_c(t)$ is constant and equal to its dc value I_c. Figure 2.23 shows the waveforms of I_c, I_c minus the external ramp, $i_e(t)$, and two different versions of the inductor current. The first version ($i_{Lss}(t)$, solid line) shows how the inductor current waveform is in steady state, i.e. when there are no perturbations of the inductor current slopes $m_1(t)$ and $-m_2(t)$. The dashed line shows an example of how the inductor current waveform is if there are perturbations of the inductor current slopes. The transistor is assumed to turn on at the points $t = nT_s$, where n is an integer. In steady state the transistor will then turn off at the points $t = (n + D)T_s$. To find out how much the inductor current changes, the inductor current slopes are integrated. The following two equations are obtained from Figure 2.23:

$$I_c - i_L(T_s k) = M_e T_s \left(D + \hat{d}(k-1) \right) + \int_{T_s(k-1+D+\hat{d}(k-1))}^{T_s k} m_2(t) dt, \qquad (2.52)$$

$$I_c - i_L(T_s k) = M_e T_s \left(D + \hat{d}(k) \right) + \int_{T_s k}^{T_s(k+D+\hat{d}(k))} m_1(t) dt. \qquad (2.53)$$

Using (2.52) and (2.53) it is possible to derive the following expression for $\hat{d}(n)$:

$$\hat{d}(n) = \frac{1}{(M_e + M_1) T_s} (M_e - M_2) T_s \hat{d}(n-1) +$$

$$\frac{1}{(M_e + M_1) T_s} \left(\int_{-\infty}^{T_s n} \hat{m}_2(t) dt - \int_{-\infty}^{T_s(n-1+D)} \hat{m}_2(t) dt - \int_{-\infty}^{T_s(n+D)} \hat{m}_1(t) dt + \int_{-\infty}^{T_s n} \hat{m}_1(t) dt \right). \qquad (2.54)$$

Note that the integer variable k in (2.52) and (2.53) is substituted by the integer variable n in (2.54). The discrete-time signal $\hat{d}(n)$ is the result of sampling the continuous-time signal $\hat{d}(t)$. The sampling interval changes if the converter is not in steady state. Similarly to the discussion in Section 2.3, sampling at the points $t = (n+D)T_s$ is a good approximation if the magnitude of $\hat{d}(t)$ is small and the changes of $\hat{d}(t)$ are slow in the surroundings of these sampling points. From (2.54), it is seen that $\hat{d}(n)$ is a sum of a discrete-time part (first term) and a continuous-time part (last term). To be able to create the discrete-time signal $\hat{d}(n)$, the continuous-time part must deliver its value at $t = (n+D)T_s$ so that it can be sampled and added to the discrete-time part of (2.54). In the first integral in (2.54),

$$\int_{-\infty}^{T_s n} \hat{m}_2(t) dt,$$

the signal $\hat{m}_2(t)$ is integrated up to $t = nT_s$ so the value of the integral is known at $t = nT_s$. Since the value of the integral has to be delivered at $t = (n+D)T_s$, the value must be delayed by DT_s. The delay for the three remaining integrals must be T_s, 0, and DT_s, respectively. Therefore, the signal $\hat{d}(n)$ can be created as shown in Figure 2.24.

The block diagram in Figure 2.24 is transformed from the time domain to the frequency domain and the result is shown in Figure 2.25. A feedback is included in Figure 2.25 to eliminate one of the input signals. The feedback is transformed from the discrete-time part to the continuous-time part if z is substituted with e^{sT_s} and the result is shown in Figure 2.26.

In Figure 2.26, the signal $\hat{x}(s)$ is introduced. The following expression can be derived:

$$\hat{x}(s) = \frac{\dfrac{e^{-sDT_s} - e^{-sT_s}}{sT_s}\hat{m}_2(s) + \dfrac{e^{-sDT_s} - 1}{sT_s}\hat{m}_1(s)}{M_1 D'^{-1}\left(m_c D'\left(1 - e^{-sT_s}\right) + e^{-sT_s}\right)}. \tag{2.55}$$

By using (2.50), (2.51), (2.55), and Table 2.2, the block diagram in Figure 2.27 is obtained and it is a model for $\hat{d}(z)$. Note that this block diagram is derived without the prerequisite that $\hat{v}_g(t)$ and $\hat{v}_o(t)$ are sinusoidal.

If the spectrums of $\hat{d}(n)$ and $\hat{v}_o(t)$ are examined the following conclusions are obtained for the case where $\hat{v}_g(t)$ is a sinusoidal with the frequency ω_m and ω_m is in the interval [0, π/T_s] rad/s:

- The discrete-time signal $d(n)$ consists approximately of just one Fourier component (in the interval [0, π/T_s] rad/s) and it has the frequency ω_m. Therefore, $d(n)$ can be obtained by sampling a sinusoidal signal with the sampling interval T_s.
- A good approximation of the signal $\hat{x}(t)$ (the inverse Laplace transform of $\hat{x}(s)$) in Figure 2.27 is obtained if the input signal $\hat{v}_o(t)$ (the inverse Laplace transform of $\hat{v}_o(s)$) is replaced with a signal consisting of just the Fourier component in $\hat{v}_o(t)$ with the frequency ω_m.

To find a linear model of the audio susceptibility that is accurate from dc to half the switching frequency it is sufficient to consider just the case where the perturbation in the input voltage, $\hat{v}_g(t)$, is a sinusoidal signal with the frequency ω_m. The model should be accurate for any ω_m in the frequency interval. From the two conclusions above, it seems reasonable that an accurate model of the audio susceptibility can be obtained from the block diagram in Figure 2.28, where the block diagram in Figure 2.27 is combined with
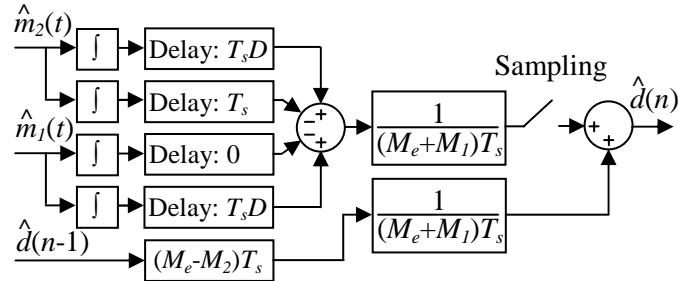
Figure 2.24: A time-domain model for the duty cycle perturbation signal.
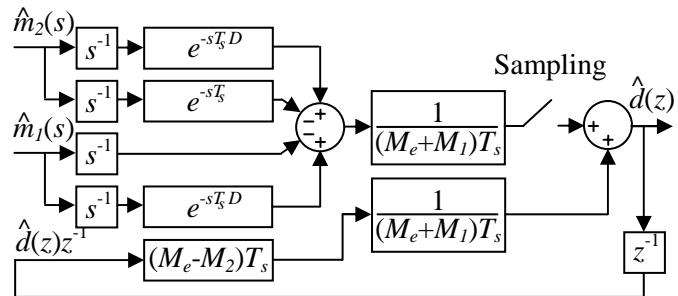
Figure 2.25: A frequency-domain model for the duty cycle perturbation signal.
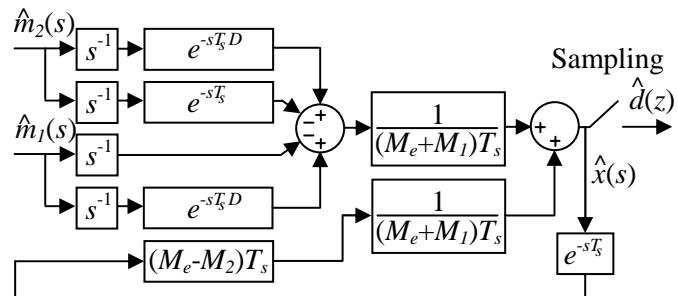
Figure 2.26. The feedback is moved to the continuous-time part.
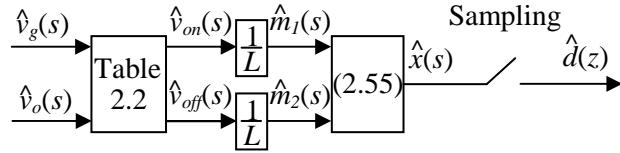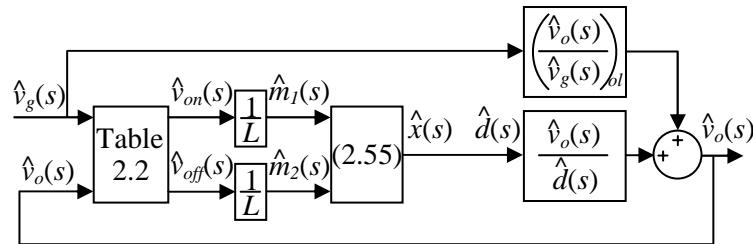
Figure 2.27: The block diagram with $\hat{v}_g(t)$ and $\hat{v}_o(t)$ as input signals.

Figure 2.28: A model of the audio susceptibility.

equation (2.49). $\hat{x}(s)$ is used as $\hat{d}(s)$ and the output $\hat{v}_o(s)$ from (2.49) is fed back to the input $\hat{v}_o(s)$ in the block diagram in Figure 2.27. The Fourier component in the output voltage with the frequency ω_m (see Section 2.2) is correctly predicted in (2.49) and it is enough to use this component as the $\hat{v}_o(s)$-input in the block diagram in Figure 2.27.

Audio Susceptibility of the Buck Converter

In this subsection, the audio susceptibility obtained by applying the novel model to the buck converter is presented. It is compared with simulation results, experimental result and the Ridley and Tan models.

By applying the novel model to the buck converter the following result is obtained:

$$\frac{\hat{v}_o(s)}{\hat{v}_g(s)} = \frac{\dfrac{RT_s}{L} D\big(m_c D' - F_f(s)\big)\big(1 + sR_cC\big)}{den(s)}, \tag{2.56}$$

where

$$F_f(s) = \frac{1}{sT_s}\left(\frac{sT_s}{1-e^{-sT_s}}\frac{1-e^{-sDT_s}}{sDT_s} - \frac{sT_s}{e^{sT_s}-1}\right) =$$

$$\left(1-\frac{D}{2}\right) - \frac{(3-2D)DT_s}{12}s - \frac{\left(1-2D+D^2\right)DT_s^2}{24}s^2 + \ldots, \tag{2.57}$$

$$den(s) = \left(1 + s(R+R_c)C\right)\left(H_e(s) + sT_s m_c D'\right) +$$

$$\frac{RT_s}{L}\left(m_c D' - \frac{1-H_e(s)}{sT_s}\right)(1+sR_cC), \tag{2.58}$$

and $H_e(s)$ is the same as in (2.18). The Taylor series of $F_f(s)$ is also shown in (2.57).

   If the approximations (2.22) and (2.23) are used, it can be shown that the denominator (2.58) is exactly the same as (2.47), i.e. the denominator in the Tan model. In Section 2.3, it was concluded that the denominator in the Tan model is almost the same as the denominator in the Ridley model, (2.43). The novel expression and the audio susceptibility predicted by the Ridley and Tan models thus have approximately the same denominator but three different numerators, compare (2.56), (2.42), and (2.46).

   The novel expression (2.56) is now compared with simulation results, experimental result, and the Ridley and Tan models.

   Figure 2.29 shows the Bode plot for the audio susceptibility according to the novel expression in (2.56) together with the results presented in Figure 2.21, i.e. the simulation results and the audio susceptibilities predicted by the Ridley and Tan models. From the figure it is seen that the novel expression agrees closely with the simulation results also at high frequencies.

   Figure 2.30 shows the same as Figure 2.29 except m_c is changed from 2 to 1.5 and experimental result presented by Ridley is included (copied manually from plot in Ridley (1991)). From the figure it is seen that the novel expression agrees closely with the simulation results also at high frequencies. The choice $m_c = 1.5$ makes the audio susceptibility very small at dc since there is a subtraction between two almost equal values in the numerator of transfer function. The modeling errors in the Ridley and Tan models cause larger relative errors at high frequencies in this case. This is most evident in the Ridley model. Ridley (1991) explains the difference between the audio susceptibility predicted by his model and experimental result at
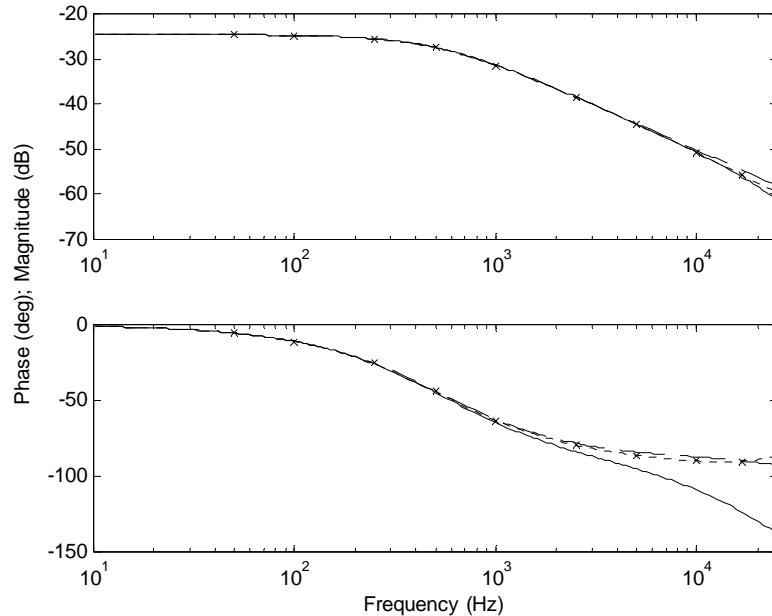
Figure 2.29: The audio susceptibility of a buck converter with a current controller (m_c =2). X: the simulation results. Dotted line: the novel expression. Solid line: the Ridley model. Dashed line: the Tan model.

m_c =1.5 by saying that the measurements were unreliable due to noise and grounding problems. The experimental result from Ridley agrees closely (if we take into consideration that it is an experimental result) with the simulation results and the novel expression as seen from Figure 2.30. This indicates that it is Ridley's measurements that are correct, not his model.

Figure 2.31 shows the same as Figure 2.29 except m_c is changed to 1. From the figure it is seen that the novel expression agrees closely with the simulation results also at high frequencies. The choice m_c =1 does not make the audio susceptibility small at dc. The result of the subtraction in the numerator of the transfer function is of opposite sign at dc compared to the case where m_c =2. This is seen from the phase shift curves in Figure 2.29 and Figure 2.31.
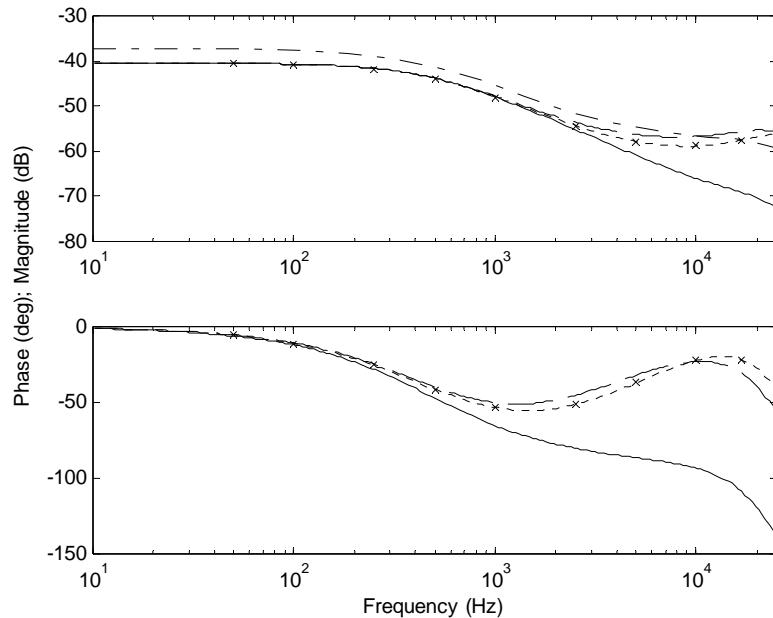
Figure 2.30: The audio susceptibility of a buck converter with a current controller (m_c =1.5). X: the simulation results. Dotted line: the novel expression. Solid line: the Ridley model. Dashed line: the Tan model. Dash-dotted line: the measurement made by Ridley (the phase shift curve is not available).

The transfer function for the audio susceptibility obtained by applying the novel model to the boost converters is found in Johansson (2003, Section 4.4, Equation 4.38). The corresponding result for the buck-boost converter is found in Johansson (2003, Section 4.5, Equation 4.63). If these two transfer functions are compared with simulation results, it is found that they agree closely with the simulation results at high frequencies but not at low frequencies. It can be shown that the predictions made by the novel model of the gain at low frequencies are very sensitive to modeling errors in the different blocks in Figure 2.28. If these predictions agree closely with the simulation results, this is due to more good luck than good management.
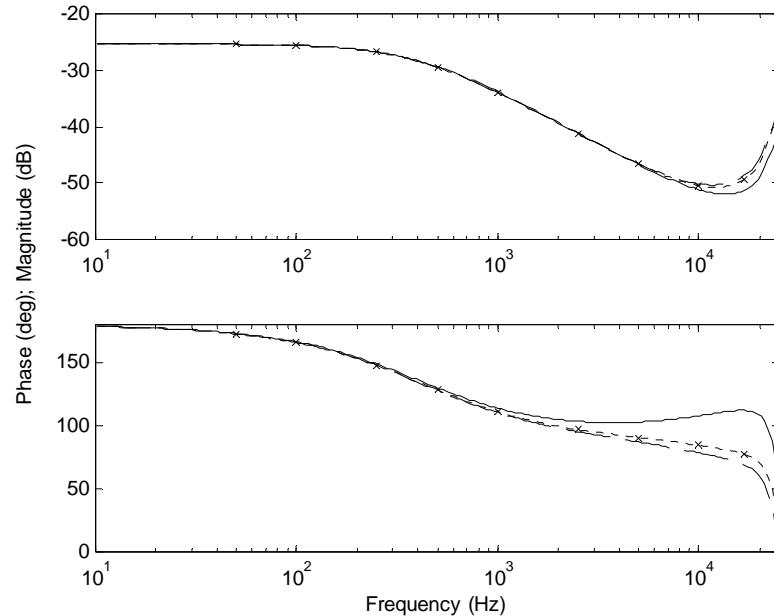
Figure 2.31: The audio susceptibility of a buck converter with a current controller ($m_c = 1$). X: the simulation results. Dotted line: the novel expression. Solid line: the Ridley model. Dashed line: the Tan model.

2.5   Improved Models

Models for converters with current-mode control were considered in Section 2.3. We showed that the way the changes in the input and output voltages are treated in the Ridley and Tan models introduces a modeling error at high frequencies. We also showed that this modeling error is significant for the audio susceptibility. A novel model for the audio susceptibility was derived in Section 2.4. In this section, this model is utilized to improve the Ridley and Tan models. In Section 2.6, the improved Ridley model will be approximated and then, in Section 2.7, used to analyze some properties that can be obtained when load current measurements are utilized for control.

In Section 2.4, it was concluded that the three expressions for the audio susceptibility for the buck converter, (2.42), (2.46), and (2.56), have approximately the same denominator but three different numerators. One way to improve the Ridley and Tan models is to modify the numerators in (2.42) and (2.46) in some way so that they are equal to the numerator in (2.56).

The improvement of the Ridley model is first considered. In the derivation of (2.42), (2.37) is used to substitute k_f. If k_f is not substituted in the derivation of the audio susceptibility, the result is

$$\frac{\hat{v}_o(s)}{\hat{v}_g(s)} = \frac{\frac{RT_s}{L} D \left(m_c D' + \frac{L}{DT_s R_i} k_f \right) (1 + sR_c C)}{den(s)} , \qquad (2.59)$$

where $den(s)$ is defined in (2.43). Hence, the feedforward gain k_f is not present in the denominator and may therefore be used to modify the numerator without changing the denominator. Note that predictions of the control-to-output transfer function and the output impedance made by the Ridley model are not affected when k_f is changed. This parameter is the gain of the feedforward of the input voltage, which is constant in the case where the control-to-output transfer function and the output impedance are considered. An equation is obtained if the numerator in (2.59) is put equal to the numerator in (2.56) and its solution is

$$k_f(s) = -\frac{DT_s R_i}{L} F_f(s) , \qquad (2.60)$$

where $F_f(s)$ is defined in (2.57). Since the new k_f depends on s, it is denoted $k_f(s)$. Note that the s^0 term in (2.60) is equal to (2.37). The audio susceptibility according to the improved Ridley model is obtained by substituting k_f in (2.59) with (2.60):

$$\frac{\hat{v}_o(s)}{\hat{v}_g(s)} = \frac{\frac{RT_s}{L} D \left(m_c D' - F_f(s) \right) (1 + sR_c C)}{den(s)} , \qquad (2.61)$$

where $F_f(s)$ is defined in (2.57) and $den(s)$ is defined in (2.43).

If the Tan model is improved in a corresponding way the new $k_f(s)$ is

$$k_f(s) = -\frac{DT_s}{L}\left(F_f(s) - \frac{1}{2}\left(1 - s\frac{2}{\pi\omega_n}\right)\right), \qquad (2.62)$$

where $F_f(s)$ is defined in (2.57).

In the licentiate thesis, the Ridley model is improved also for the boost and buck-boost converters. The novel model is inaccurate at low frequencies for these two converters but the improvements are made in such a way that this shortcoming is not transferred to the improved models. For the boost converter, the audio susceptibility according to the improved Ridley model and the new $k_f(s)$ are found in Johansson (2003, Section 5.3, Equations 5.21 and 5.27). The corresponding results for the buck-boost converter are found in Johansson (2003, Section 5.4, Equations 5.38 and 5.44). The new $k_f(s)$ are unstable transfer functions for the boost and buck-boost converters.

2.6   Approximations of Obtained Expressions

Models for converters with current-mode control were considered in Section 2.3 and they were improved regarding the audio susceptibility in Section 2.5. The expressions obtained from all these models are rather complicated. In this section, approximate versions of the expressions for the control-to-output transfer function, the output impedance, and the audio susceptibility obtained by applying the improved Ridley model to the buck converter are presented. In Section 2.7, these approximate expressions will be used to analyze some properties that can be obtained when load current measurements are utilized for control.

The denominator (2.43) is common for the control-to-output transfer function (2.40), the output impedance (2.41), and the audio susceptibility (2.61). The transfer functions have three poles since the denominator (2.43) is a third order polynomial. The poles depend on m_c, which is the relative slope of the external ramp (see (2.25)), according to Figure 2.32 (see Ridley (1990b, Section 5.2.2)). If m_c is not to large, there are two high-frequency poles (i.e. poles far from the origin) and one low-frequency pole. In this case it is possible to approximate the denominator with a product of a second order polynomial and a first order polynomial. The second order polynomial
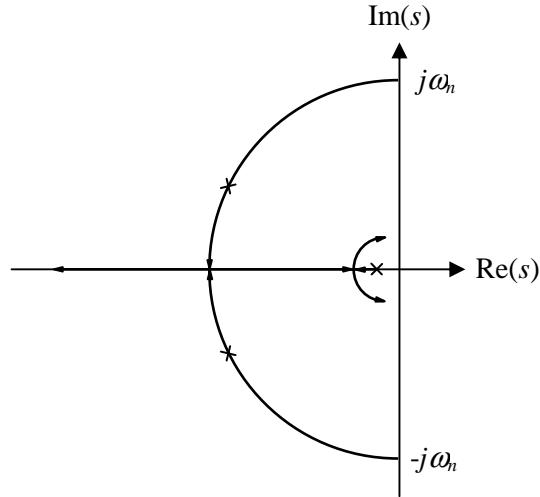
Figure 2.32: The root-locus of the three poles for increasing m_c.

corresponds to the two high-frequency poles and the first order polynomial corresponds to the low-frequency pole. This fact is used as the starting point for the derivation of an approximate model and the result is now presented.

If the conditions

$$R_c << R, \tag{2.63}$$

$$\frac{R_c T_s}{L}\left(m_c D'-0.5\right) << 1, \tag{2.64}$$

$$\frac{1}{\sqrt{LC}} << \omega_n, \tag{2.65}$$

$$\frac{1}{RCK} << \omega_n, \tag{2.66}$$

$$\frac{1}{RCK} << \omega_n Q, \tag{2.67}$$

where

$$K = \frac{1}{1 + \dfrac{RT_s}{L}\left(m_c D' - 0.5\right)} \,, \tag{2.68}$$

and Q is defined in (2.24), are fulfilled, then approximate versions of the control-to-output transfer function, the output impedance, and the audio susceptibility for the buck converter are

$$\frac{\hat{v}_o(s)}{\hat{i}_c(s)} = RKF_l(s)F_{ESR}(s)F_h(s) \,, \tag{2.69}$$

$$Z_{out}(s) = RKF_l(s)F_{ESR}(s) \,, \tag{2.70}$$

$$\frac{\hat{v}_o(s)}{\hat{v}_g(s)} = \frac{RT_s D}{L}\left(m_c D' - F_f(s)\right)KF_l(s)F_{ESR}(s)F_h(s) \,, \tag{2.71}$$

where

$$F_l(s) = \frac{1}{1 + sRCK} \,, \tag{2.72}$$

$$F_{ESR}(s) = 1 + sR_c C \,, \tag{2.73}$$

$F_h(s)$ is defined in (2.23), K is defined in (2.68), and $F_f(s)$ is defined in (2.57). The approximate versions (2.69) and (2.70) are exactly the same as the ones proposed by Ridley (1991). In the approximate version (2.70), two poles are cancelled by two zeros compared to the original version (2.41).

Since $F_f(s)$ is a rather complicated expression, it is desirable to find an approximate expression. $F_f(s)$ can be approximated by a Taylor polynomial, i.e. a truncated version of the Taylor series in (2.57). The higher degree of the Taylor polynomial that is used, the better approximation is obtained. If a Taylor polynomial of degree 0 is used, $k_f(s)$ in (2.60) is the same as k_f in (2.37) and the Ridley model is not improved. If a Taylor polynomial of degree 1 is used, there is an extra zero in the improved Ridley model. In Section 2.3, it was observed that the Tan model includes an extra zero

compared to the Ridley model (compare (2.42) and (2.46)). If a Taylor polynomial of degree 1 is used to improve the Tan model, the extra zero that is already present in the Tan model, is moved to a more suitable position. The extra zero in the Tan model explains why the Tan model is better than the Ridley model in Figure 2.30. However, the Ridley model is better than the Tan model in some cases since the extra zero in the Tan model is not placed at the most suitable position. This is for instance the case if D is small.

A Taylor polynomial approximates a function in a neighborhood of a point. There are other methods that approximate a function in an interval. For instance, the method of least squares can be used to minimize the integral of the squared errors. This can give a smaller maximum error.

Approximate versions of the control-to-output transfer function, the output impedance, and the audio susceptibility for the boost converter are found in Johansson (2003, Section 6.3, Equations 6.109, 6.118, and 6.121). The corresponding results for the buck-boost converter are found in Johansson (2003, Section 6.4, Equations 6.157, 6.166, and 6.178).

2.7   Using Load Current for Control

The output voltage and the inductor current are measured in the case where current-mode control is utilized. In this section, some properties that can be obtained when the controller also utilizes load current measurements are analyzed. The results of this analysis are compared with simulation results.

The outline of this section is as follows. First, some of the previous works made in this area are reviewed. Two concepts in control theory, feedforward and gain scheduling, will be needed and are therefore also reviewed. Next, a simple model of the buck converter with current-mode control is used to give a simple explanation of the following principal properties that are obtained when using load current measurements to control the converter:

- Low output impedance.
- An almost invariant control-to-output transfer function for different loads.
- Risk of instability.

Finally, the model obtained in Section 2.6 for the buck converter with current-mode control is used to analyze the properties.
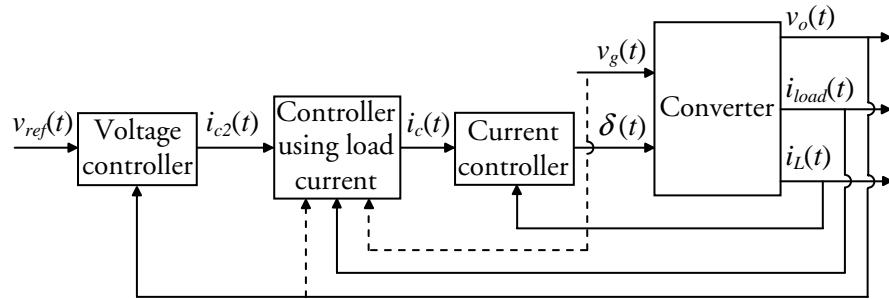
Figure 2.33: The configuration of the controller.

A Review

A number of papers suggest that the load current should be measured in order to improve the control of dc-dc converters. A few of them are mentioned in this subsection.

Redl and Sokal (1986) show that the transient in the output voltage due to a step change in the load can be much reduced if the load current is measured and used to control the converter. They only consider the case where current-mode control is used. The configuration of the controller is shown in Figure 2.33. The inductor current, $i_L(t)$, is fed back in the inner loop. The load current, $i_{load}(t)$, is used in the middle loop. (The input voltage, $v_g(t)$, and output voltage, $v_o(t)$, are in some cases also used in the middle loop.) The output voltage, $v_o(t)$, is fed back in the outer loop. The control method includes an extra middle controller compared to current-mode control (compare Figure 2.33 and Figure 2.11). The middle controller should be as follows according to Redl and Sokal (1986).

Buck:
$$i_c(t) = i_{c2}(t) + i_{load}(t), \qquad (2.74)$$

Boost:
$$i_c(t) = i_{c2}(t) + \frac{v_o(t)}{v_g(t)} i_{load}(t), \qquad (2.75)$$

Buck-boost:
$$i_c(t) = i_{c2}(t) + \frac{v_o(t) + v_g(t)}{v_g(t)} i_{load}(t). \qquad (2.76)$$

(The expression in (2.76) is actually obtained from Kislovski, Redl and Sokal (1991, Section 11.2).)

Schoneman and Mitchell (1989) analyze the proposed use of load current further in the case of the buck converter, i.e. (2.74).

Redl and Sokal (1986) suggest that the load current is not measured directly but calculated indirectly. For example, in the buck converter, the inductor current, $i_L(t)$, and the current to the output capacitor, $i_{cap}(t)$, are measured. The load current can then be calculated as the difference (see Figure 2.1):

$$i_{load}(t) = i_L(t) - i_{cap}(t). \qquad (2.77)$$

Note that the inductor current is measured in current-mode control so it is still only necessary to measure one extra current compared to current-mode control.

Schoneman and Mitchell (1989) propose an alternative approach. From Figure 2.14, it is seen that the difference $i_c(t) - i_L(t)$ is calculated in the current controller. This difference is rewritten by using (2.74) and (2.77):

$$\begin{aligned} i_c(t) - i_L(t) &= i_{c2}(t) + i_{load}(t) - i_L(t) = \\ i_{c2}(t) &+ i_L(t) - i_{cap}(t) - i_L(t) = i_{c2}(t) - i_{cap}(t). \end{aligned} \qquad (2.78)$$

Hence, it is not necessary to measure the inductor and load currents. Only the current to the output capacitor must be measured.

Hiti and Borojevic (1993) use the measured load current to modify the current-mode control for the boost converter. The modification is made in such a way that the dc gain of the closed middle loop in Figure 2.33 (i.e. the dc gain of the transfer function that describes how $v_o(t)$ is affected by $i_{c2}(t)$) is independent of the load. The modification turns out to be the same as the one presented for the boost converter by Redl and Sokal (1986), i.e. (2.75).

Feedforward and Gain Scheduling

Two concepts in control theory, feedforward and gain scheduling, will be needed in some of the next subsections and are therefore reviewed in this subsection.
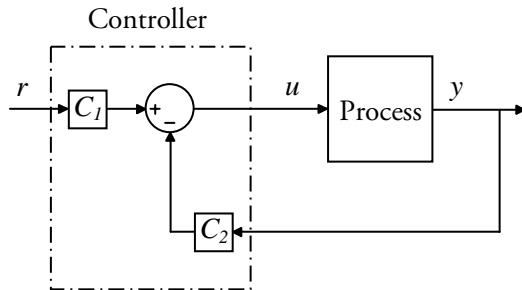
Figure 2.34: The basic configuration of the controller.

Figure 2.34 shows the configuration of the controller used as a base here. The control signal of the controller is called u and controls the input signal of the process that should be controlled. The output signal of the process is called y and it is fed back to the controller. The reference signal of the controller is called r. The controller is very general since the compensators C_1 and C_2 can be chosen independently.

The definition of feedforward is that a disturbance signal is measured and used to make a change in the control signal before the disturbance has caused any change in the output of the process (Åström and Hägglund, 1995, Section 7.3). Figure 2.35 shows an example where the controller in Figure 2.34 is extended to also include feedforward. The disturbance signal is called v and it is multiplied with C_{ff} to obtain the contribution to the control signal from the feedforward part. Feedforward does not cause any stability problems (Åström and Hägglund, 1995, Section 7.3). A consequence of this is that, for linear systems, feedforward does not affect the loop gain.

A definition of gain scheduling is found in Åström and Wittenmark (1995, Chapter 9). If the operating conditions of a process vary with time and the controller that controls the process is time invariant, the dynamics of the closed loop system also vary with time. Assume that some variables that reflect the operating conditions of a process are measured. If these variables are used to change the values of the parameters in the controller, it should be possible to reduce the influence of changed operating conditions on the dynamics of the closed loop system. This method is called gain scheduling and an example is shown in Figure 2.36. P_{cal} is a time-varying parameter in the controller. It is calculated by using the gain schedule and the scheduling variables, which
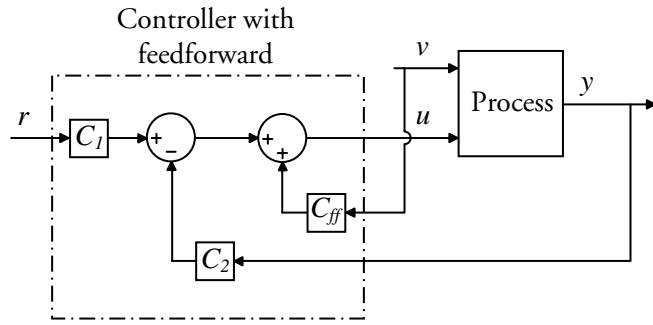
Figure 2.35: A controller with feedforward.
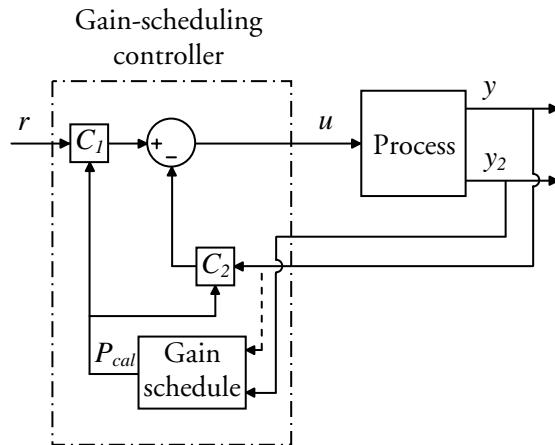
Figure 2.36: A gain-scheduling controller.

are the input signals to the gain schedule. The scheduling variables should reflect the operating conditions of the process. The signal y_2 is an extra output of the process that is measured and used as a scheduling variable. The signal y that is measured and fed back to the original controller could also be used as a scheduling variable if it reflects the operating conditions of the process in some way.
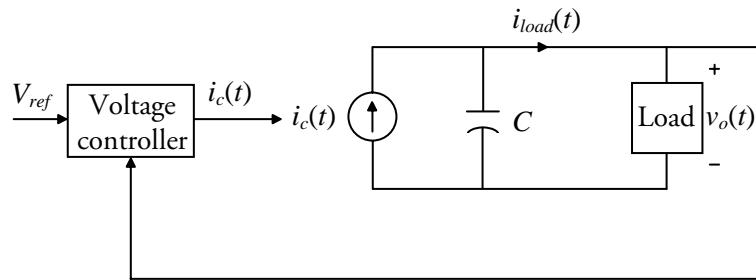
Figure 2.37: A simple model of the buck converter with current-mode control.
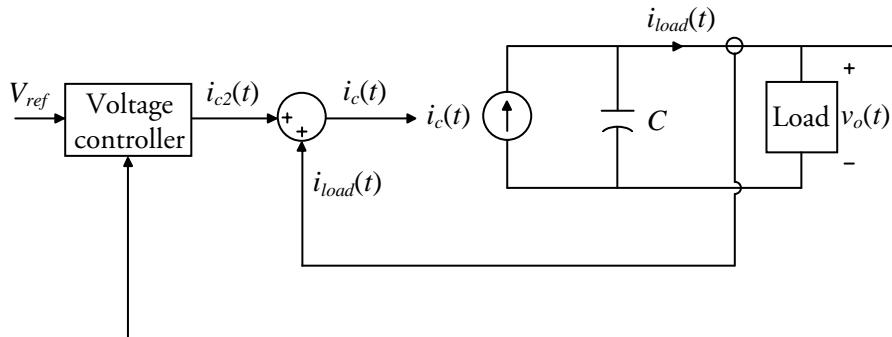
Figure 2.38: The measured load current affects the control signal.

Low Output Impedance

In this subsection, the output impedance obtained when using measured load current for control is analyzed by using a simple model of the buck converter with current-mode control.

The current through the inductor is controlled in current-mode control. If this control has high bandwidth, the inductor can be approximated by a controlled current source. The buck converter with current-mode control can then be modeled as in Figure 2.37 (compare Figure 2.37 and Figure 1.2). The current from the current source is equal to the reference signal for the current controller, $i_c(t)$. The ESR of the capacitor is neglected in Figure 2.37.

Figure 2.38 shows how the measured load current should be used to control the buck converter according to (2.74). If $i_{load}(t)$ changes, $i_c(t)$ changes by the same amount, provided that $i_{c2}(t)$ is constant. Consequently, the capacitor current does not change. The conclusion is that changes in load current do not affect the output voltage, that is, the output impedance is zero:

$$Z_{out}(s) = -\frac{v_o(s)}{i_{load}(s)} = 0 . \tag{2.79}$$

Note that the definition of output impedance used in (2.79) is not the same as the one used previously (e.g. (2.13)).

An Almost Invariant Control-to-Output Transfer Function for Different Loads

In this subsection, the control-to-output transfer function that describes how $i_{c2}(t)$ affects $v_o(t)$ is analyzed by using the simple model. Two different types of loads are considered. The first type is a current source, i.e. the load current is independent of the output voltage. The second type is a linear resistive load.

First assume that the load is a current source. If the load current is not used, $i_c(t)$ is equal to $i_{c2}(t)$ and the output voltage is

$$v_o(s) = \frac{1}{sC}\big(i_{c2}(s) - i_{load}(s)\big). \tag{2.80}$$

Since $i_{load}(t)$ is determined by the current source, it can be regarded as an input signal in addition to $i_{c2}(t)$. The control-to-output transfer function that describes how $i_{c2}(t)$ affects $v_o(t)$ is therefore obtained if $i_{load}(t)$ is set to zero:

$$G_{v_o i_{c2}}(s) = \frac{v_o(s)}{i_{c2}(s)}\bigg|_{i_{load}(s)=0} = \frac{1}{sC} . \tag{2.81}$$

If the load current is used, $i_c(t)$ is given by (2.74) and the output voltage is

$$v_o(s) = \frac{1}{sC}\big(i_c(s) - i_{load}(s)\big) =$$

$$\frac{1}{sC}\big(i_{c2}(s) + i_{load}(s) - i_{load}(s)\big) = \frac{1}{sC} i_{c2}(s) \tag{2.82}$$

and $G_{v_o i_{c2}}(s)$ is

$$G_{v_o i_{c2}}(s) = \frac{v_o(s)}{i_{c2}(s)} = \frac{1}{sC}. \tag{2.83}$$

It is seen from (2.81) and (2.83) that the control-to-output transfer function $G_{v_o i_{c2}}(s)$ does not change when the measured load current is introduced for control. Therefore, the loop gain and the stability properties do not change. Since the load current does not depend on the states of the converter, it can be seen as a disturbance signal. The conclusion is that the use of measured load current for control is feedforward in the case where the load is a current source.

Now assume that the load is a resistor with resistance R. If the load current is not used, $G_{v_o i_{c2}}(s)$ is

$$G_{v_o i_{c2}}(s) = \frac{v_o(s)}{i_{c2}(s)} = \frac{R\dfrac{1}{sC}}{R + \dfrac{1}{sC}}. \tag{2.84}$$

If the load current is used, the output voltage is given by (2.82) and $G_{v_o i_{c2}}(s)$ is given by (2.83). It is seen from (2.84) and (2.83) that $G_{v_o i_{c2}}(s)$ changes from the impedance of the parallel of the capacitor and resistor to just the impedance of the capacitor when the measured load current is introduced for control. Since R is not present in (2.83), the use of the load current makes the control-to-output transfer function $G_{v_o i_{c2}}(s)$ invariant for different values of R, i.e. different linear resistive loads.

If the load is a resistor and the measured load current is introduced for control, the control-to-output transfer function $G_{v_o i_{c2}}(s)$ changes, as shown above, and can also become unstable, as will be shown in the next subsection. The conclusion is that the use of measured load current for control is not
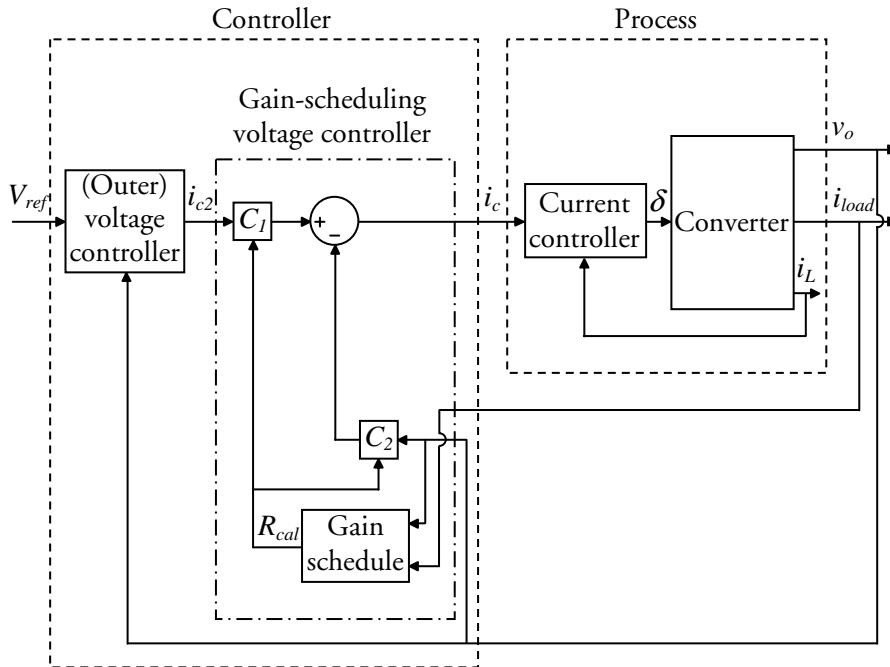
Figure 2.39: A configuration of the controller where the gain-scheduling property is emphasized.

feedforward in the case where the load is a resistor. It can instead be seen as gain scheduling, as now will be shown. Figure 2.39 is a modified version of Figure 2.33. The closed inner loop in Figure 2.33 is regarded as the process to be controlled in Figure 2.39. The controller in Figure 2.39 controls the input signal of the process, $i_c(t)$. The output signals of the process, $v_o(t)$ and $i_{load}(t)$, are measured and used by the controller. The controller consists of two voltage controllers in cascade: an outer voltage controller and a gain-scheduling voltage controller. The outer voltage controller then controls a "process" which is the closed loop of the gain-scheduling voltage controller and the process. Assume that the gain-scheduling voltage controller is designed just to make this "process" invariant for different linear resistive loads. Assume further that the outer voltage controller is designed thereafter to obtain the wanted properties of the whole closed loop system. If the designed gain-scheduling voltage controller is

$$C_1(t) = 1, \tag{2.85}$$

$$C_2(t) = \frac{-1}{R_{cal}(t)}, \tag{2.86}$$

$$R_{cal}(t) = \frac{v_o(t)}{i_{load}(t)}, \tag{2.87}$$

then the control signal is

$$i_c(t) = C_1(t)i_{c2}(t) - C_2(t)v_o(t) = i_{c2}(t) + \frac{1}{R_{cal}(t)}v_o(t) =$$

$$i_{c2}(t) + \frac{1}{\dfrac{v_o(t)}{i_{load}(t)}}v_o(t) = i_{c2}(t) + i_{load}(t). \tag{2.88}$$

Hence, the gain-scheduling voltage controller is exactly the same as the middle controller in Figure 2.33 for the buck converter, i.e. (2.74). The use of measured load current for control can therefore be seen as gain scheduling.

It was shown previously that the control-to-output transfer function $G_{v_o i_{c2}}(s)$ is invariant for different linear resistive loads if (2.74) is used. The designed gain-scheduling voltage controller, (2.85)-(2.87), is therefore reasonable since it is equivalent to (2.74) and the purpose was to obtain invariance for different linear resistive loads.

By using the simple model in Figure 2.37, the following description of the process in Figure 2.39 is obtained in the case where the load is a resistor:

$$G_{v_o i_c}(s) = \frac{v_o(s)}{i_c(s)} = \frac{R\dfrac{1}{sC}}{R + \dfrac{1}{sC}}, \tag{2.89}$$

$$i_{load}(s) = \frac{v_o(s)}{R}. \tag{2.90}$$

This is a first order system and the most natural choice for the state variable is the voltage across the capacitor, which is the same as the output voltage, $v_o(t)$. $v_o(t)$ and $i_{load}(t)$ are both measurements of this state, where the latter one is scaled by the factor $1/R$. If the controller knows the value of R, it will control the process equally well with only $i_{load}(t)$ measured compared to if only $v_o(t)$ is measured.

That both signals are measured and used by the controller is in the above gain-scheduling approach interpreted as follows. $v_o(t)$ is a measurement of the state and is fed back to the controller. The controller shall try to control the process such that $v_o(t)$ is equal to reference signal V_{ref} and it is therefore a voltage controller. The value of the load resistance, R, will be a parameter in the voltage controller. The operating conditions of the process vary with time since the load resistance varies. To reduce the influence of the changed dynamics of the process, the parameter R in the controller is replaced by the time-varying parameter $R_{cal}(t)$. It should be an estimate of the load resistance. To be able to calculate this estimate, an extra variable that reflects the operating conditions of a process must be measured and it is the load current, $i_{load}(t)$. An estimate of the load resistance can now be calculated with the gain schedule (2.87). $i_{load}(t)$ and also $v_o(t)$ are used as scheduling variables. The calculated estimate, $R_{cal}(t)$, is equal to the load resistance, R, if there are no measurement errors.

An alternative interpretation of that $v_o(t)$ and $i_{load}(t)$ are both measured, is that it is the output power, $v_o(t)i_{load}(t)$, that is measured and used to control the input power (Hiti and Borojevic, 1993).

Schoneman and Mitchell (1989) use a load consisting of both a resistor and a current source. The load current is in this case dependent of the output voltage. The authors say that the load current is fed forward, but this is thus not correct, strictly speaking. They also claim that the "feedforward" does not affect the loop gain. The reason for this erroneous conclusion is that the authors at a point in the derivation neglect the changes of the current through the resistor.

Risk of Instability

From Figure 2.38, it is seen that there is positive feedback in the load current loop. This indicates that there can be a problem with the stability in the case where the load is a resistor. To investigate the stability, Figure 2.38 is generalized to obtain Figure 2.40, where the gain in the measurement of the
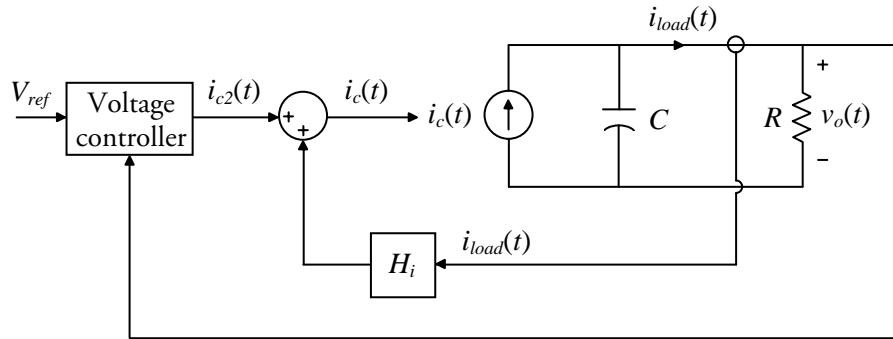
Figure 2.40: A measurement gain, H_i, is introduced for the load current.

load current is H_i. In a real system, H_i is not exactly equal to 1, but the measurement can be made such that H_i is close to 1. The output voltage is

$$v_o(s) = \frac{1}{sC}\left(i_c(s) - i_{load}(s)\right) = \frac{1}{sC}\left(i_{c2}(s) + H_i\frac{v_o(s)}{R} - \frac{v_o(s)}{R}\right). \quad (2.91)$$

Hence, the control-to-output transfer function $G_{v_o i_{c2}}(s)$ is

$$G_{v_o i_{c2}}(s) = \frac{v_o(s)}{i_{c2}(s)} = \frac{\dfrac{1}{sC}}{1 - \dfrac{1}{sRC}(H_i - 1)} = \frac{1}{C\left(s + (1 - H_i)\dfrac{1}{RC}\right)}. \quad (2.92)$$

$G_{v_o i_{c2}}(s)$ has a pole at

$$p_1 = -(1 - H_i)\frac{1}{RC}. \quad (2.93)$$

If $H_i > 1$, the system is unstable since the pole is in the right half plane in the complex s-plane. If $H_i = 1$, the system has a pole in the origin and the system acts as an integrator. If $H_i < 1$, the system is stable and the dc gain is $R/(1 - H_i)$, i.e. very high if H_i is close to 1. The conclusion of all this is that it is difficult or impossible to obtain a specific output voltage by

manually setting a value for $i_{c2}(t)$ if H_i is close to 1. Instead, an outer voltage controller is used to set $i_{c2}(t)$ and the system can be stabilized.

Analysis Using Approximate Expressions

In Section 2.5, approximate expressions for the buck converter with current-mode control were presented. In this subsection, these expressions are used to analyze how the control-to-output transfer function, the output impedance and the audio susceptibility are affected when using load current measurements to control the converter. The results are also compared with simulation results.

To make the analysis in this subsection general, a transfer function, $H_i(s)$, is introduced in (2.74):
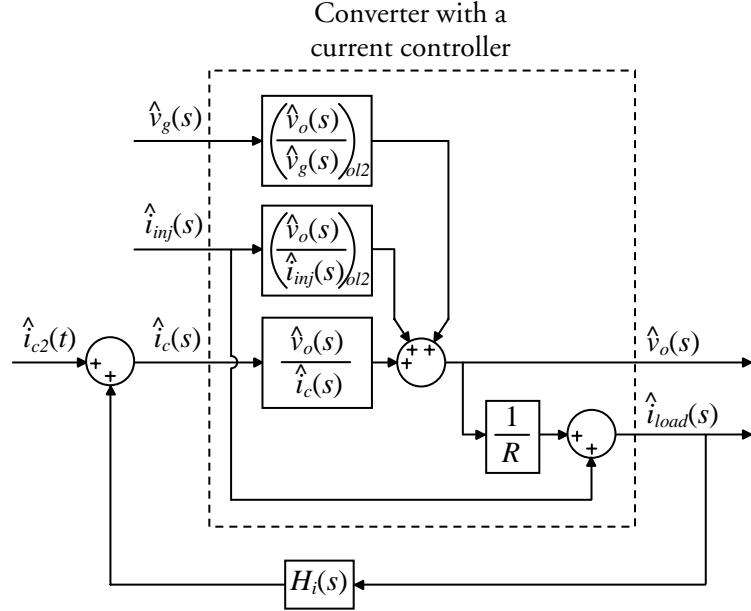
$$\hat{i}_c(s) = \hat{i}_{c2}(s) + H_i(s)\hat{i}_{load}(s). \tag{2.94}$$

$H_i(s)$ can represent the dynamics of a filter, which filters the signal from the load-current sensor, and also the sensor itself. From Figure 2.6, it is seen that the load current is

$$i_{load}(t) = \frac{v_o(t)}{R} + i_{inj}(t). \tag{2.95}$$

Figure 2.41 shows the system obtained by using (2.94) and (2.95). In Section 2.4, the subscript ol was introduced to denote the converter transfer functions, i.e. the open loop system. This system is controlled by changing the duty cycle of $\delta(t)$. If the inductor current is fed back, a new system is obtained which is controlled by changing $i_c(t)$. The transfer functions for this new system will be denoted with the subscript $ol2$. However, it is not used for the control-to-output transfer function since there is no risk of confusion in that case. Since linear models are used, the output voltage is obtained by adding the contribution from each input signal as shown in Figure 2.41.

By using (2.69)-(2.71) and Figure 2.41 the following results are obtained for the three major transfer functions:

Figure 2.41: The system obtained when using $H_i(s)$ in the control law.

$$G_{v_o i_{c2}}(s) = \frac{\hat{v}_o(s)}{\hat{i}_{c2}(s)} =$$

$$\frac{F_{ESR}(s)F_h(s)}{C\left(s + (1 - F_{ESR}(s)F_h(s)H_i(s))\frac{1}{RC} + \frac{T_s}{LC}(m_c D' - 0.5)\right)}, \qquad (2.96)$$

$$Z_{out}(s) = \frac{(1 - F_h(s)H_i(s))F_{ESR}(s)}{C\left(s + (1 - F_{ESR}(s)F_h(s)H_i(s))\frac{1}{RC} + \frac{T_s}{LC}(m_c D' - 0.5)\right)}, \qquad (2.97)$$

$$\frac{\hat{v}_o(s)}{\hat{v}_g(s)} = \frac{\frac{T_s D}{L}(m_c D' - F_f(s))F_{ESR}(s)F_h(s)}{C\left(s + (1 - F_{ESR}(s)F_h(s)H_i(s))\frac{1}{RC} + \frac{T_s}{LC}(m_c D' - 0.5)\right)}, \qquad (2.98)$$

where $F_{ESR}(s)$ is defined in (2.73) and $F_h(s)$ is defined in (2.23). $F_f(s)$ is in this subsection a Taylor polynomial of degree 2 of $F_f(s)$ in (2.57).

The control-to-output transfer function (2.96) is first considered. A new variable, $F(s)$, is introduced:

$$F(s) = F_{ESR}(s)F_h(s). \qquad (2.99)$$

The load resistance, R, shows up only at one place in (2.96) and the more $H_i(s)$ is in accordance with $1/F(s)$, the closer invariance for different loads is the control-to-output transfer function. $1/F(s)$ is approximately equal to 1 at low frequencies since both $F_{ESR}(s)$ and $F_h(s)$ are approximately equal to 1 at low frequencies. If (2.74) is used, i.e. $H_i(s)$ is equal to 1, the control-to-output transfer function is almost invariant for different loads at low frequencies. It can be shown that the absolute value of the second term is much smaller than the absolute value of the first term, s, in the (largest) parenthesis in the denominator of (2.96) if $H_i(s)$ is equal to 1. This means that the control-to-output transfer function is almost invariant for different loads for all frequencies in the interval $[0, \omega_n]$. The conclusion is that there is not so much to gain by trying to get $H_i(s)$ in accordance with $1/F(s)$ compared to setting $H_i(s)$ equal to 1.

It is seen from (2.73) and (2.23) that $F_{ESR}(s)$ has one high-frequency zero and $F_h(s)$ has two high-frequency poles. If $H_i(s)$ is equal to 0, i.e. the measured load current is not used in the control law, the low-frequency pole in (2.96) is

$$p_1 = -\left(\frac{1}{RC} + \frac{T_s}{LC}\left(m_c D'-0.5\right) \right). \qquad (2.100)$$

If $H_i(s)$ is equal to 1, i.e. the control law (2.74) is used, the low-frequency pole in (2.96) is approximately

$$p_1 \approx -\frac{T_s}{LC}\left(m_c D'-0.5\right). \qquad (2.101)$$

The results obtained here for the position of the low-frequency pole are compared with the results obtained in the previous subsection where a simple model was used. According to (2.93), the pole moves from $-1/(RC)$ to the origin if H_i is increases from 0 to 1. The pole moves into the right half plane

in the complex s-plane if H_i increases further and the system becomes unstable. From (2.100) and (2.101), it is seen that the position of the low-frequency pole is shifted approximately $T_s(m_c D'-0.5)/(LC)$ to the left in the s-plane compared to the position of the pole in the simple model. A greater $H_i(s)$ is therefore needed to obtain instability according to the model used in this subsection compared to what is needed according to the simple model.

It is seen from (2.96) that the dc gain is approximately inversely proportional to the distance between the low-frequency pole and the origin. Therefore, the dc gain approximately increases by the same degree as the first (lowest) corner frequency decreases if $H_i(s)$ is changed from 0 to 1.

Figure 2.42 shows the Bode plot for $G_{v_o i_{c2}}(s)$ in (2.96) when different $H_i(s)$ and loads, $R_{\min}=1$ Ω and $R_{\max}=4$ Ω, are used. Except for R, the parameter values shown in Table 2.1 are used. m_c is set to 2. From the figure it is seen that for $H_i(s)=0$, the gain and phase shift changes considerably for different loads. For $H_i(s)=1$, the gain and phase shift is almost invariant for different loads. Simulation results are also plotted in Figure 2.42 and they are in good agreement with (2.96). An extended version of the simulation model in Figure 2.18 is used.

Previously in this subsection, we concluded from (2.96) that the more $H_i(s)$ is in accordance with $1/F(s)$, the closer invariance for different loads is the control-to-output transfer function. Simulation results have showed that when $H_i(s)$ is set to $1/F(s)$ in series with a second order Butterworth low-pass filter with corner frequency at the switching frequency, the transfer function is closer to invariance for different loads than when $H_i(s)$ is set equal to 1. This is in accordance with the conclusion.

According to (2.96), $H_i(s)$ should be equal to $1/F(s)$ to obtain invariance for different loads. It will now be shown that this result also can be obtained by applying gain scheduling. Assume that the only goal with the gain scheduling controller is to make the closed loop invariant for different loads and an outer controller is designed later to control the output voltage (see Figure 2.39).

The first step in designing the gain scheduling controller is to design a controller as if the resistance of the load is constant and known. This controller is here designed by using model matching (Chen, 1999, Section 9.3), which is similar to pole placement but the zeros are also placed. The process to be controlled is $G_{v_o i_c}(s)$ and it has one zero and three poles according to (2.69). The position of the zero associated with $F_{ESR}(s)$ does not depend on R. The same is true for the two high-frequency poles
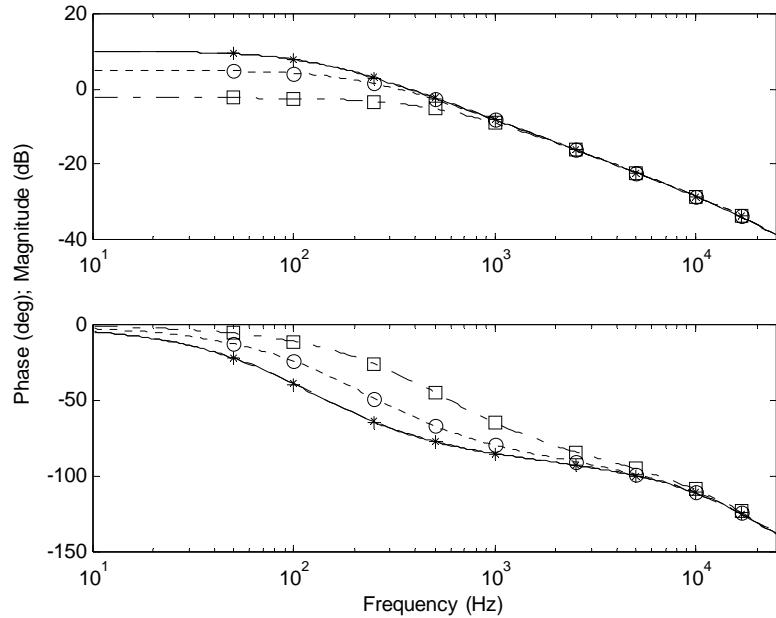
Figure 2.42: The control-to-output transfer function of a buck converter controlled by (2.94). Symbol for simulation result is in parenthesis. Dash-dotted line ($\square$): $H_i(s) = 0$ and $R = R_{min}$. Dotted line (O): $H_i(s) = 0$ and $R = R_{max}$. Solid line (+): $H_i(s) = 1$ and $R = R_{min}$. Dashed line (x): $H_i(s) = 1$ and $R = R_{max}$. Note that the two last mentioned lines almost coincide.

connected with $F_h(s)$. However, the position of the low-frequency pole, p_1, connected with $F_l(s)$ and the dc gain of $G_{v_o i_c}(s)$ depend on R.

The expressions for the dc gain and the position of all the poles and zeros of the closed loop system $G_{v_o i_{c2}}(s)$ should be independent of R. Since this is the only goal with the controller, the dc gain and the positions are chosen such that the expression of the controller is simple. Two poles and a zero are therefore placed at the same position as the two high-frequency poles and the zero in $G_{v_o i_c}(s)$. It turns out that it is suitable to place the last pole at

$$p_{1n} = -\frac{T_s}{LC}\left(m_c D' - 0.5\right) \qquad (2.102)$$

and to choose the dc gain $-1/(Cp_{1n})$. With these choices, the controller is

$$\hat{i}_c(s) = \hat{i}_{c2}(s) - \frac{-1}{F(s)R}\hat{v}_o(s), \qquad (2.103)$$

where $F(s)$ is defined in (2.99).

The second step in designing the gain scheduling controller is to replace the parameter R in the control law (2.103) with the time-varying parameter $R_{cal}(t)$ defined in (2.87) and the result is

$$\hat{i}_c(s) = \hat{i}_{c2}(s) - \frac{-1}{F(s)R_{cal}(s)}\hat{v}_o(s) = \hat{i}_{c2}(s) + \frac{1}{F(s)}\hat{i}_{load}(s). \qquad (2.104)$$

By comparing (2.104) and (2.94), it is concluded that $H_i(s)$ should be equal to $1/F(s)$ to obtain invariance for different loads. It has now been shown that this result could be obtained by applying gain scheduling. Note that if $H_i(s)$ is equal to $1/F(s)$ in (2.96), then the dc gain and the low-frequency pole in (2.96) are exactly the same as the choices made above in the model matching design.

The output impedance (2.97) is now considered. Note that the denominator is exactly the same as in (2.96) and that the numerator is independent of R. The conclusions about invariance of R for the control-to-output transfer function are therefore also valid in this case. From (2.97), it is seen that the more $H_i(s)$ is in accordance with $1/F_h(s)$, the lower is the output impedance. $1/F_h(s)$ is approximately equal to 1 at low frequencies. If (2.74) is used, i.e. $H_i(s)$ is equal to 1, the output impedance will be low at low frequencies.

Figure 2.43 shows the Bode plot for the output impedance in (2.97) when different $H_i(s)$ and loads are used. The parameter values used for the control-to-output transfer function are also used here. From the figure it is seen that for $H_i(s) = 0$, the output impedance is high at low frequencies. When $H_i(s)$ is changed to 1, the output impedance is reduced at low frequencies and it becomes almost invariant for different loads. Simulation results are also plotted in Figure 2.43 and they are in good agreement with
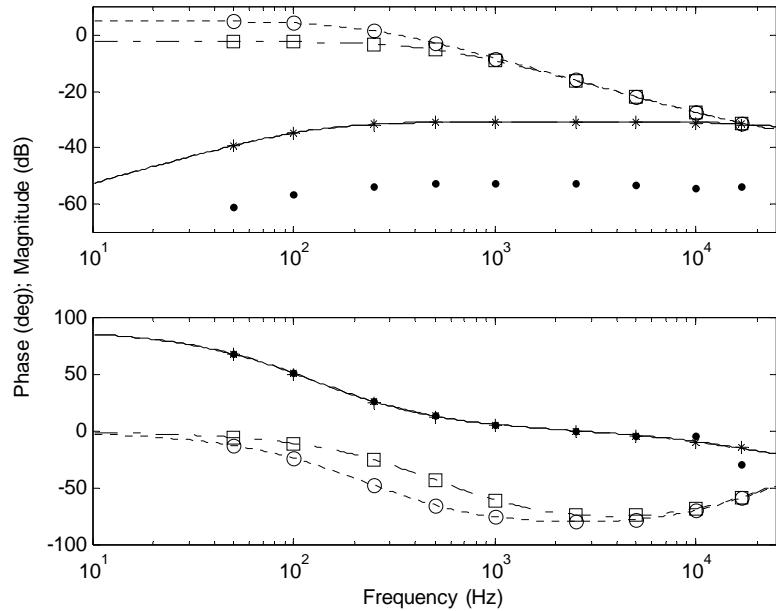
Figure 2.43: The output impedance of a buck converter controlled by (2.94).
Dash-dotted line ($\square$): $H_i(s) = 0$ and $R = R_{\min}$. Dotted line (O):
$H_i(s) = 0$ and $R = R_{\max}$. Solid line (+): $H_i(s) = 1$ and
$R = R_{\min}$. Dashed line (x): $H_i(s) = 1$ and $R = R_{\max}$. Note that
the two last mentioned lines almost coincide. Points: Simulation
with $R = R_{\max}$ and $H_i(s)$ equal to $1/F_h(s)$ in series with a
second order filter.

(2.97). When $H_i(s)$ is changed to $1/F_h(s)$ in series with a second order
Butterworth low-pass filter with corner frequency at five times the switching
frequency, simulation results show (see Figure 2.43) that the output
impedance is further decreased by approximately 20 dB for all the tested
frequencies. Note that (2.97) is not valid for frequencies over half the
switching frequency. Therefore, it cannot be used to predict what happens
when there is a step change in the load, since the load current in this case
consists of frequency components that are also over half the switching
frequency.
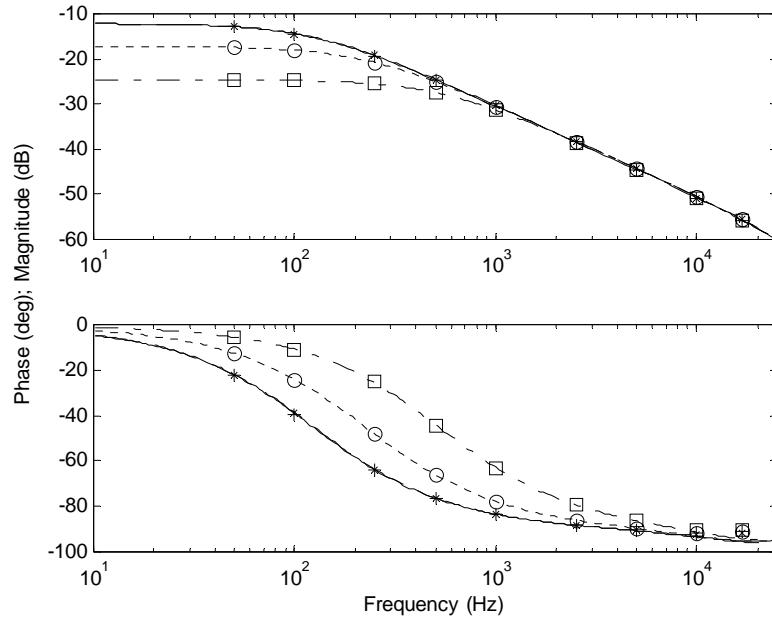
Figure 2.44: The audio susceptibility of a buck converter controlled by (2.94). Dash-dotted line ($\square$): $H_i(s)=0$ and $R=R_{\min}$. Dotted line (O): $H_i(s)=0$ and $R=R_{\max}$. Solid line (+): $H_i(s)=1$ and $R=R_{\min}$. Dashed line (x): $H_i(s)=1$ and $R=R_{\max}$. Note that the two last mentioned lines almost coincide.

Finally, the audio susceptibility (2.98) is considered. Note that the denominator is exactly the same as in (2.96) and that the numerator is independent of R. The conclusions about invariance of R for the control-to-output transfer function are therefore also valid in this case. According to Section 2.4, it is possible to choose m_c such that the audio susceptibility is very small at dc. This ability still remains in the case where the control law (2.94) is used since the expression $m_c D' - F_f(s)$ in (2.71) also is present in the numerator of (2.98).

Figure 2.44 shows the Bode plot for the audio susceptibility in (2.98) when different $H_i(s)$ and loads are used. The parameter values used for the control-to-output transfer function are also used here. From the figure it is seen that for $H_i(s)=0$, the gain changes considerably for different loads. For

$H_i(s) = 1$, the gain is almost invariant for different loads. Simulation results are also plotted in Figure 2.44 and they are in good agreement with (2.98).

In the case where a linearized version of (2.75) is used to control a boost converter, the control-to-output transfer function, the output impedance, and the audio susceptibility are found in Johansson (2003, Section 7.5, Equations 7.122, 7.151, and 7.156). The corresponding results for the buck-boost converter are found in Johansson (2003, Section 7.6, Equations 7.187, 7.192, and 7.198). For boost and buck-boost converters, it is not possible to obtain invariance for different loads at high frequencies due to the presence of zeros in the right half plane of the complex s-plane.

2.8   Summary and Concluding Remarks

This section explains which major models were obtained and how they were derived. The main conclusions are also presented. However, the method used to verify the obtained models is first explained.

Verification

Evaluation of a converter by means of a network analyzer is common and this is one of the reasons for the interest in models that can predict the frequency functions.

To verify the derived small-signal models, the frequency functions predicted by them were compared with simulation results. Switched (large-signal) simulation models were utilized and the output voltage then consists of several Fourier components. To obtain the frequency function, one frequency at the time was evaluated. A sinusoidal signal with frequency ω_m was injected and only the Fourier component with frequency ω_m in the output voltage was considered. A network analyzer also just considers this Fourier component.

The control signal can be considered to be sampled with the switching frequency. The frequency functions were therefore only evaluated for the frequency interval dc to half the switching frequency.

State-Space averaging

State-space averaging was used to derive a linear continuous-time time-invariant model for the buck converter. The control-to-output transfer function, the output impedance, and the audio susceptibility were extracted

from this model. We concluded that these transfer functions are in good agreement with the simulation results.

Current-Mode Control

The Ridley and Tan models were applied to the buck converter with current-mode control. We concluded that the obtained control-to-output transfer functions and the output impedances are in good agreement with the simulation results but the obtained audio susceptibility is not.

The high-frequency extensions in the Ridley and Tan models are based on an accurate control-to-current transfer function, which is derived with the assumption that the changes in the input and output voltages are negligible. The actual changes in the input and output voltages are in the Ridley and Tan models taken into consideration by including two feedforward gains, k_f and k_r. These gains are designed such that the dc gain should be correct. This design results in modeling errors, especially for the audio susceptibility at high frequencies. The reason is that the amplitude of the perturbation in the input voltage does not decrease at high frequencies since the injection signal from the network analyzer affects the input voltage directly. However, when the control-to-output transfer function and the output impedance are considered, the input voltage is not affected and the changes in the output voltage is negligible at high frequencies due to the low-pass character of the output filter of the converters.

A Novel Model

A novel model for the audio susceptibility of converters with current-mode control was derived by treating the changes in the input and output voltages in a more refined way. The novel model was applied to the buck converter. We concluded that the obtained audio susceptibility is in good agreement with simulation results.

Improved Models

The novel model was used to improve the Ridley and Tan models. The feedforward gains k_f were changed such that the two models became equal to the novel model.

Approximations of Obtained Expressions

The control-to-output transfer function, the output impedance, and the audio susceptibility obtained from the improved Ridley model were approximated. To be able to do this, several assumptions were introduced.

Using Load Current for Control

The output voltage and the inductor current are measured in the case where current-mode control is used. Some properties that can be obtained when the controller also uses load current measurements were analyzed. The control-to-output transfer function, the output impedance, and the audio susceptibility were derived for the buck converter. The main conclusions are presented here.

1. The analysis confirms that low output impedance can be obtained.

2. The analysis shows that in the case where the load is a current source the following properties are obtained:
    *   The use of measured load current for control is feedforward.
    *   The control-to-output transfer function does not change when this feedforward is introduced.

3. The analysis shows that in the case where the load is a linear resistor, the following properties are obtained:
    *   The control-to-output transfer function can change when the measured load current is introduced for control.
    *   The converter can become unstable when the measured load current is introduced for control.
    *   The control-to-output transfer function can be almost invariant for different linear resistive loads if the measured load current is used for control.
    *   The use of measured load current for control is not feedforward. It can instead be seen as gain scheduling.

The derived approximate expressions were used as a starting point when expressions were derived for the closed loop system where the load current is used for control. This is not the best way to derive reliable expressions. Instead, the non-approximate expressions should have been used as a starting

point and the derived expressions for the closed loop system should have been approximated afterwards.

Chapter 3 Model   Including Stray Resistances

If the frequency functions predicted by the transfer functions for the buck converter derived in the licentiate thesis, Johansson (2003), are compared with experimental results obtained by means of a network analyzer, it is found that there is a large difference in one case. The transfer function for the output impedance does not predict the experimental results at low frequencies when the measured load current is utilized for control. The reason for the difference is that the stray resistances in the inductor, transistor, and diode were not considered in the licentiate thesis. In this chapter a new transfer function for the output impedance is derived where the stray resistances are considered. It will be compared with experimental results in Chapter 4.

3.1   Introduction

Figure 2.1 shows the circuit of the buck converter that is used in the licentiate thesis. Only one non-ideality is considered and it is the ESR of the capacitor, R_c. Figure 3.1 shows the circuit of the buck converter that is used in this chapter to derive a new transfer function for the output impedance. Three stray resistances are added compared to the circuit in Figure 2.1. It is the resistance in the inductor, R_L, the resistance in the transistor while it operates in the on state, R_t, and the resistance in the diode while it conducts, R_d. The inductor, transistor, and diode are each modeled as an ideal component in series with an ideal resistor.

The methodology used in the derivation is analogous to the one used in the licentiate thesis. In Section 3.2, state-space averaging is used to derive a model of the buck converter. In Section 3.3, the Ridley model is used to obtain a model of the buck converter with current-mode control. The output
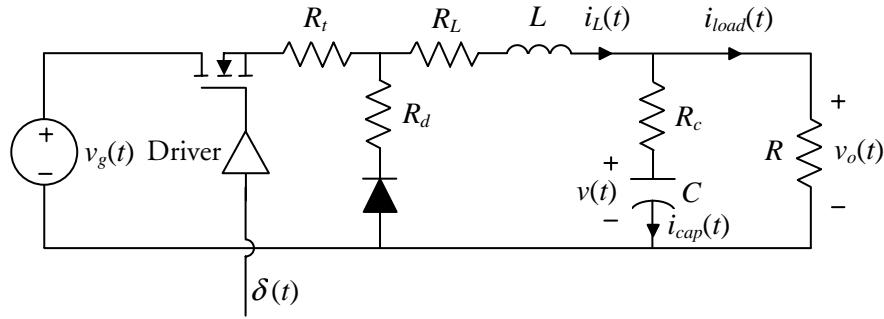
Figure 3.1: The circuit of the buck converter where stray resistances are included.

impedance for the case where the measured load current is utilized for control is derived in Section 3.4. A summary and concluding remarks are presented in Section 3.5.
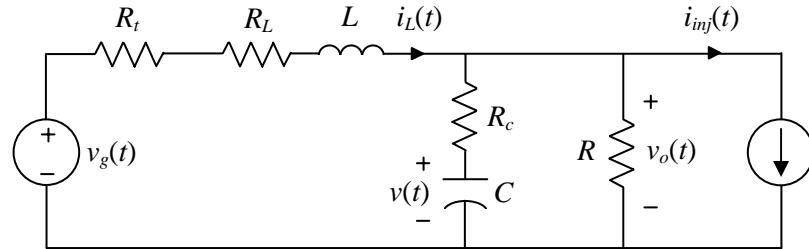
3.2   State-Space Averaging

In this section, a linear time-invariant model of the buck converter is derived by means of state-space averaging. The converter can be described as switching between different time-invariant systems and the state-space description of each one of these systems is first derived. These state-space descriptions are used as a starting point in the method of state-space averaging. This method is then applied to the buck converter and the result is a linear time-invariant model in state-space description. Finally, several transfer functions are extracted from this model.

State-Space Description for Each Time Interval

Since it is assumed that the converter is operated in continuous conduction mode, two different systems must be considered. The state-space description of each one of these two systems is derived in this subsection.

The circuit in Figure 3.2 is used as a model of the buck converter during t_{on} (compare Figure 3.2 and Figure 3.1). The transistor is on during t_{on} and is modeled with R_t. The diode does not conduct and is therefore removed. As in Figure 2.3, a current source is added and it injects the current $i_{inj}(t)$.

Figure 3.2: The circuit of the buck converter during t_{on}.

A new parameter, R_{on}, is introduced:

$$R_{on} = R_L + R_t .$$ (3.1)

From Figure 3.2, the following equations are obtained:

$$\frac{di_L(t)}{dt} = \frac{1}{L}\left(v_g(t) - R_{on}i_L(t) - v_o(t)\right),$$ (3.2)

$$\frac{dv(t)}{dt} = \frac{1}{C}\left(i_L(t) - \frac{v_o(t)}{R} - i_{inj}(t)\right),$$ (3.3)

$$v_o(t) = v(t) + R_c\left(i_L(t) - \frac{v_o(t)}{R} - i_{inj}(t)\right).$$ (3.4)

The circuit in Figure 3.2 is a second order system. Let $i_L(t)$ and $v(t)$ be chosen as the state variables. Regard $v_g(t)$ and $i_{inj}(t)$ as the input signals and $v_o(t)$ as the output signal. The following state-space system is obtained from (3.2)-(3.4) according to the appendix (Section 3.6):

$$\begin{cases} \dfrac{d\mathbf{x}(t)}{dt} = \mathbf{A_1}\mathbf{x}(t) + \mathbf{B_1}\mathbf{u}(t) \\ \mathbf{y}(t) = \mathbf{C_1}\mathbf{x}(t) + \mathbf{E_1}\mathbf{u}(t) \end{cases},$$ (3.5)

where

$$\mathbf{x}(t) = \begin{bmatrix} i_L(t) \\ v(t) \end{bmatrix}, \tag{3.6}$$

$$\mathbf{u}(t) = \begin{bmatrix} v_g(t) \\ i_{inj}(t) \end{bmatrix}, \tag{3.7}$$

$$\mathbf{y}(t) = v_o(t), \tag{3.8}$$

$$\mathbf{A_1} = \begin{bmatrix} -\dfrac{R_{on}}{L} - \dfrac{RR_c}{(R+R_c)L} & -\dfrac{R}{(R+R_c)L} \\[2mm] \dfrac{R}{(R+R_c)C} & -\dfrac{1}{(R+R_c)C} \end{bmatrix}, \tag{3.9}$$

$$\mathbf{B_1} = \begin{bmatrix} \dfrac{1}{L} & \dfrac{RR_c}{(R+R_c)L} \\[2mm] 0 & -\dfrac{R}{(R+R_c)C} \end{bmatrix}, \tag{3.10}$$

$$\mathbf{C_1} = \begin{bmatrix} \dfrac{RR_c}{R+R_c} & \dfrac{R}{R+R_c} \end{bmatrix}, \tag{3.11}$$
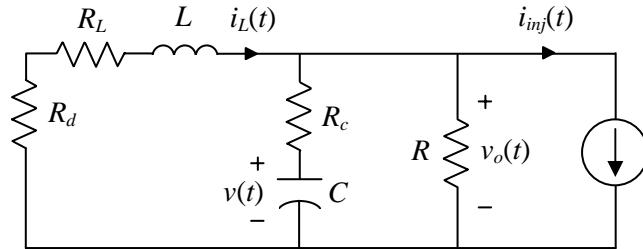
$$\mathbf{E_1} = \begin{bmatrix} 0 & -\dfrac{RR_c}{R+R_c} \end{bmatrix}. \tag{3.12}$$

The circuit in Figure 3.3 is used as a model of the buck converter during t_{off} (compare Figure 3.3 and Figure 3.1). The transistor is off during t_{off} and is therefore removed together with the input voltage source. The diode conducts and is modeled with the resistance R_d.

A new parameter, R_{off}, is introduced:

$$R_{off} = R_L + R_d . \tag{3.13}$$

The circuit in Figure 3.2 is the same as the circuit in Figure 3.3 if $v_g(t)$ is set

Figure 3.3: The circuit of the buck converter during t_{off} .

to zero and R_t is replaced by R_d . Therefore, a state-space model for the circuit in Figure 3.3 can be obtained by setting all the coefficients for $v_g(t)$ to zero and by replacing R_{on} with R_{off} in (3.5):

$$\begin{cases} \dfrac{d\mathbf{x}(t)}{dt} = \mathbf{A}_2\mathbf{x}(t) + \mathbf{B}_2\mathbf{u}(t) \\ \mathbf{y}(t) = \mathbf{C}_2\mathbf{x}(t) + \mathbf{E}_2\mathbf{u}(t) \end{cases} , \tag{3.14}$$

where

$$\mathbf{A}_2 = \begin{bmatrix} -\dfrac{R_{off}}{L} - \dfrac{RR_c}{(R+R_c)L} & -\dfrac{R}{(R+R_c)L} \\ \dfrac{R}{(R+R_c)C} & -\dfrac{1}{(R+R_c)C} \end{bmatrix}, \tag{3.15}$$

$$\mathbf{B}_2 = \begin{bmatrix} 0 & \dfrac{RR_c}{(R+R_c)L} \\ 0 & -\dfrac{R}{(R+R_c)C} \end{bmatrix}, \tag{3.16}$$

$$\mathbf{C}_2 = \mathbf{C}_1 , \tag{3.17}$$

$$\mathbf{E}_2 = \mathbf{E}_1 . \tag{3.18}$$

Applying State-Space Averaging

The method of state-space averaging is applied to the buck converter in this subsection.

A new parameter, R_a, is introduced:

$$R_a = DR_{on} + D'R_{off} \ .$$
(3.19)

where D' is defined in (2.15). R_a is the average stray resistance.

A dc model is first derived from (2.6) by setting $\hat{\mathbf{x}}(t)$, $\hat{\mathbf{u}}'(t)$, $\hat{\mathbf{y}}(t)$, and $d\mathbf{x}(t)/dt$ to zero:

$$\begin{cases} \mathbf{0} = \mathbf{A}\mathbf{X} + \mathbf{B}\mathbf{U} \\ \mathbf{Y} = \mathbf{C}\mathbf{X} + \mathbf{E}\mathbf{U} \end{cases} ,$$
(3.20)

where

$$\mathbf{A} = D\mathbf{A_1} + D'\mathbf{A_2} = \begin{bmatrix} -\dfrac{R_a}{L} - \dfrac{RR_c}{(R+R_c)L} & -\dfrac{R}{(R+R_c)L} \\ \dfrac{R}{(R+R_c)C} & -\dfrac{1}{(R+R_c)C} \end{bmatrix},$$
(3.21)

$$\mathbf{B} = D\mathbf{B_1} + D'\mathbf{B_2} = \begin{bmatrix} D\dfrac{1}{L} & \dfrac{RR_c}{(R+R_c)L} \\ 0 & -\dfrac{R}{(R+R_c)C} \end{bmatrix},$$
(3.22)

$$\mathbf{C} = D\mathbf{C_1} + D'\mathbf{C_2} = \begin{bmatrix} \dfrac{RR_c}{R+R_c} & \dfrac{R}{R+R_c} \end{bmatrix},$$
(3.23)

$$\mathbf{E} = D\mathbf{E_1} + D'\mathbf{E_2} = \begin{bmatrix} 0 & -\dfrac{RR_c}{R+R_c} \end{bmatrix}.$$
(3.24)

Assume that the dc value of $i_{inj}(t)$ is zero. The following equations are then obtained if (3.20) is expanded:

$$0 = -\frac{R_a}{L}I_L - \frac{RR_c}{(R+R_c)L}I_L - \frac{R}{(R+R_c)L}V + \frac{D}{L}V_g \ , \qquad (3.25)$$

$$0 = \frac{R}{(R+R_c)C}I_L - \frac{1}{(R+R_c)C}V \ , \qquad (3.26)$$

$$V_o = \frac{RR_c}{R+R_c}I_L + \frac{R}{R+R_c}V \ . \qquad (3.27)$$

(3.26) is simplified to:

$$V = RI_L \ . \qquad (3.28)$$

(3.28) is inserted into (3.27):

$$V_o = \frac{R_c}{R+R_c}V + \frac{R}{R+R_c}V = V \ . \qquad (3.29)$$

(3.28) is inserted in (3.25):

$$0 = -\frac{R_a}{R}V - \frac{R_c}{(R+R_c)}V - \frac{R}{(R+R_c)}V + DV_g \ , \qquad (3.30)$$

$$\frac{V}{V_g} = \frac{D}{1+R_a/R} \ . \qquad (3.31)$$

Finally, an ac model is derived from (2.6). According to Johansson (2003, Section 2.3), the following linear system is obtained if (2.6) is linearized:

$$\begin{cases} \dfrac{d\hat{\mathbf{x}}(t)}{dt} = \mathbf{A}\hat{\mathbf{x}}(t) + \mathbf{B'}\hat{\mathbf{u}}'(t) \\ \hat{\mathbf{y}}(t) = \mathbf{C}\hat{\mathbf{x}}(t) + \mathbf{E'}\hat{\mathbf{u}}'(t) \end{cases} \ , \qquad (3.32)$$

where

$$\mathbf{B'} = \begin{bmatrix} \mathbf{B} & \mathbf{B_d} \end{bmatrix}, \tag{3.33}$$

$$\mathbf{E'} = \begin{bmatrix} \mathbf{E} & \mathbf{E_d} \end{bmatrix}, \tag{3.34}$$

$$\mathbf{B_d} = (\mathbf{A_1} - \mathbf{A_2})\mathbf{X} + (\mathbf{B_1} - \mathbf{B_2})\mathbf{U}, \tag{3.35}$$

$$\mathbf{E_d} = (\mathbf{C_1} - \mathbf{C_2})\mathbf{X} + (\mathbf{E_1} - \mathbf{E_2})\mathbf{U}. \tag{3.36}$$

(3.35) and (3.36) are expanded and written on an explicit form:

$$\mathbf{B_d} = \begin{bmatrix} \dfrac{R_{off} - R_{on}}{L} & 0 \\ 0 & 0 \end{bmatrix} \mathbf{X} + \begin{bmatrix} \dfrac{1}{L} & 0 \\ 0 & 0 \end{bmatrix} \mathbf{U} = \begin{bmatrix} \dfrac{(R_{off} - R_{on})I_L + V_g}{L} \\ 0 \end{bmatrix}, \quad (3.37)$$

$$\mathbf{E_d} = \mathbf{0X} + \mathbf{0U} = 0. \tag{3.38}$$

One expression in (3.37) is rewritten by using (3.28), (3.31), (3.19), and (2.15):

$$(R_{off} - R_{on})I_L + V_g = (R_{off} - R_{on})\frac{V_g D}{R(1 + R_a/R)} + V_g =$$

$$V_g \left(\frac{DR_{off} - DR_{on}}{R + R_a} + 1 \right) = \tag{3.39}$$

$$V_g \frac{DR_{off} - DR_{on} + R + DR_{on} + D'R_{off}}{R + R_a} = V_g \frac{R + R_{off}}{R + R_a}.$$

(3.33) and (3.34) are expanded:

$$\mathbf{B'} = \begin{bmatrix} \dfrac{D}{L} & \dfrac{RR_c}{(R + R_c)L} & \dfrac{V_g(R + R_{off})}{(R + R_a)L} \\ 0 & -\dfrac{R}{(R + R_c)C} & 0 \end{bmatrix}, \tag{3.40}$$

$$\mathbf{E'} = \begin{bmatrix} 0 & -\dfrac{RR_c}{R + R_c} & 0 \end{bmatrix}. \tag{3.41}$$

All the coefficient matrices in the ac model (3.32) are now available.

Extracting the Transfer Functions

The control-to-output transfer function, the output impedance and the audio susceptibility will now be derived from the linearized system in (3.32).

Assume that the state is zero initially. The Laplace transform of (3.32) is

$$\begin{cases} s\hat{\mathbf{x}}(s) = \mathbf{A}\hat{\mathbf{x}}(s) + \mathbf{B'}\hat{\mathbf{u}}'(s) \\ \hat{\mathbf{y}}(s) = \mathbf{C}\hat{\mathbf{x}}(s) + \mathbf{E'}\hat{\mathbf{u}}'(s) \end{cases}. \tag{3.42}$$

(3.42) is rewritten:

$$\begin{cases} \hat{\mathbf{x}}(s) = (s\mathbf{I} - \mathbf{A})^{-1}\mathbf{B'}\hat{\mathbf{u}}'(s) \\ \hat{\mathbf{y}}(s) = \mathbf{C}\hat{\mathbf{x}}(s) + \mathbf{E'}\hat{\mathbf{u}}'(s) \end{cases}. \tag{3.43}$$

The following six transfer functions are obtained from the first equation in (3.43) according to the appendix (Section 3.6):

$$\frac{\hat{i}_L(s)}{\hat{d}(s)} = \frac{V_g\left(R + R_{off}\right)\left(R + R_a\right)^{-1}\left(1 + s(R + R_c)C\right)}{den_{ol}(s)}, \tag{3.44}$$

$$\frac{\hat{v}(s)}{\hat{d}(s)} = \frac{RV_g\left(R + R_{off}\right)\left(R + R_a\right)^{-1}}{den_{ol}(s)}, \tag{3.45}$$

$$\frac{\hat{i}_L(s)}{\hat{i}_{inj}(s)} = \frac{R\left(1 + sR_cC\right)}{den_{ol}(s)}, \tag{3.46}$$

$$\frac{\hat{v}(s)}{\hat{i}_{inj}(s)} = \frac{-R\left(R_a + sL\right)}{den_{ol}(s)}, \tag{3.47}$$

$$\frac{\hat{i}_L(s)}{\hat{v}_g(s)} = \frac{D(1 + s(R + R_c)C)}{den_{ol}(s)}, \qquad (3.48)$$

$$\frac{\hat{v}(s)}{\hat{v}_g(s)} = \frac{RD}{den_{ol}(s)}, \qquad (3.49)$$

where

$$den_{ol}(s) =$$
$$R_a + R + s(L + (R + R_c)R_aC + RR_cC) + s^2(R + R_c)LC = \qquad (3.50)$$
$$R(1 + sR_cC) + (R_a + sL)(1 + s(R + R_c)C).$$

The control-to-output transfer function, the output impedance, and the audio susceptibility are obtained by combining (3.44)-(3.49) and the second equation in (3.43) (see appendix):

$$\frac{\hat{v}_o(s)}{\hat{d}(s)} = \frac{RV_g(R + R_{off})(R + R_a)^{-1}(1 + sR_cC)}{den_{ol}(s)}, \qquad (3.51)$$

$$Z_{out}(s) = -\frac{\hat{v}_o(s)}{\hat{i}_{inj}(s)} = \frac{R(R_a + sL)(1 + sR_cC)}{den_{ol}(s)}, \qquad (3.52)$$

$$\frac{\hat{v}_o(s)}{\hat{v}_g(s)} = \frac{RD(1 + sR_cC)}{den_{ol}(s)}, \qquad (3.53)$$

where $den_{ol}(s)$ is defined in (3.50). By comparing (3.51)-(3.53) with (2.12)-(2.14), it is concluded that the stray resistances R_L, R_t, and R_d do not affect the number of poles and zeros in the transfer functions. Furthermore, if these stray resistances are set to zero in (3.51)-(3.53), the equations (2.12)-(2.14) are obtained as expected.

3.3   Current-Mode Control

In this section, the Ridley model is used to obtain a model of the buck converter with current-mode control. One part of this model is the model of the converter derived in the previous section.

To obtain a model where the stray resistances are considered, the block diagram in Figure 2.17 must be changed. In Figure 2.17, changes in the input and output voltages are taken into account by using the feedforward gains k_f and k_r. These feedforward gains depend on the converter topology. The contribution to the input of the modulator block $F_m(s)$ is

$$k_f \hat{v}_g(s) + k_r \hat{v}_o(s). \tag{3.54}$$

In Ridley (1991), a more general block diagram is presented where $\hat{v}_{on}(s)$ and $\hat{v}_{off}(s)$ are used instead of $\hat{v}_g(s)$ and $\hat{v}_o(s)$. $\hat{v}_{on}(s)$ is the voltage across the inductor during t_{on} and $\hat{v}_{off}(s)$ is the voltage across the inductor during t_{off}. The contribution to the input of the modulator block $F_m(s)$ is

$$k_f{}'\hat{v}_{on}(s) + k_r{}'\hat{v}_{off}(s), \tag{3.55}$$

where

$$k_f{}' = -\frac{DT_s R_i}{L}\left(1 - \frac{D}{2}\right), \tag{3.56}$$

$$k_r{}' = \frac{D'^2 T_s R_i}{2L}. \tag{3.57}$$

The feedforward gains $k_f{}'$ and $k_r{}'$ do not depend on the converter topology which is an advantage. Note that the feedforward gains k_f and k_r depend on the converter topology.

If the stray resistances are not considered, the following expressions for $\hat{v}_{on}(s)$ and $\hat{v}_{off}(s)$ are valid for the buck converter (see Table 2.2):

$$\hat{v}_{on}(s) = \hat{v}_g(s) - \hat{v}_o(s), \tag{3.58}$$

$$\hat{v}_{off}(s) = \hat{v}_o(s). \tag{3.59}$$

(3.55) is rewritten for this case:

$$k_f'\hat{v}_{on}(s) + k_r'\hat{v}_{off}(s) = k_f'\left(\hat{v}_g(s) - \hat{v}_o(s)\right) + k_r'\hat{v}_o(s) = \\ k_f'\hat{v}_g(s) + \left(-k_f'+k_r'\right)\hat{v}_o(s). \tag{3.60}$$

By comparing (3.54) and (3.60), it is concluded that k_f should be equal to k_f' and so it is (compare (2.37) and (3.56)). Furthermore, k_r should be equal to $-k_f'+k_r'$ and this is also the case since (2.38) is the same as

$$-k_f'+k_r' = \frac{DT_sR_i}{L}\left(1 - \frac{D}{2}\right) + \frac{D'^2\,T_sR_i}{2L} = \\ \frac{2DT_sR_i - D^2T_sR_i + (1-D)^2T_sR_i}{2L} = \frac{T_sR_i}{2L}. \tag{3.61}$$

According to Figure 2.17, the duty cycle is

$$\hat{d}(s) = F_m(s)\left(k_f\hat{v}_g(s) + k_r\hat{v}_o(s) + R_i\hat{i}_c(s) - H_e(s)R_i\hat{i}_L(s)\right). \tag{3.62}$$

If the stray resistances are considered, the following expressions for $\hat{v}_{on}(s)$ and $\hat{v}_{off}(s)$ are valid for the buck converter (see Figure 3.2 and Figure 3.3):

$$\hat{v}_{on}(s) = \hat{v}_g(s) - R_{on}\hat{i}_L(s) - \hat{v}_o(s), \tag{3.63}$$

$$\hat{v}_{off}(s) = \hat{v}_o(s) + R_{off}\hat{i}_L(s). \tag{3.64}$$

For this case, the Ridley model is according to Figure 3.4 and the duty cycle is
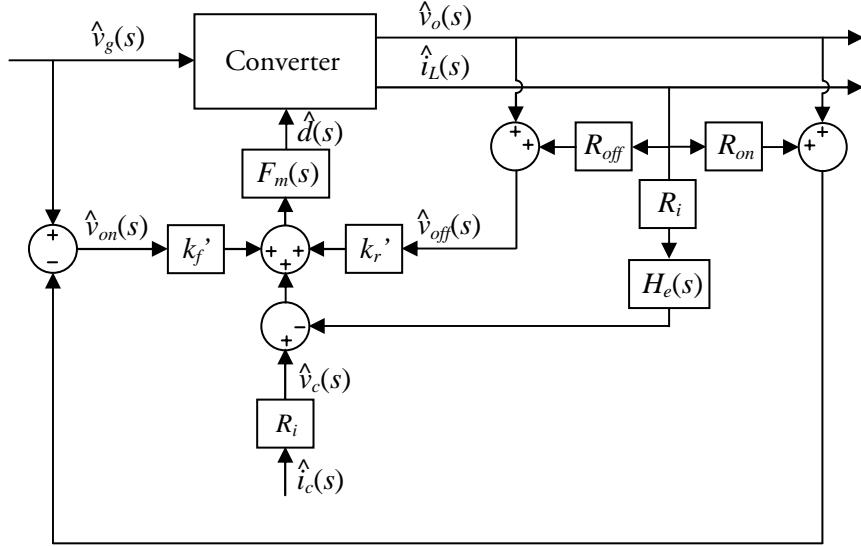
Figure 3.4: The Ridley model for the buck converter including stray resistances.

$$\hat{d}(s) = F_m(s)\Big(k_f{}'\big(\hat{v}_g(s) - R_{on}\hat{i}_L(s) - \hat{v}_o(s)\big) +$$
$$k_r{}'\big(\hat{v}_o(s) + R_{off}\hat{i}_L(s)\big) + R_i\hat{i}_c(s) - H_e(s)R_i\hat{i}_L(s)\Big) =$$
$$F_m(s)\Big(k_f{}'\hat{v}_g(s) + \big(-k_f{}' + k_r{}'\big)\hat{v}_o(s) + \qquad\qquad (3.65)$$
$$R_i\hat{i}_c(s) - \big(H_e(s) + R_i^{-1}k_f{}'R_{on} - R_i^{-1}k_r{}'R_{off}\big)R_i\hat{i}_L(s)\Big) =$$
$$F_m(s)\Big(k_f\hat{v}_g(s) + k_r\hat{v}_o(s) + R_i\hat{i}_c(s) - H_{ee}(s)R_i\hat{i}_L(s)\Big),$$

where

$$H_{ee}(s) = H_e(s) + R_i^{-1}k_f{}'R_{on} - R_i^{-1}k_r{}'R_{off} \ , \qquad\qquad (3.66)$$

k_f is defined in (2.37), and k_r is defined in (2.38). (3.66) is an extended version of $H_e(s)$ and is used temporarily to reduce the size of the expressions below.

The model of the converter is linear and the outputs are therefore

$$\hat{v}_o(s) = \frac{\hat{v}_o(s)}{\hat{d}(s)}\hat{d}(s) + \frac{\hat{v}_o(s)}{\hat{i}_{inj}(s)}\hat{i}_{inj}(s) + \frac{\hat{v}_o(s)}{\hat{v}_g(s)}\hat{v}_g(s), \qquad (3.67)$$

$$\hat{i}_L(s) = \frac{\hat{i}_L(s)}{\hat{d}(s)}\hat{d}(s) + \frac{\hat{i}_L(s)}{\hat{i}_{inj}(s)}\hat{i}_{inj}(s) + \frac{\hat{i}_L(s)}{\hat{v}_g(s)}\hat{v}_g(s). \qquad (3.68)$$

(3.65) is rewritten by using (3.67) and (3.68):

$$\hat{d}(s)F_m^{-1}(s) = k_f\hat{v}_g(s) +$$
$$k_r\left(\frac{\hat{v}_o(s)}{\hat{d}(s)}\hat{d}(s) + \frac{\hat{v}_o(s)}{\hat{i}_{inj}(s)}\hat{i}_{inj}(s) + \frac{\hat{v}_o(s)}{\hat{v}_g(s)}\hat{v}_g(s)\right) +$$
$$R_i\hat{i}_c(s) - \qquad\qquad\qquad\qquad\qquad\qquad (3.69)$$
$$H_{ee}(s)R_i\left(\frac{\hat{i}_L(s)}{\hat{d}(s)}\hat{d}(s) + \frac{\hat{i}_L(s)}{\hat{i}_{inj}(s)}\hat{i}_{inj}(s) + \frac{\hat{i}_L(s)}{\hat{v}_g(s)}\hat{v}_g(s)\right).$$

All the terms containing $\hat{d}(s)$ in (3.69) are moved to the left:

$$\left(F_m^{-1}(s) - k_r\frac{\hat{v}_o(s)}{\hat{d}(s)} + H_{ee}(s)R_i\frac{\hat{i}_L(s)}{\hat{d}(s)}\right)\hat{d}(s) =$$
$$\left(k_f + k_r\frac{\hat{v}_o(s)}{\hat{v}_g(s)} - H_{ee}(s)R_i\frac{\hat{i}_L(s)}{\hat{v}_g(s)}\right)\hat{v}_g(s) + \qquad (3.70)$$
$$\left(k_r\frac{\hat{v}_o(s)}{\hat{i}_{inj}(s)} - H_{ee}(s)R_i\frac{\hat{i}_L(s)}{\hat{i}_{inj}(s)}\right)\hat{i}_{inj}(s) + R_i\hat{i}_c(s).$$

(3.70) is rewritten:

$$\hat{d}(s) = \left(F_m^{-1}(s) - k_r \frac{\hat{v}_o(s)}{\hat{d}(s)} + H_{ee}(s)R_i \frac{\hat{i}_L(s)}{\hat{d}(s)} \right)^{-1} \bullet$$

$$\left(\left(k_f + k_r \frac{\hat{v}_o(s)}{\hat{v}_g(s)} - H_{ee}(s)R_i \frac{\hat{i}_L(s)}{\hat{v}_g(s)} \right) \hat{v}_g(s) + \right. \tag{3.71}$$

$$\left. \left(k_r \frac{\hat{v}_o(s)}{\hat{i}_{inj}(s)} - H_{ee}(s)R_i \frac{\hat{i}_L(s)}{\hat{i}_{inj}(s)} \right) \hat{i}_{inj}(s) + R_i \hat{i}_c(s) \right).$$

(3.67) is now modified using (3.71):

$$\hat{v}_o(s) = \frac{\hat{v}_o(s)}{\hat{d}(s)} \left(F_m^{-1}(s) - k_r \frac{\hat{v}_o(s)}{\hat{d}(s)} + H_{ee}(s)R_i \frac{\hat{i}_L(s)}{\hat{d}(s)} \right)^{-1} \bullet$$

$$\left(\left(k_f + k_r \frac{\hat{v}_o(s)}{\hat{v}_g(s)} - H_{ee}(s)R_i \frac{\hat{i}_L(s)}{\hat{v}_g(s)} \right) \hat{v}_g(s) + \right.$$

$$\left. \left(k_r \frac{\hat{v}_o(s)}{\hat{i}_{inj}(s)} - H_{ee}(s)R_i \frac{\hat{i}_L(s)}{\hat{i}_{inj}(s)} \right) \hat{i}_{inj}(s) + R_i \hat{i}_c(s) \right) + \tag{3.72}$$

$$\frac{\hat{v}_o(s)}{\hat{i}_{inj}(s)} \hat{i}_{inj}(s) + \frac{\hat{v}_o(s)}{\hat{v}_g(s)} \hat{v}_g(s).$$

The control-to-output transfer function of the closed loop system, which includes the converter and the current controller, is obtained from (3.72):

$$\frac{\hat{v}_o(s)}{\hat{i}_c(s)} = \frac{\hat{v}_o(s)}{\hat{d}(s)} \left(F_m^{-1}(s) - k_r \frac{\hat{v}_o(s)}{\hat{d}(s)} + H_{ee}(s)R_i \frac{\hat{i}_L(s)}{\hat{d}(s)} \right)^{-1} R_i =$$

$$\frac{R_i}{F_m^{-1}(s)\left(\dfrac{\hat{v}_o(s)}{\hat{d}(s)} \right)^{-1} - k_r + H_{ee}(s)R_i \dfrac{\hat{i}_L(s)}{\hat{d}(s)}\left(\dfrac{\hat{v}_o(s)}{\hat{d}(s)} \right)^{-1}}. \tag{3.73}$$

As in Chapter 2, the subscript *ol* will be used for the converter transfer functions, i.e. for the open loop system. When otherwise obvious the subscript will be excluded. The output impedance of the closed loop system is obtained from (3.72):

$$Z_{out}(s) = -\frac{\hat{v}_o(s)}{\hat{i}_{inj}(s)} =$$

$$-\frac{k_r\left(\dfrac{\hat{v}_o(s)}{\hat{i}_{inj}(s)}\right)_{ol} - H_{ee}(s)R_i\left(\dfrac{\hat{i}_L(s)}{\hat{i}_{inj}(s)}\right)_{ol}}{F_m^{-1}(s)\left(\dfrac{\hat{v}_o(s)}{\hat{d}(s)}\right)^{-1} - k_r + H_{ee}(s)R_i\dfrac{\hat{i}_L(s)}{\hat{d}(s)}\left(\dfrac{\hat{v}_o(s)}{\hat{d}(s)}\right)^{-1}} - \left(\frac{\hat{v}_o(s)}{\hat{i}_{inj}(s)}\right)_{ol}. \qquad (3.74)$$

The audio susceptibility of the closed loop system can be obtained from (3.72):

$$\frac{\hat{v}_o(s)}{\hat{v}_g(s)} =$$

$$\frac{k_f + k_r\left(\dfrac{\hat{v}_o(s)}{\hat{v}_g(s)}\right)_{ol} - H_{ee}(s)R_i\left(\dfrac{\hat{i}_L(s)}{\hat{v}_g(s)}\right)_{ol}}{F_m^{-1}(s)\left(\dfrac{\hat{v}_o(s)}{\hat{d}(s)}\right)^{-1} - k_r + H_{ee}(s)R_i\dfrac{\hat{i}_L(s)}{\hat{d}(s)}\left(\dfrac{\hat{v}_o(s)}{\hat{d}(s)}\right)^{-1}} + \left(\frac{\hat{v}_o(s)}{\hat{v}_g(s)}\right)_{ol}. \qquad (3.75)$$

(3.73)-(3.75) are rewritten in the appendix (Section 3.6) by using the converter transfer functions derived in Section 3.2 and the results are

$$\frac{\hat{v}_o(s)}{\hat{i}_c(s)} = \frac{\hat{v}_o(s)}{\hat{v}_c(s)/R_i} = \frac{R(1 + sR_cC)}{den(s)}, \qquad (3.76)$$

$$Z_{out}(s) = -\frac{\hat{v}_o(s)}{\hat{i}_{inj}(s)} = \frac{R(1 + sR_cC)\left(F_h^{-1}(s) + K_{sr}\right)}{den(s)}, \qquad (3.77)$$

$$\frac{\hat{v}_o(s)}{\hat{v}_g(s)} = \frac{\frac{RT_s}{L}D\left(m_c D' - \left(1 - \frac{D}{2}\right)\right)(1 + sR_cC)}{den(s)}, \tag{3.78}$$

where

$$den(s) =$$
$$\left(1 + s(R + R_c)C\right)\left(F_h^{-1}(s) + K_{sr}\right) + \frac{RT_s}{L}(m_c D' - 0.5)(1 + sR_cC), \tag{3.79}$$

$$K_{sr} = \frac{T_s}{L}\left(R_a(m_c D' - 0.5) + 0.5DD'(R_{off} - R_{on})\right), \tag{3.80}$$

and $F_h(s)$ is defined in (2.23). The parameter K_{sr} shows the influence of the stray resistances R_L, R_t, and R_d. If these stray resistances are zero, then K_{sr} is also zero. Note that R_L, R_t, and R_d do not affect the number of poles and zeros in the transfer functions (3.76)-(3.78).

The new expression for the output impedance can be derived without considering the audio susceptibility. The audio susceptibility has been considered so far in this chapter since it has given a more complete model without too much extra work. However, the audio susceptibility and the control-to-output transfer function will not be considered any more in this chapter. The audio susceptibility predicted by the Ridley model in (3.78) will for instance not be improved by using the novel model presented in Section 2.4.

3.4   Using Load Current for Control

In this section, the output impedance is derived for the case where the measured load current is used for control. The result is analyzed and compared with simulation results. A discussion about the control method is also included. Finally, a heuristic approximation of the obtained expression is presented.

Derivation of the output impedance

An expression for the output impedance is first derived and it is assumed that the control law (2.94) is used. Figure 2.41 shows the system obtained when (2.94) is used. The following is obtained from the figure:

$$
\begin{aligned}
\hat{v}_o(s) &= \frac{\hat{v}_o(s)}{\hat{i}_c(s)} \hat{i}_c(s) + \left(\frac{\hat{v}_o(s)}{\hat{i}_{inj}(s)} \right)_{ol2} \hat{i}_{inj}(s) + \left(\frac{\hat{v}_o(s)}{\hat{v}_g(s)} \right)_{ol2} \hat{v}_g(s) = \\
&\frac{\hat{v}_o(s)}{\hat{i}_c(s)} \left(\hat{i}_{c2}(s) + H_i(s) \left(\frac{\hat{v}_o(s)}{R} + \hat{i}_{inj}(s) \right) \right) + \\
&\left(\frac{\hat{v}_o(s)}{\hat{i}_{inj}(s)} \right)_{ol2} \hat{i}_{inj}(s) + \left(\frac{\hat{v}_o(s)}{\hat{v}_g(s)} \right)_{ol2} \hat{v}_g(s).
\end{aligned}
\tag{3.81}
$$

An expression for the output voltage is obtained from (3.81):

$$
\begin{aligned}
\hat{v}_o(s) &= \left(\frac{\hat{v}_o(s)}{\hat{i}_c(s)} \hat{i}_{c2}(s) + \left(\frac{\hat{v}_o(s)}{\hat{i}_c(s)} H_i(s) + \left(\frac{\hat{v}_o(s)}{\hat{i}_{inj}(s)} \right)_{ol2} \right) \hat{i}_{inj}(s) + \right. \\
&\left. \left(\frac{\hat{v}_o(s)}{\hat{v}_g(s)} \right)_{ol2} \hat{v}_g(s) \right) \left(1 - \frac{\hat{v}_o(s)}{\hat{i}_c(s)} H_i(s) \frac{1}{R} \right)^{-1}.
\end{aligned}
\tag{3.82}
$$

To obtain the output impedance, the two input signals $\hat{v}_g(s)$ and $\hat{i}_{c2}(s)$ are set to zero in (3.82):

$$
Z_{out}(s) = -\frac{\hat{v}_o(s)}{\hat{i}_{inj}(s)} = -\frac{\dfrac{\hat{v}_o(s)}{\hat{i}_c(s)} H_i(s) + \left(\dfrac{\hat{v}_o(s)}{\hat{i}_{inj}(s)} \right)_{ol2}}{1 - \dfrac{\hat{v}_o(s)}{\hat{i}_c(s)} H_i(s) \dfrac{1}{R}}.
\tag{3.83}
$$

(3.83) is rewritten by using (3.76) and (3.77):

$$Z_{out}(s) = -\frac{\dfrac{RF_{ESR}(s)}{den(s)}H_i(s) - \dfrac{RF_{ESR}(s)\left(F_h^{-1}(s) + K_{sr}\right)}{den(s)}}{1 - \dfrac{F_{ESR}(s)}{den(s)}H_i(s)} =$$

$$\frac{\left(1 - \left(F_h^{-1}(s) + K_{sr}\right)^{-1}H_i(s)\right)F_{ESR}(s)}{R^{-1}den(s)\left(F_h^{-1}(s) + K_{sr}\right)^{-1} - R^{-1}F_{ESR}(s)\left(F_h^{-1}(s) + K_{sr}\right)^{-1}H_i(s)},$$

(3.84)

where $F_{ESR}(s)$ is defined in (2.73), $F_h(s)$ is defined in (2.23), $K_{sr}(s)$ is defined in (3.80), and $den(s)$ is defined in (3.79).

Analysis of the obtained expression

The obtained expression (3.84) is analyzed and compared with simulation results in this subsection. A discussion about the control method is also included.

From (3.84), it is seen that the more $H_i(s)$ is in accordance with $F_h^{-1}(s) + K_{sr}$, the lower is the output impedance. $F_h^{-1}(s)$ is approximately equal to 1 at low frequencies. If (2.74) is used, i.e. $H_i(s)$ is equal to 1, and $|K_{sr}| \ll 1$, the output impedance will be low at low frequencies. If $H_i(s)$ is equal to $1 + K_{sr}$, the output impedance will be even lower at low frequencies.

The curves and the simulation results in Figure 2.43 for $R = R_{min}$ and two different $H_i(s)$ are shown again in Figure 3.5. R_L, R_t, and R_d were not considered when these results were generated. Figure 3.5 also shows the corresponding results for the case where R_L =20 mΩ, R_t =60 mΩ, and R_d =25 mΩ. For this case, the curves are generated with (3.84) and the simulation results are generated with the model shown in Figure 3.6. Two transfer functions, $H_i(s)$ and $H_v(s)$, are added in the simulation model compared to the model in Figure 2.18. $H_v(s)$ should be used only when the boost and buck-boost converters are considered and $H_v(s)$ is therefore set to zero. The constant *Ic2* is adjusted manually so that the average value of the duty cycle, D, is equal to 0.455. Note that the average value of the output voltage, V_o, is lower in the case where R_a >0 compared to the case where R_a is zero according to (3.31) and (3.29). M_e is calculated by using (2.25) and (3.108):
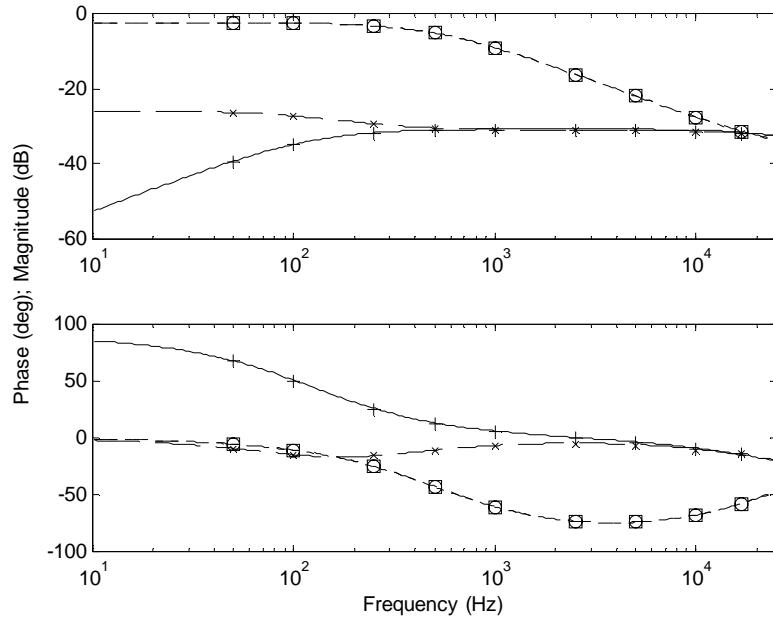
Figure 3.5: The output impedance of a buck converter controlled by (2.94). Dash-dotted line ($\Box$): $H_i(s) = 0$ and without R_L, R_t, and R_d. Dotted line (O): $H_i(s) = 0$ and with R_L, R_t, and R_d. Solid line (+): $H_i(s) = 1$ and without R_L, R_t, and R_d. Dashed line (x): $H_i(s) = 1$ and with R_L, R_t, and R_d. Note that the two first mentioned lines almost coincide.

$$M_e = \frac{V_g D'(R + R_{off})}{L(R + R_a)}(m_c - 1). \tag{3.85}$$

The buck converter subsystem shown in Figure 3.7 is used and it includes R_L, R_t, and R_d. According to Figure 3.5, the simulation results are in good agreement with (3.84).

From Figure 3.5 it is seen that for $H_i(s) = 0$, the output impedance is high at low frequencies and it is insensitive to R_L, R_t, and R_d. When $H_i(s)$ is changed to 1, the output impedance is reduced at low frequencies and it is sensitive to R_L, R_t, and R_d.
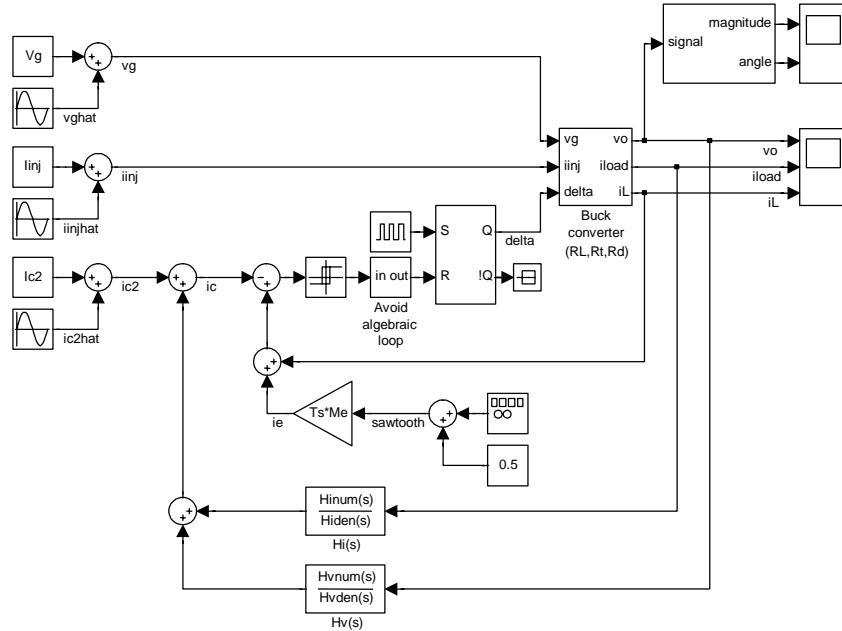
Figure 3.6: The simulation model where two transfer functions, $H_i(s)$ and $H_v(s)$, are included.
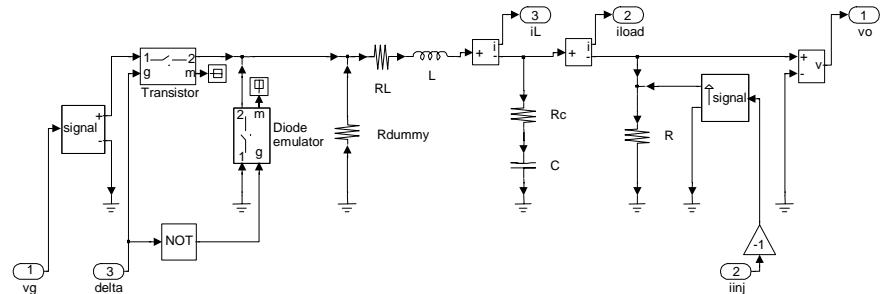
Figure 3.7: The buck converter subsystem where R_L, R_t, and R_d are included. R_t and R_d are parameters in the transistor and diode emulator block, respectively.

To explain these results, consider first the output impedance for the open loop system (3.52). If R_a is zero, the output impedance tends to zero as the frequency tends to zero (see Figure 2.9). The output impedance is mainly determined by the ideal inductor at low frequencies since the impedance of the capacitor and the load resistor is much higher than the impedance of the inductor. If $R_a > 0$, the output impedance is mainly determined by the ideal inductor and the average stray resistance R_a at low frequencies. At dc, the output impedance is equal to R_a connected in parallel with R. Hence, the output impedance is sensitive to R_L, R_t, and R_d.

Now consider the case where current-mode control is used ($H_i(s) = 0$). The inductor current is controlled and the simple model in Figure 2.37 can be used at low frequencies. In this model, the capacitor and the load is fed by a current source. The impedance of the current source is infinite. Therefore, the output impedance is mainly determined by the load resistor at low frequencies (according to the simple model). Since the current through the inductor is controlled, the closed loop system is insensitive to resistances in series with the inductor.

Finally, consider the case where the load current is measured and used for control ($H_i(s) = 1$). In Figure 2.33, the interpretation of this case is that an outer controller (the middle controller in the figure) is added. Since the inductor current controller makes the inner closed loop system insensitive to R_L, R_t, and R_d, it is surprising that the new closed loop system, where the outer controller i added, is sensitive to R_L, R_t, and R_d. (2.78) shows why Figure 2.33 is misleading. The two measured signals, $i_L(t)$ and $i_{load}(t)$, enter the control law with opposite signs. $i_{load}(t)$ works against the decrease in sensitivity to R_L, R_t, and R_d obtained by $i_L(t)$. An alternative interpretation is also obtained from (2.78): It is the current to the output capacitor, $i_{cap}(t)$, that is controlled in the new closed loop system. Hence, there is only one controller and one measured signal, not two controllers and two measured signals. Since the current through the inductor is no longer controlled, the new closed loop system is sensitive to resistances in series with the inductor. If the capacitor current really is calculated from measurements of $i_L(t)$ and $i_{load}(t)$, the two measured signals can be seen as internal signals in the capacitor current sensor.

The alternative interpretation presented above, where the capacitor current is measured, is now investigated further. The circuit in Figure 2.1 (or Figure 3.1) is a second order system. The most natural choice for the state variables is the voltage across the capacitor, $v(t)$, and the inductor current, $i_L(t)$. However, assume that the output voltage, $v_o(t)$, and the capacitor

current, $i_{cap}(t)$, are chosen instead. When an outer voltage controller is added to the controller discussed above, each of the two states is measured (once). Hence, the total controller is a standard state feedback controller where all the states are measured. Cascade control can be seen as a special case of state feedback and our case fulfills the requirements of cascade control. In fact, it is a very common type of cascade control (if we neglect the ESR of the capacitor). In the outer loop the output voltage is controlled and in the inner loop the derivative of the output voltage is controlled (the capacitor current is proportional to the derivative of the output voltage). The advantage of using such a cascade control instead of a PID control is that the derivative part is measured instead of calculated which makes it less sensitive to measurement noise.

There seems to be a contradiction between the discussion above and the one made in Section 2.7 where it was concluded that the control can be seen as gain scheduling. This is now investigated. Assume that $v_o(t)$, $i_L(t)$, and $i_{load}(t)$ are measured. (The measurement of $i_{load}(t)$ can be replaced by measurement of $i_{cap}(t)$ since $i_{load}(t)$ then can be calculated.) $v_o(t)$ and $i_L(t)$ can be chosen as the two state variables of the converter. Hence, the two states are measured. $i_{load}(t)$ is used to estimate the load resistance so that gain scheduling can be applied. In the general case where the load is a dynamic system, $i_{load}(t)$ is used to estimate a dynamic model of the load so that adaptive control can be applied. If $i_L(t)$ and $i_{load}(t)$ are measured, more information is available compared to the case where only $i_{cap}(t)$ is measured. If a gain-scheduling controller is designed in such a way that the measurements of $i_L(t)$ and $i_{load}(t)$ are used only to calculate the difference $i_L(t) - i_{load}(t)$, then the extra information is wasted. In this case, the same control can be obtained from measurements of only $v_o(t)$ and $i_{cap}(t)$ and this can be regarded as cascade control according to the previous discussion. One interpretation can be that the cascade controller is a special case of the gain-scheduling controller. Another interpretation is that if the potential of gain scheduling is not fully utilized during the design, the obtained gain scheduling controller can deteriorate to a cascade controller.

It was concluded previously that the output impedance will be lower at low frequencies if $H_i(s)$ is changed from 1 to $1 + K_{sr}$. The output impedance is zero at dc with this choice. In some cases, it is possible to obtain this even if $H_i(s) = 1$ by changing the relative slope of the external ramp, m_c. From (3.84), it is seen that K_{sr} must be zero and m_c is therefore calculated as follows:

$$0 = \frac{T_s}{L}\left(R_a\left(m_c D' - 0.5\right) + 0.5DD'\left(R_{off} - R_{on}\right)\right), \tag{3.86}$$

$$m_c D' - 0.5 = \frac{0.5DD'\left(R_{on} - R_{off}\right)}{R_a}, \tag{3.87}$$

$$m_c = \frac{1}{2D'} + \frac{D\left(R_{on} - R_{off}\right)}{2R_a}. \tag{3.88}$$

One restriction when choosing m_c is that the control of the inductor current can be unstable if m_c is small. According to Johansson (2003, Section 6.2), $m_c D'$ must be greater than 0.5 to obtain stability. Hence, it is not possible to obtain zero output impedance at dc if R_{on} is smaller than R_{off} (see (3.87)).

Figure 3.8 shows the Bode plot for the output impedance in (3.84) for two different cases. In the first case, $H_i(s)$ is set to $1 + K_{sr}$ (=1.01686). In the second case, $H_i(s) = 1$ and m_c is changed from 2 to 1.04812 according to (3.88). The values for the other parameters are the same as the ones used in Figure 3.5. From Figure 3.8 it is seen that the output impedance tends to zero as the frequency tends to zero in both cases as expected. Note that the output impedance in the first case is almost the same as the output impedance obtained for the case where $H_i(s) = 1$ and R_L, R_t, and R_d are zero (compare Figure 3.8 and Figure 3.5).

Simulation results are also plotted in Figure 3.8. Note that simulation results for the frequency 10 Hz is included this time. For the first case, simulation results agree closely with the magnitude curve. However, there is a significant difference in the phase curve at 10 Hz. For the second case, there is a significant difference in both the magnitude and phase curves at low frequencies. By adjusting m_c, it is found that the simulation model predicts a minimum for the output impedance at $m_c = 1.0542$. The simulation results are plotted in Figure 3.8 also for this m_c and it is seen that they agree closely with the magnitude and phase curves. It seems reasonable that small modeling errors can cause large relative errors in (3.84) in the case where low output impedance is to be predicted since there is a subtraction between two almost equally large values in this case. Hence, the prediction of low output impedance is very sensitive to errors in m_c.
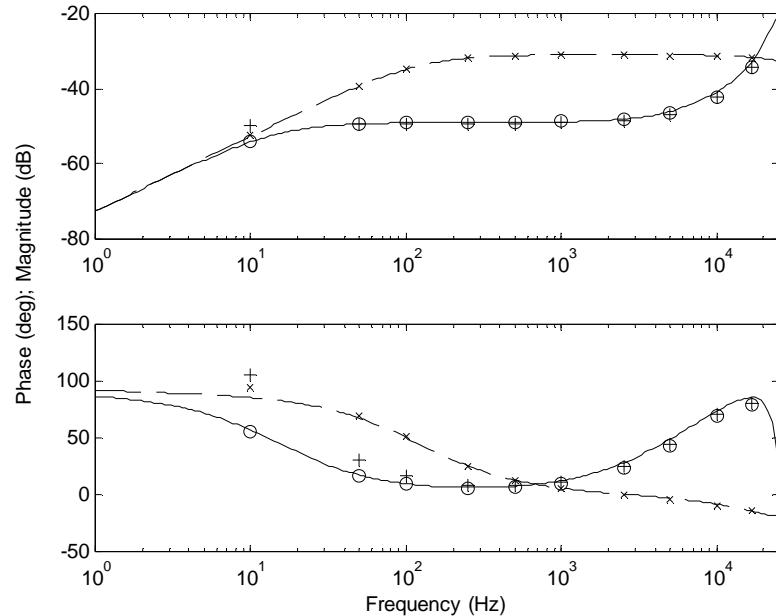
Figure 3.8: The output impedance of a buck converter with R_L, R_t, and R_d and controlled by (2.94). Dashed line (x): $H_i(s) = 1.01686$ (and $m_c = 2$). Solid line (+): $H_i(s) = 1$ and $m_c = 1.04812$. Simulation results with $H_i(s) = 1$ and $m_c = 1.0542$ are also included (O).

Heuristic approximation of the obtained expression

Figure 3.9 shows the Bode plots for the denominators in (3.84) and (2.97). The parameter values used in Figure 3.5 are also used here and $H_i(s) = 1$. From Figure 3.9 it is seen that the denominator in (2.97) is a good approximation of the denominator in (3.84) even though R_L, R_t, and R_d are not considered and some other approximations are made. Therefore, a heuristic approximation of the output impedance is
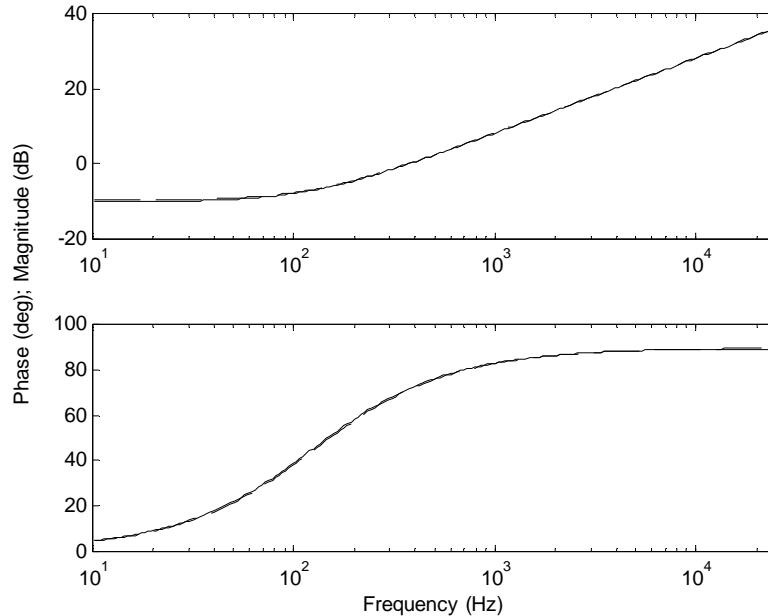
Figure 3.9: Bode plots of two denominators. Dashed line: denominator in (3.84). Solid line: denominator in (2.97). Note that the two lines almost coincide.

$$Z_{out}(s) = \frac{\left(1 - \left(F_h^{-1}(s) + K_{sr}\right)^{-1} H_i(s)\right) F_{ESR}(s)}{C\left(s + \left(1 - F_{ESR}(s)F_h(s)H_i(s)\right)\dfrac{1}{RC} + \dfrac{T_s}{LC}\left(m_c D' - 0.5\right)\right)}, \qquad (3.89)$$

where $F_{ESR}(s)$ is defined in (2.73), $F_h(s)$ is defined in (2.23), and $K_{sr}(s)$ is defined in (3.80). Note that (3.89) is exactly the same as (2.97) if $H_i(s) = 0$.

3.5   Summary and Concluding Remarks

A new transfer function for the output impedance has been derived in this chapter where the stray resistances in the inductor, transistor, and diode

have been considered. The methodology used in the derivation is analogous to the one used in the licentiate thesis, Johansson (2003).

The new transfer function shows that the output impedance is sensitive to the stray resistances if the load current is used for control as proposed by Redl and Sokal (1986). In this control the measured inductor and load currents are only used to calculate the difference, i.e. the capacitor current. Hence, the capacitor current is controlled. Since the inductor current is not controlled, the output impedance is sensitive to the stray resistances. In current-mode control, not applying the load current for control, the inductor current is controlled and the indictor acts as a current source. Therefore, the output impedance is insensitive to the stray resistances, which are connected in series with the inductor.

Since the capacitor current is controlled in the control proposed by Redl and Sokal (1986), cascade control is obtained when an outer voltage controller is added. If a gain-scheduling controller is designed in such a way that the measurements of the inductor and load currents are used only to calculate the difference, i.e. the capacitor current, the obtained gain scheduling controller will simply act as a cascade controller.

In this chapter, it was also shown that the output impedance (theoretically) can become zero at dc also in the case where the stray resistances are larger than zero by adjusting the control ($H_i(s)$ or m_c). Furthermore, a heuristic approximation of the new transfer function for the output impedance was presented. Simulation results were also presented and they verified the main analytical results in the chapter.

3.6   Appendix

Some results presented previously in this chapter are derived in this section. First, the derivation of (3.5)-(3.12) is presented. Next, (3.44)-(3.49) are derived. The derivation of (3.51)-(3.53) is then presented. Finally, (3.76)-(3.78) are derived.

Derivation of (3.5)-(3.12)

(3.4) is rearranged to:

$$v_o(t) + \frac{R_c}{R} v_o(t) = v(t) + R_c \left(i_L(t) - i_{inj}(t) \right), \qquad (3.90)$$

$$v_o(t) = \frac{v(t) + R_c\left(i_L(t) - i_{inj}(t)\right)}{1 + R_c/R}, \qquad (3.91)$$

$$v_o(t) = \frac{RR_c}{R + R_c}i_L(t) + \frac{R}{R + R_c}v(t) - \frac{RR_c}{R + R_c}i_{inj}(t). \qquad (3.92)$$

(3.92) is used to substitute $v_o(t)$ in (3.2) and (3.3):

$$\frac{di_L(t)}{dt} = -\frac{R_{on}}{L}i_L(t) - \frac{RR_c}{(R + R_c)L}i_L(t) - \frac{R}{(R + R_c)L}v(t) +$$
$$\frac{1}{L}v_g(t) + \frac{RR_c}{(R + R_c)L}i_{inj}(t), \qquad (3.93)$$

$$\frac{dv(t)}{dt} = \frac{1}{C}i_L(t) - \frac{R_c}{(R + R_c)C}i_L(t) - \frac{1}{(R + R_c)C}v(t) +$$
$$\frac{R_c}{(R + R_c)C}i_{inj}(t) - \frac{1}{C}i_{inj}(t). \qquad (3.94)$$

(3.94) is simplified:

$$\frac{dv(t)}{dt} = \frac{R}{(R + R_c)C}i_L(t) - \frac{1}{(R + R_c)C}v(t) - \frac{R}{(R + R_c)C}i_{inj}(t). \qquad (3.95)$$

By using (3.93), (3.95), and (3.92), the state-space system in (3.5)-(3.12) is obtained.

Derivation of (3.44)-(3.49)

The first equation in (3.43) is expanded:

$$\hat{\mathbf{x}}(s) = \begin{bmatrix} \dfrac{(R+R_c)R_a + RR_c}{(R+R_c)L} + s & \dfrac{R}{(R+R_c)L} \\ -\dfrac{R}{(R+R_c)C} & \dfrac{1}{(R+R_c)C} + s \end{bmatrix}^{-1} \bullet$$

$$\begin{bmatrix} \dfrac{D}{L} & \dfrac{RR_c}{(R+R_c)L} & \dfrac{V_g(R+R_{off})}{(R+R_a)L} \\ 0 & -\dfrac{R}{(R+R_c)C} & 0 \end{bmatrix} \hat{\mathbf{u}}'(s).$$

$$(3.96)$$

The matrix inversion in (3.96) is calculated:

$$\hat{\mathbf{x}}(s) =$$

$$\frac{1}{\left(\dfrac{(R+R_c)R_a + RR_c}{(R+R_c)L} + s\right)\left(\dfrac{1}{(R+R_c)C} + s\right) + \dfrac{R^2}{(R+R_c)^2 LC}} \bullet$$

$$\begin{bmatrix} \dfrac{1}{(R+R_c)C} + s & -\dfrac{R}{(R+R_c)L} \\ \dfrac{R}{(R+R_c)C} & \dfrac{(R+R_c)R_a + RR_c}{(R+R_c)L} + s \end{bmatrix} \bullet$$

$$\begin{bmatrix} \dfrac{D}{L} & \dfrac{RR_c}{(R+R_c)L} & \dfrac{V_g(R+R_{off})}{(R+R_a)L} \\ 0 & -\dfrac{R}{(R+R_c)C} & 0 \end{bmatrix} \hat{\mathbf{u}}'(s).$$

$$(3.97)$$

(3.97) is simplified:

$\hat{\mathbf{x}}(s) =$

$$\frac{1}{\dfrac{(R+R_c)R_a + RR_c + R^2}{(R+R_c)^2 LC} + s\dfrac{L + (R+R_c)R_a C + RR_c C}{(R+R_c)LC} + s^2} \bullet$$

$$\begin{bmatrix} \dfrac{D}{(R+R_c)LC} + s\dfrac{D}{L} \\ \dfrac{RD}{(R+R_c)LC} \end{bmatrix}$$

$$\left[\begin{matrix} \dfrac{RR_c}{(R+R_c)^2 LC} + s\dfrac{RR_c}{(R+R_c)L} + \dfrac{R^2}{(R+R_c)^2 LC} \\ \dfrac{R^2 R_c}{(R+R_c)^2 LC} - \dfrac{R(R+R_c)R_a + R^2 R_c}{(R+R_c)^2 LC} - s\dfrac{R}{(R+R_c)C} \\ \dfrac{V_g(R+R_{off})}{(R+R_a)(R+R_c)LC} + s\dfrac{V_g(R+R_{off})}{(R+R_a)L} \\ \dfrac{RV_g(R+R_{off})}{(R+R_a)(R+R_c)LC} \end{matrix} \right] \hat{\mathbf{u}}'(s),$$

(3.98)

$$\hat{\mathbf{x}}(s) = \frac{1}{R_a + R + s(L + (R+R_c)R_a C + RR_c C) + s^2(R+R_c)LC} \bullet$$

$$\begin{bmatrix} D(1 + s(R+R_c)C) & R(1 + sR_c C) \\ RD & -R(R_a + sL) \\ V_g(R+R_{off})(R+R_a)^{-1}(1 + s(R+R_c)C) \\ RV_g(R+R_{off})(R+R_a)^{-1} \end{bmatrix} \hat{\mathbf{u}}'(s).$$

(3.99)

The six transfer functions (3.44)-(3.49) are obtained from (3.99).

Derivation of (3.51)-(3.53)

The second equation in (3.43) is expanded:

$$\hat{\mathbf{y}}(s) = \left[\frac{RR_c}{R + R_c} \quad \frac{R}{R + R_c} \right] \hat{\mathbf{x}}(s) + \left[0 \quad -\frac{RR_c}{R + R_c} \quad 0 \right] \hat{\mathbf{u}}'(s). \qquad (3.100)$$

The control-to-output transfer function is obtained by combining (3.100), (3.44), and (3.45):

$$\frac{\hat{v}_o(s)}{\hat{d}(s)} = \frac{RR_c}{R + R_c} \frac{\hat{i}_L(s)}{\hat{d}(s)} + \frac{R}{R + R_c} \frac{\hat{v}(s)}{\hat{d}(s)} =$$

$$\frac{RR_c V_g \left(R + R_{off}\right)\left(R + R_a\right)^{-1}\left(1 + s\left(R + R_c\right)C\right)}{\left(R + R_c\right)den_{ol}(s)} +$$

$$\frac{R^2 V_g \left(R + R_{off}\right)\left(R + R_a\right)^{-1}}{\left(R + R_c\right)den_{ol}(s)} = \qquad (3.101)$$

$$\frac{RV_g \left(R + R_{off}\right)\left(R + R_a\right)^{-1}\left(R + R_c\left(1 + s\left(R + R_c\right)C\right)\right)}{\left(R + R_c\right)den_{ol}(s)} =$$

$$\frac{RV_g \left(R + R_{off}\right)\left(R + R_a\right)^{-1}\left(1 + sR_cC\right)}{den_{ol}(s)}.$$

The output impedance is obtained by combining (3.100), (3.46), and (3.47):

$$Z_{out}(s) = -\frac{\hat{v}_o(s)}{\hat{i}_{inj}(s)} =$$

$$-\frac{RR_c}{R+R_c}\frac{\hat{i}_L(s)}{\hat{i}_{inj}(s)} - \frac{R}{R+R_c}\frac{\hat{v}(s)}{\hat{i}_{inj}(s)} + \frac{RR_c}{R+R_c} =$$

$$\frac{-RR_cR(1+sR_cC)+R^2(R_a+sL)}{(R+R_c)den_{ol}(s)} +$$

$$\frac{RR_cR(1+sR_cC)+RR_c(R_a+sL)(1+s(R+R_c)C)}{(R+R_c)den_{ol}(s)} = \qquad (3.102)$$

$$\frac{R^2(R_a+sL)+RR_c(R_a+sL)(1+s(R+R_c)C)}{(R+R_c)den_{ol}(s)} =$$

$$\frac{R(R_a+sL)(R+R_c(1+s(R+R_c)C))}{(R+R_c)den_{ol}(s)} = \frac{R(R_a+sL)(1+sR_cC)}{den_{ol}(s)}.$$

The audio susceptibility is derived by combining (3.100), (3.48), and (3.49):

$$\frac{\hat{v}_o(s)}{\hat{v}_g(s)} = \frac{RR_c}{R+R_c}\frac{\hat{i}_L(s)}{\hat{v}_g(s)} + \frac{R}{R+R_c}\frac{\hat{v}(s)}{\hat{v}_g(s)} =$$

$$\frac{RR_cD(1+s(R+R_c)C)+R^2D}{(R+R_c)den_{ol}(s)} = \qquad (3.103)$$

$$\frac{RD(R+R_c(1+s(R+R_c)C))}{(R+R_c)den_{ol}(s)} = \frac{RD(1+sR_cC)}{den_{ol}(s)}.$$

Derivation of (3.76)-(3.78)

(3.73) is rewritten by using (3.44) and (3.51):

$$\frac{\hat{v}_o(s)}{\hat{i}_c(s)} =$$

$$\frac{R_i}{\dfrac{F_m^{-1}(s)(R+R_a)den_{ol}(s)}{RV_g(R+R_{off})(1+sR_cC)} - k_r + H_{ee}(s)R_i\dfrac{1+s(R+R_c)C}{R(1+sR_cC)}} =$$

$$R(1+sR_cC)\left(\frac{F_m^{-1}(s)(R+R_a)den_{ol}(s)}{R_iV_g(R+R_{off})} - \frac{k_r}{R_i}R(1+sR_cC)+\right.$$

$$\left. H_{ee}(s)(1+s(R+R_c)C)\right)^{-1} = \frac{R(1+sR_cC)}{den(s)},$$

(3.104)

where

$$den(s) =$$

$$R_i^{-1}F_m^{-1}(s)V_g^{-1}(R+R_{off})^{-1}(R+R_a)den_{ol}(s) - R_i^{-1}k_rR(1+sR_cC)+ \quad (3.105)$$

$$H_{ee}(s)(1+s(R+R_c)C)$$

and $den_{ol}(s)$ is defined in (3.50). Hence, the numerator in (3.76) is derived.
    (3.74) can be rewritten by using (3.46), (3.52), and the fact that (3.73) can be rewritten as in (3.104):

$$Z_{out}(s) = -\frac{\hat{v}_o(s)}{\hat{i}_{inj}(s)} =$$

$$\frac{R_i^{-1}R(1+sR_cC)\left(k_r\dfrac{R(R_a+sL)(1+sR_cC)}{den_{ol}(s)} + H_{ee}(s)R_i\dfrac{R(1+sR_cC)}{den_{ol}(s)}\right)}{den(s)} +$$

$$\frac{R(R_a+sL)(1+sR_cC)}{den_{ol}(s)} =$$

(3.106)

$$\frac{R(1+sR_cC)}{den(s)}\frac{1}{den_{ol}(s)}\bullet$$

$$\left(R_i^{-1}k_rR(R_a+sL)(1+sR_cC) + H_{ee}(s)R(1+sR_cC)+(R_a+sL)den(s)\right).$$

(3.75) is modified by using (3.48), (3.53), and the fact that (3.73) can be rewritten as in (3.104):

$$
\frac{\hat{v}_o(s)}{\hat{v}_g(s)} = R_i^{-1} R(1 + sR_c C) \bullet
$$

$$
\frac{\left(k_f + k_r \dfrac{RD(1 + sR_c C)}{den_{ol}(s)} - H_{ee}(s)R_i \dfrac{D(1 + s(R + R_c)C)}{den_{ol}(s)} \right)}{den(s)} +
$$

$$
\frac{RD(1 + sR_c C)}{den_{ol}(s)} =
$$

$$
\frac{R(1 + sR_c C)}{den(s)} \frac{1}{den_{ol}(s)} \left(R_i^{-1} k_f den_{ol}(s) +
$$

$$
R_i^{-1} k_r RD(1 + sR_c C) - H_{ee}(s)D(1 + s(R + R_c)C) + Dden(s) \right).
$$

(3.107)

An expression for the slope of the inductor current while the transistor is on is obtained by using (3.2), (3.28), (3.29), (3.31), (3.19), and (2.15):

$$
M_1 = \frac{1}{L}\left(V_g - R_{on} I_L - V_o \right) = \frac{1}{L}\left(V_g - R_{on} \frac{V_o}{R} - V_o \right) =
$$

$$
\frac{1}{L}\left(V_g - \left(\frac{R_{on}}{R} + 1 \right) \frac{D}{1 + R_a/R} V_g \right) = \frac{V_g}{L}\left(\frac{R + R_a}{R + R_a} - \frac{D(R + R_{on})}{R + R_a} \right) =
$$

$$
\frac{V_g}{L(R + R_a)}\left(R + DR_{on} + D'R_{off} - DR - DR_{on} \right) = \frac{V_g D'(R + R_{off})}{L(R + R_a)}.
$$

(3.108)

The first term in (3.105) is modified by using (2.36), (2.33), and (3.108):

$$
R_i^{-1} F_m^{-1}(s) V_g^{-1}(R + R_{off})^{-1}(R + R_a) den_{ol}(s) =
$$

$$
R_i^{-1} m_c S_n T_s V_g^{-1}(R + R_{off})^{-1}(R + R_a) den_{ol}(s) =
$$

$$
R_i^{-1} m_c R_i M_1 T_s V_g^{-1}(R + R_{off})^{-1}(R + R_a) den_{ol}(s) =
$$

$$
m_c \frac{V_g D'(R + R_{off})}{L(R + R_a)} \frac{T_s(R + R_a)}{V_g(R + R_{off})} den_{ol}(s) = \frac{T_s m_c D'}{L} den_{ol}(s).
$$

(3.109)

(3.105) is rewritten using (3.109):

$$den(s) =$$
$$\frac{T_s m_c D'}{L} den_{ol}(s) - R_i^{-1} k_r R(1 + sR_c C) + H_{ee}(s)(1 + s(R + R_c)C).$$

(3.110)

(3.110) is rewritten using (3.50) and (2.38):

$$den(s) =$$
$$\frac{T_s m_c D'}{L} R(1 + sR_c C) + \frac{T_s m_c D'}{L}(R_a + sL)(1 + s(R + R_c)C) -$$
$$R_i^{-1} \frac{T_s R_i}{2L} R(1 + sR_c C) + H_{ee}(s)(1 + s(R + R_c)C) =$$
$$(1 + s(R + R_c)C)\left(H_{ee}(s) + \frac{T_s m_c D'}{L}(R_a + sL) \right) +$$
$$\frac{RT_s}{L}(m_c D' - 0.5)(1 + sR_c C).$$

(3.111)

The following is obtained from (2.23), (2.24), (2.20), and (2.21):

$$F_h^{-1}(s) = 1 + \frac{s}{\omega_n Q} + \frac{s^2}{\omega_n^2} = 1 + \frac{s\pi(m_c D' - 0.5)}{\omega_n} + \frac{s^2}{\omega_n^2} =$$
$$1 + \frac{s\pi}{-2\omega_n} + \frac{s\pi}{\omega_n} m_c D' + \frac{s^2}{\omega_n^2} = 1 + \frac{s}{\omega_n Q_z} + \frac{s^2}{\omega_n^2} + \frac{s\pi}{\pi/T_s} m_c D' =$$
$$H_e(s) + sT_s m_c D',$$

(3.112)

where $H_e(s)$ is defined in (2.22). One part of (3.111) is rewritten by using (3.66), (3.112), (3.56), (3.57), (2.15), and (3.19):

$$H_{ee}(s) + \frac{T_s m_c D'}{L}(R_a + sL) =$$

$$H_e(s) + R_i^{-1} k_f' R_{on} - R_i^{-1} k_r' R_{off} + \frac{T_s m_c D'}{L} R_a + s T_s m_c D' =$$

$$F_h^{-1}(s) + R_i^{-1} k_f' R_{on} - R_i^{-1} k_r' R_{off} + \frac{T_s m_c D'}{L} R_a =$$

$$F_h^{-1}(s) - \frac{DT_s}{L}\left(1 - \frac{D}{2}\right) R_{on} - \frac{D'^2 T_s}{2L} R_{off} + \frac{T_s m_c D'}{L} R_a =$$

$$F_h^{-1}(s) + \frac{T_s}{L}\left(-DR_{on} + \frac{D^2}{2} R_{on} - \frac{(1-D)D'}{2} R_{off} + m_c D' R_a\right) = \qquad (3.113)$$

$$F_h^{-1}(s) + \frac{T_s}{L} \bullet$$

$$\left(-\frac{D}{2} R_{on} - \frac{D(1-D)}{2} R_{on} - \frac{D'}{2} R_{off} + \frac{DD'}{2} R_{off} + m_c D' R_a\right) =$$

$$F_h^{-1}(s) + \frac{T_s}{L}\left(-\frac{DR_{on} + D' R_{off}}{2} + \frac{DD'}{2}\left(R_{off} - R_{on}\right) + m_c D' R_a\right) =$$

$$F_h^{-1}(s) + \frac{T_s}{L}\left(R_a\left(m_c D' - \frac{1}{2}\right) + \frac{DD'}{2}\left(R_{off} - R_{on}\right)\right) = F_h^{-1}(s) + K_{sr} \ ,$$

where

$$K_{sr} = \frac{T_s}{L}\left(R_a\left(m_c D' - 0.5\right) + 0.5 DD'\left(R_{off} - R_{on}\right)\right). \qquad (3.114)$$

The following is obtained if (3.113) is inserted into (3.111):

$$den(s) =$$
$$\left(1 + s(R + R_c)C\right)\left(F_h^{-1}(s) + K_{sr}\right) + \frac{RT_s}{L}\left(m_c D' - 0.5\right)\left(1 + sR_c C\right). \qquad (3.115)$$

Hence, the denominator in (3.76) is derived.

The large parenthesis in (3.106) is rewritten by using (3.110), (3.50), and (3.113):

$$R_i^{-1}k_r R(R_a + sL)(1 + sR_c C) + H_{ee}(s)R(1 + sR_c C) +$$
$$(R_a + sL)den(s) =$$
$$R_i^{-1}k_r R(R_a + sL)(1 + sR_c C) + H_{ee}(s)R(1 + sR_c C) + (R_a + sL)\bullet$$
$$\left(\frac{T_s m_c D'}{L}den_{ol}(s) - R_i^{-1}k_r R(1 + sR_c C) + H_{ee}(s)(1 + s(R + R_c)C)\right) =$$
$$H_{ee}(s)(R(1 + sR_c C) + (R_a + sL)(1 + s(R + R_c)C)) +$$
$$(R_a + sL)\frac{T_s m_c D'}{L}den_{ol}(s) =$$
$$\left(H_{ee}(s) + \frac{T_s m_c D'}{L}(R_a + sL)\right)den_{ol}(s) = \left(F_h^{-1}(s) + K_{sr}\right)den_{ol}(s).$$

(3.116)

(3.106) is rewritten by using (3.116):

$$Z_{out}(s) = -\frac{\hat{v}_o(s)}{\hat{i}_{inj}(s)} = \frac{R(1 + sR_c C)\left(F_h^{-1}(s) + K_{sr}\right)}{den(s)}.$$

(3.117)

Hence, (3.77) is derived.

The large parenthesis in (3.107) is rewritten by using (3.110):

$$R_i^{-1}k_f den_{ol}(s) + R_i^{-1}k_r RD(1 + sR_c C) -$$
$$H_{ee}(s)D(1 + s(R + R_c)C) + Dden(s) =$$
$$R_i^{-1}k_f den_{ol}(s) + R_i^{-1}k_r RD(1 + sR_c C) -$$
$$H_{ee}(s)D(1 + s(R + R_c)C) + D\frac{T_s m_c D'}{L}den_{ol}(s) -$$
$$DR_i^{-1}k_r R(1 + sR_c C) + DH_{ee}(s)(1 + s(R + R_c)C) =$$
$$R_i^{-1}k_f den_{ol}(s) + D\frac{T_s m_c D'}{L}den_{ol}(s) =$$
$$\frac{T_s}{L}D\left(m_c D' + \frac{L}{DT_s R_i}k_f\right)den_{ol}(s).$$

(3.118)

(3.107) is rewritten by using (3.118) and (2.37):

$$\frac{\hat{v}_o(s)}{\hat{v}_g(s)} = \frac{\frac{RT_s}{L} D\left(m_c D' - \left(1 - \frac{D}{2}\right)\right)(1 + sR_cC)}{den(s)}.$$

$$(3.119)$$

Hence, (3.78) is derived.

Chapter 4 Experimental Verification

The control-to-output transfer function and the audio susceptibility for the buck converter were presented in Chapter 2. The frequency functions predicted by these two transfer functions and the new transfer function for the output impedance, presented in Chapter 3, are experimentally verified in this chapter.

The buck converter used to obtain experimental results is presented in Section 4.1. The frequency functions predicted by the presented transfer functions and simulation model are compared with experimental results in Section 4.2. A summary and concluding remarks are presented in Section 4.3.

4.1　Experimental Converter

To obtain experimental results, an experimental buck converter was built and it is presented in this section.

The circuit of the buck converter is shown in Figure 3.1. The components in the converter and the operating point are to some extent chosen such that non-idealities do not affect the measurement results so much. The input voltage, V_g, is 24 V and the output voltage, V_o, is 12 V. The experiments are made with two different resistive loads. The load resistance, R, is either equal to 2 Ω ($= R_{min}$) or 6 Ω ($= R_{max}$). Therefore, the load current, I_{load}, is either equal to 6 A or 2 A.

The transistor is a IRF540 from Intersil. According to the data sheet, it is a 28 A, 100 V, N-channel power MOSFET and $r_{DS(ON)}$ is typically 60 mΩ (at junction temperature 25 °C).

A MBR4060PT from TSC contains two diodes but we only use one of them. The circuit is a 40 A, 60 V, Schottky barrier rectifier according to the data sheet. The diagram that shows forward current versus forward voltage is

127

considered to obtain a value for R_d. The slope is 33 mΩ at 2A and 17 mΩ at 6A (at junction temperature 25 °C). For simplicity, the average value, 25 mΩ, will be used in the models.

The inductor consists of a molybdenum permalloy powder (MPP) toroidal core and a copper winding. The core is a 55907-A2 from Magnetics. According to the data sheet, the initial permeability is equal to 60 and the A_L value is equal to 85 nH/turn^2. Each core of this type is stamped with a grade and it is zero for our core. This means that the manufacturer has checked that the A_L value for our core is in the interval [99, 101] % of the nominal value. The outer diameter of the core is 7.78 cm, the inner diameter is 4.92 cm, and the height is 1.59 cm. The winding consists of 48 turns of copper wire. The diameter of the wire is 0.18 cm and the length of each turn is 6.3 cm. The inductance is calculated as follows:

$$L = A_L N^2 = 85 \bullet 10^{-9} \bullet 48^2 \approx 196 \, \mu H. \tag{4.1}$$

The resistivity of copper is 1.72 μΩ-cm (at temperature 20 °C). Therefore, the dc resistance of the winding is calculated as follows:

$$R_L = \rho \frac{l}{A} = 1.72 \bullet 10^{-6} \bullet \frac{48 \bullet 6.3}{\pi (0.18/2)^2} \approx 20 \, m\Omega. \tag{4.2}$$

The capacitor actually consists of two capacitors connected in parallel. Each one of the capacitors is a RJH-50V331MI5 from ELNA. Each one is a 330 μF, 50 V, aluminum electrolytic capacitor according to the data sheet. The maximum current ripple is 0.979 A (RMS) at 100 kHz and 105 °C. The ESR is 60 mΩ at 100 kHz and 20 °C. Totally, the capacitance is 660 μF and the ESR is 30 mΩ.

The control proposed by Redl and Sokal (1986) is implemented according to the alternative approach presented by Schoneman and Mitchell (1989), i.e. only the capacitor current is measured and used by the controller. The capacitor current is measured by using a current shunt with resistance 50 mΩ (model SR10 from Caddock). Hence, the gain of the current sensor is 50 mV/A. The case where the capacitor current is measured by using a current transformer is analyzed in the Chapter 5. The resistance of the current shunt affects the converter properties significantly at high frequencies but it is not considered in the models presented in the previous chapters. However, since
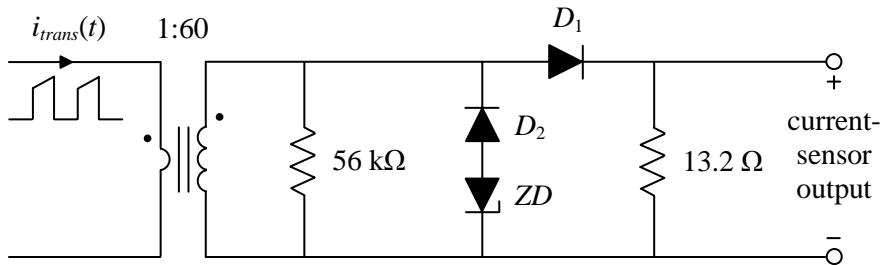
Figure 4.1: The circuit of the current sensor used to measure the transistor current.

the current shunt is connected in series with the capacitor, we can pretend that the resistance of the current shunt is a part of the ESR of the capacitor. Therefore, R_c is set to 80 mΩ and the non-ideality of the sensor is taken care of by the models.

To be able to make experiments also for the case where only current-mode control is used (neither load current nor capacitor current is used for control), the transistor current is measured by using a current transformer. The currents through the transistor and inductor are the same while the transistor is on. Therefore, the transistor current can be used instead of inductor current in peak current-mode control. It is rather easy to measure the transistor current using a current transformer since the transistor current is zero during the second part of each switching period. The circuit of the current sensor is shown in Figure 4.1. The core of the transformer is a ferrite toroid, TN36/23/15-3C11 from Ferroxcube. According to the data sheet, the initial permeability is equal to 4300 and the A_L value is equal to 5800 nH/turn^2. The secondary winding consists of 60 turns and the primary winding consists of 1 turn, i.e. the lead from the transistor goes straight through the toroid. D_1 and D_2 are diodes of type 1N4148. ZD is a zener diode of type 1N4744A and the zener voltage is 15 V. While the transistor operates in the on state, the current in the secondary winding mainly goes through D_1 and the magnetizing current increases. The gain of the current sensor is approximately 13.2/60=0.22 V/A. While the transistor operates in the off state, D_1 does not conduct and the output voltage of the current sensor is zero as it should be. At the same time, the magnetizing current mainly goes through the 56 kΩ resistor. The voltage across the resistor makes the magnetizing current to decrease towards zero. To protect the components,

the maximum voltage is limited by the zener diode. The impedance of the current sensor at the primary winding affects the transistor current but this will be neglected in the models.

The outer voltage controller is excluded in the models presented in the previous chapters. Therefore, no voltage controller is implemented and we are actually not using current-mode control according to the definition. The output voltage 12 V is obtained by manually adjusting the current reference. The slope of the external ramp, M_e, is 56000 A/s and the switching period, T_s, is 20 μs.

Referring to Figure 3.1 and the last section all the parameter values that will be needed are summarized in Table 4.1.

Table 4.1: The parameter values for the experimental buck converter.

Parameter	Value
L	196 μH
R_L	20 mΩ
C	660 μF
R_c	80 mΩ
R_{min}	2 Ω
R_{max}	6 Ω
R_t	60 mΩ
R_d	25 mΩ
V_g	24 V
V_o	12 V
T_s	20 μs
M_e	56000 A/s

4.2   Results

The frequency functions predicted by the presented transfer functions and simulation model are compared with experimental results in this section. However, the conditions used to obtain the various results are first presented.

Conditions

A network analyzer, MS4630B from Anritsu, is used to measure the frequency functions. In each experiment, the gain and the phase shift are measured at 251 different frequencies in the interval [10 Hz, 100 kHz]. The frequencies are logarithmically equally spaced in the interval. Only the results for the frequencies in the interval [10 Hz, 25 kHz] will be presented since the switching frequency of the converter is 50 kHz. The network analyzer can make measurements in the frequency interval [10 Hz, 300 MHz] and this explains why a lower limit than 10 Hz is not chosen. The duration of each experiment, i.e. the sweep time, is 200 s and the resolution bandwidth is 3 Hz. Neither averaging nor smoothing is used to improve the signal-to-noise ratio.

The simulation model in Figure 3.6 and the parameter values in Table 4.1 are used to obtain the simulation results that will be presented. Note that the stray resistances R_L, R_t, and R_d are included in the simulation model. $H_v(s)$ is set to zero and I_{c2} is adjusted manually to obtain V_o equal to 12 V. The duty cycle, D, is then a little larger than 0.5 according to (3.31) and (3.29). Note that a different method was used to obtain the simulation results presented in Section 3.4 since I_{c2} was adjusted such that D became equal to 0.5.

The parameter values in Table 4.1 are used also in the transfer functions. According to the model for the buck converter in Johansson (2003), D is equal to V_o/V_g. Therefore, D is set to 0.5 in the transfer functions to obtain a fair verification. Furthermore, m_c is calculated as follows:

$$m_c = 1 + \frac{M_e}{M_1} = 1 + \frac{M_e}{(V_g - V_o)/L} \approx 1.915. \tag{4.3}$$

The values of both D and m_c are used also in the case where the new (approximate) transfer function for the output impedance (3.89) is used.
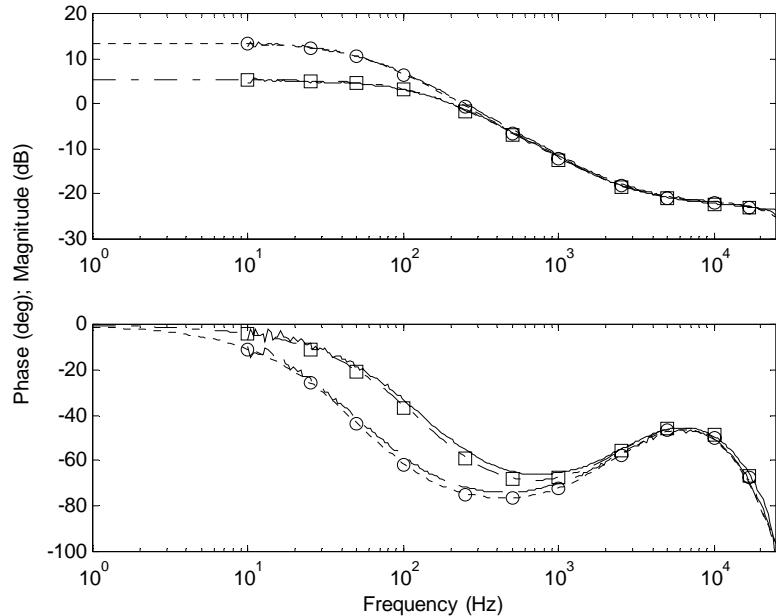
Figure 4.2: The control-to-output transfer function of the experimental buck converter with an inductor-current controller. □: Simulation with $R = R_{\min}$. Dash-dotted line: Analytic model with $R = R_{\min}$. Solid line: Experiment with $R = R_{\min}$. O: Simulation with $R = R_{\max}$. Dotted line: Analytic model with $R = R_{\max}$. Dashed line: Experiment with $R = R_{\max}$.

Control-to-Output Transfer Function

Figure 4.2 shows the Bode plot for the control-to-output transfer functions in (2.96) when $H_i(s) = 0$ (i.e. the measured load current is not used for control) and different loads are used. Only the inductor current is measured and used for control in this case. Simulation and experimental results are also shown in the figure for frequencies higher or equal to 10 Hz. From the figure it is seen that (2.96) is in good agreement with the simulation and experimental results.

Figure 4.3 shows the same as Figure 4.2 except that $H_i(s) = 1$ (i.e. the
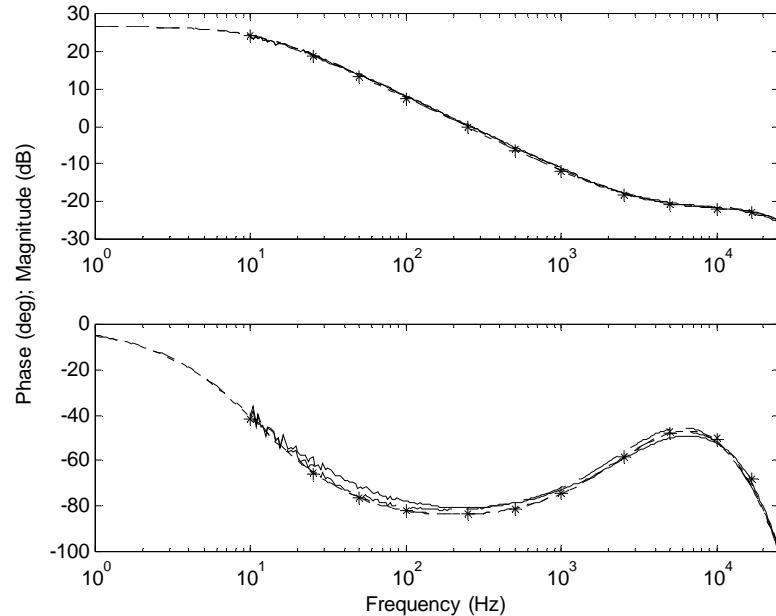
Figure 4.3: The control-to-output transfer function of the experimental buck
converter when load current (or capacitor current) is used for
control. +: Simulation with $R = R_{min}$. Dash-dotted line: Analytic
model with $R = R_{min}$. Solid line: Experiment with $R = R_{min}$. x:
Simulation with $R = R_{max}$. Dotted line: Analytic model with
$R = R_{max}$. Dashed line: Experiment with $R = R_{max}$. Note that
the dash-dotted and dotted lines almost coincide.

measured load current is used for control) in the analytic and simulation
models and that the capacitor current is measured and used for control in the
experimental converter instead of the transistor current. From the figure it is
seen that (2.96) is in good agreement with the simulation and experimental
results also in this case.

Note that (2.96) does not consider the stray resistances R_L, R_t, and R_d.
Since (2.96) makes good predictions of the simulation and experimental
results, it can be concluded that R_L, R_t, and R_d do not affect the control-
to-output transfer function significantly.
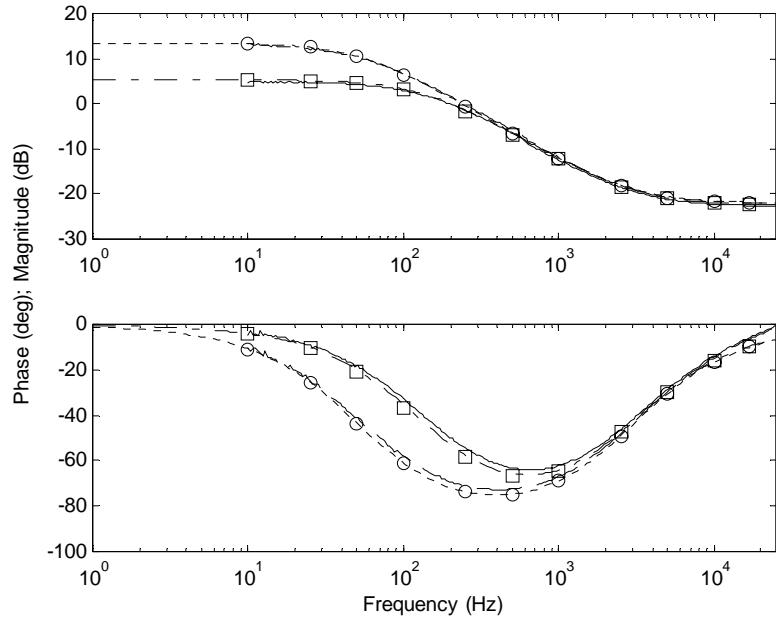
Figure 4.4: The output impedance of the experimental buck converter with
         an inductor-current controller. □: Simulation with $R = R_{\min}$.
         Dash-dotted line: Analytic model with $R = R_{\min}$. Solid line:
         Experiment with $R = R_{\min}$. O: Simulation with $R = R_{\max}$.
         Dotted line: Analytic model with $R = R_{\max}$. Dashed line:
         Experiment with $R = R_{\max}$.

Output Impedance

Figure 4.4 shows the Bode plot for the output impedance in (2.97) when
$H_i(s) = 0$ and different loads are used. Simulation and experimental results
are also shown in the figure. From the figure it is seen that (2.97) is in good
agreement with the simulation and experimental results. Hence, (2.97) makes
good predictions even though R_L, R_t, and R_d are not considered.

Figure 4.5 shows the same as Figure 4.4 except that $H_i(s) = 1$ in the
analytic and simulation models and that the capacitor current is measured
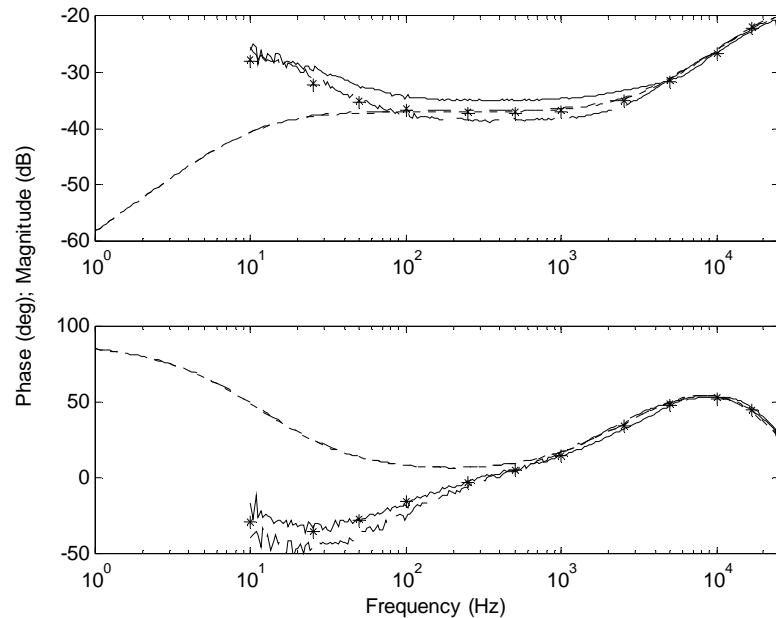
Figure 4.5: The output impedance of the experimental buck converter when load current (or capacitor current) is used for control. +: Simulation with $R = R_{min}$. Dash-dotted line: Analytic model with $R = R_{min}$. Solid line: Experiment with $R = R_{min}$. x: Simulation with $R = R_{max}$. Dotted line: Analytic model with $R = R_{max}$. Dashed line: Experiment with $R = R_{max}$. Note that the dash-dotted and dotted lines almost coincide.

and used for control in the experimental converter. From the figure it is seen that (2.97) is not in good agreement with the simulation and experimental results at low frequencies.

Figure 4.6 shows the same as Figure 4.5 except that (2.97) is replaced by the new (approximate) transfer function for the output impedance (3.89). From the figure it is seen that the analytic model now is in good agreement with the simulation and experimental results also at low frequencies. Hence, R_L, R_t, and R_d must be considered to obtain good predictions of the output impedance in the case where $H_i(s) = 1$.
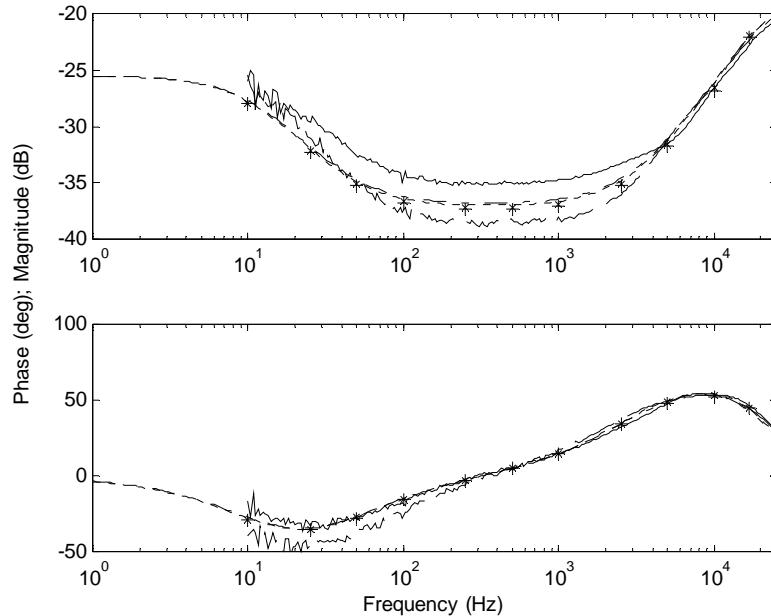
Figure 4.6: The output impedance of the experimental buck converter when load current (or capacitor current) is used for control. +: Simulation with $R = R_{\min}$. Dash-dotted line: New analytic model with $R = R_{\min}$. Solid line: Experiment with $R = R_{\min}$. x: Simulation with $R = R_{\max}$. Dotted line: New analytic model with $R = R_{\max}$. Dashed line: Experiment with $R = R_{\max}$. Note that the dash-dotted and dotted lines almost coincide.

Note that (3.89) is exactly the same as (2.97) if $H_i(s) = 0$. Hence, it is verified that (3.89) makes good predictions both when $H_i(s) = 0$ and $H_i(s) = 1$.

Audio Susceptibility

Figure 4.7 shows the Bode plot for the audio susceptibility in (2.98) when $H_i(s) = 0$ and different loads are used. $F_f(s)$ is a Taylor polynomial of degree 0 of $F_f(s)$ in (2.57), i.e. an approximate version of the original
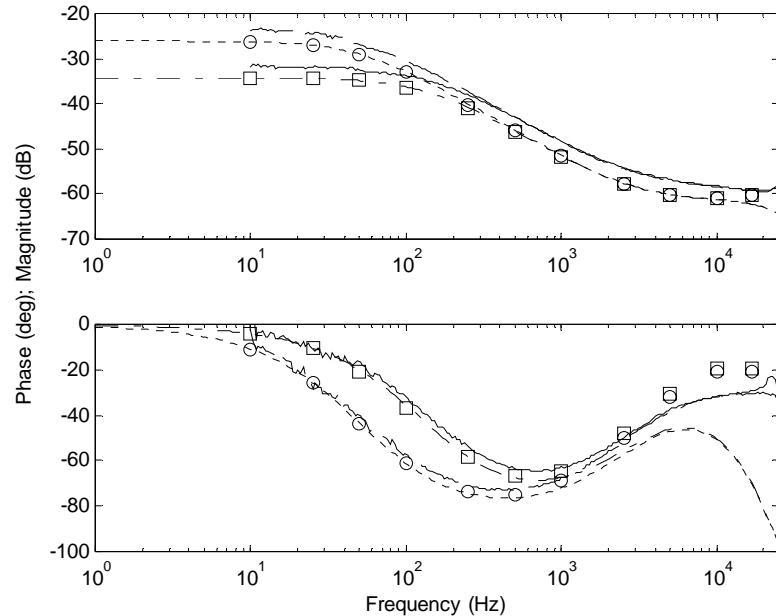
Figure 4.7: The audio susceptibility of the experimental buck converter with an inductor-current controller. $\square$: Simulation with $R = R_{\min}$. Dash-dotted line: Analytic model with $R = R_{\min}$. Solid line: Experiment with $R = R_{\min}$. O: Simulation with $R = R_{\max}$. Dotted line: Analytic model with $R = R_{\max}$. Dashed line: Experiment with $R = R_{\max}$.

Ridley model (2.42) is used. Simulation and experimental results are also shown in the figure. From the figure it is seen that the phase curves predicted by the analytic model are not in good agreement with the simulation and experimental results at high frequencies.

Figure 4.8 shows the same as Figure 4.7 except that $F_f(s)$ is a Taylor polynomial of degree 2 of $F_f(s)$ in (2.57), i.e. an improved version of the Ridley model is used. From the figure it is seen that the phase curves predicted by the analytic model now are in good agreement with the simulation and experimental results also at high frequencies. However, the magnitude curves from the experiments are (still) shifted a little compared to
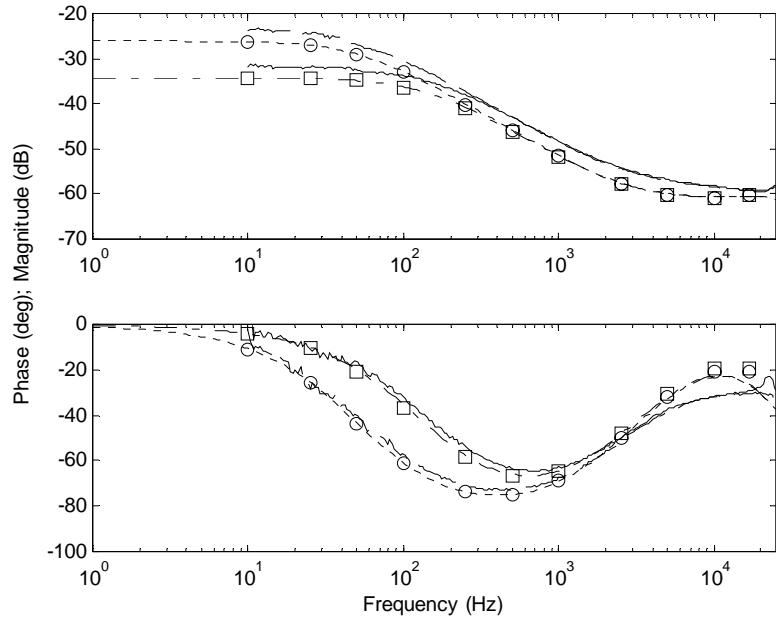
Figure 4.8: The audio susceptibility of the experimental buck converter with an inductor-current controller. □: Simulation with $R = R_{\min}$. Dash-dotted line: Improved analytic model with $R = R_{\min}$. Solid line: Experiment with $R = R_{\min}$. O: Simulation with $R = R_{\max}$. Dotted line: Improved analytic model with $R = R_{\max}$. Dashed line: Experiment with $R = R_{\max}$.

the curves predicted by the simulation and analytic models. The reason for this is not investigated here. The results presented by Ridley (1991) show the same type of difference between the experimental result and the model prediction at low and medium frequencies for some choices of m_c.

Figure 4.9 shows the same as Figure 4.8 except that $H_i(s) = 1$ in the analytic and simulation models and that the capacitor current is measured and used for control in the experimental converter. As in Figure 4.8, the curves are in good agreement except the magnitude curves from the experiments that are shifted a little compared to the curves predicted by the simulation and analytic models.
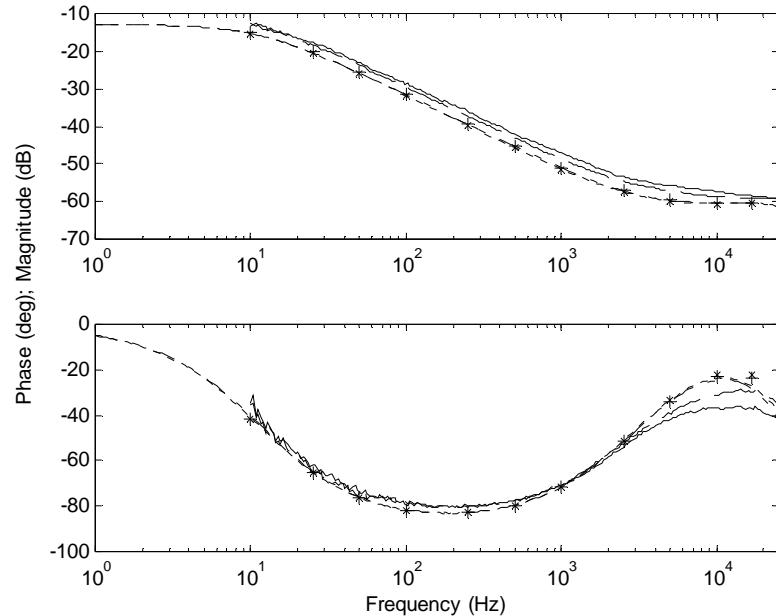
Figure 4.9: The audio susceptibility of the experimental buck converter when load current (or capacitor current) is used for control. +: Simulation with $R = R_{min}$. Dash-dotted line: Improved analytic model with $R = R_{min}$. Solid line: Experiment with $R = R_{min}$. x: Simulation with $R = R_{max}$. Dotted line: Improved analytic model with $R = R_{max}$. Dashed line: Experiment with $R = R_{max}$. Note that the dash-dotted and dotted lines almost coincide.

4.3   Summary and Concluding Remarks

The experimental buck converter was first presented. The experimental results obtained by means of a network analyzer were then presented and compared with the frequency functions predicted by the simulation and analytic models.

The main conclusion of the comparison is that the control-to-output transfer function (2.96), the audio susceptibility (2.98), and the new (approximate) transfer function for the output impedance (3.89) make good

predictions of the experimental and simulation results. However, in the case of the audio susceptibility, the magnitude curves from the experiments are shifted a little compared to the curves predicted by the simulation and analytic models.

Another conclusion is that experimental results for the audio susceptibility verify that the improved Ridley model makes better predictions than the (original) Ridley model.

It is also experimentally verified that the stray resistances R_L, R_t, and R_d must be considered in an analytic model to obtain good predictions of the output impedance in the case where $H_i(s) = 1$. Hence, (2.97) does not make good predictions of the experimental results in this case. However, in the case where $H_i(s) = 0$, (2.97) makes good predictions and (2.97) is exactly the same as (3.89).

Chapter 5 Current-Transformer Influence

In the experiments presented in Chapter 4, the capacitor current was measured using a current shunt. The case where a current transformer is used instead of a current shunt is analyzed in this chapter. The analysis is also verified by means of experimental and simulation results.

5.1 Introduction

Redl and Sokal (1986) suggest that a current transformer is used to measure the capacitor current. There are several advantages using a current transformer instead of a current shunt. The magnitude of the ripple in the output voltage is decreased and the efficiency is increased since the impedance of the sensor can be decreased. Furthermore, electrical insulation is obtained. The suggested current transformer is simple but it has high-pass-filter characteristics, which introduce a resonance in the buck converter at a low frequency. A new model is derived that can predict this resonance.

In Section 3.2, a model is derived for the capacitor-current sensor that uses a current transformer. In Section 3.3, the new converter model is derived and approximate expressions for the control-to-output transfer function, audio susceptibility, and output impedance are also presented. The frequency functions predicted by the approximate expressions are compared with experimental and simulation results in Section 3.4. A summary and concluding remarks are presented in Section 3.5.

5.2 Current Transformer

In this section, a model is derived for the capacitor-current sensor that utilizes a current transformer.

The circuit of the current sensor is shown in Figure 5.1. The core of the transformer is a ferrite toroid, TN13/7.5/5-3E25 from Ferroxcube. According to the data sheet, the initial permeability is equal to 5500 and the A_L value is equal to 2810 nH/turn^2. The number of turns in the primary winding, n_1, is equal to 1 and the number of turns in the secondary winding, n_2, is equal to 30. The burdon resistance, R_2, is equal to 6.6 Ω.

By using a simple model for a transformer (Erickson and Maksimovic, 2000, Section 13.2.2) the model in Figure 5.2 is obtained for the current sensor. The magnetizing inductance, L_M, is calculated as follows:

$$L_M = A_L n_1^2 = 2810 \bullet 10^{-9} \bullet 1^2 = 2.81\,\mu\text{H}. \tag{5.1}$$

The impedance of the current sensor at the primary winding, $Z_1(s) = v_1(s)/i_{cap}(s)$, will now be calculated. The resistance R_2 on the secondary side can be represented by an equivalent resistance, R_1, on the primary side:

$$R_1 = \left(\frac{n_1}{n_2}\right)^2 R_2 = \left(\frac{1}{30}\right)^2 6.6 \approx 7.33\,\text{m}\Omega. \tag{5.2}$$

R_1 and L_M are connected in parallel and

$$Z_1(s) = \frac{v_1(s)}{i_{cap}(s)} = \frac{R_1 s L_M}{R_1 + s L_M}. \tag{5.3}$$

The output voltage of the current sensor is obtained by using (5.3) and (5.2):

$$v_2(s) = \frac{n_2}{n_1} v_1(s) = \frac{n_2}{n_1} Z_1(s) i_{cap}(s) = \frac{n_2}{n_1} R_1 \frac{s}{R_1/L_M + s} i_{cap}(s) =$$
$$\frac{n_1}{n_2} R_2 \frac{s}{R_1/L_M + s} i_{cap}(s). \tag{5.4}$$

Therefore, the transfer function for the current sensor is
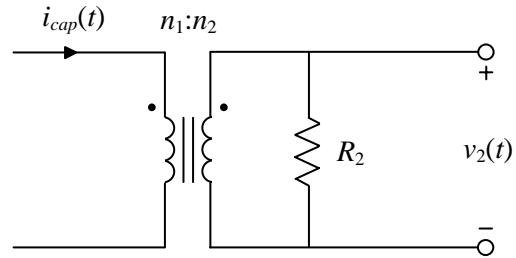
Figure 5.1: The circuit of the current sensor used to measure the capacitor current.
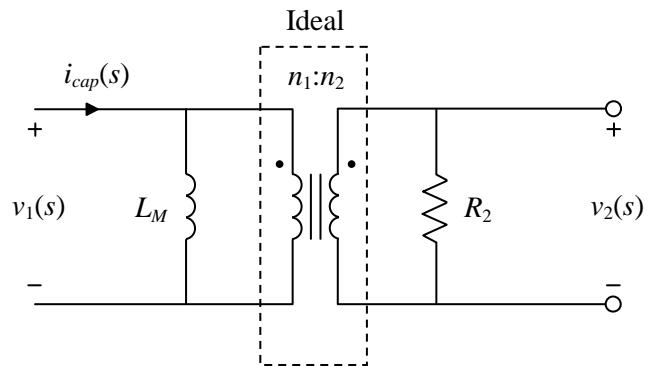

Figure 5.2: A model of the capacitor-current sensor.

$$\frac{v_2(s)}{i_{cap}(s)} = \frac{n_1}{n_2} R_2 H_c(s), \tag{5.5}$$

where

$$H_c(s) = \frac{s}{R_1/L_M + s} = \frac{s}{\left(\dfrac{n_1}{n_2}\right)^2 \dfrac{R_2}{L_M} + s}. \tag{5.6}$$

Note that $H_c(s)$ is a first order high-pass filter and the gain in the pass band is unity. Hence, the gain of the current sensor is $R_2 n_1 / n_2$ at high frequencies and it tends to zero as the frequency tends to zero.

Assume that the current sensor is extended such that a voltage-to-current converter is connected at the output. Assume further that the gain of this converter is $n_2 / (R_2 n_1)$. The transfer function for the extended current sensor is

$$\frac{i_{capm}(s)}{i_{cap}(s)} = H_c(s), \qquad\qquad (5.7)$$

where $i_{capm}(s)$ is the new output signal. $i_{capm}(s)$ is a measured version of $i_{cap}(s)$ and the high frequency components are the same in the two signals.

5.3   Model Including a Capacitor-Current Sensor

A new buck converter model, where the capacitor-current sensor is considered, is derived in this section. Approximate expressions for the control-to-output transfer function, audio susceptibility, and output impedance are also presented. However, how to treat the non-idealities of the current transformer is first discussed.

Treating the Non-Idealities of the Current Transformer

In Chapter 4, the capacitor-current sensor was a current shunt. Its non-ideality was taken care of in the converter models by increasing R_c. In this chapter, the capacitor-current sensor uses a current transformer. In Section 5.2, it was shown that the impedance of this sensor can be modeled as a resistor (R_1) and an inductor (L_M) connected in parallel. At high frequencies, the impedance of the inductor is much higher than the impedance of the resistor and the sensor can be approximated with the resistor. This approximation is not good at low frequencies since the impedance of the sensor then is much lower due to the inductor. However, this approximation error is not important if the capacitor and the sensor are considered as a unit since the impedance of the capacitor is much higher than the resistance of the resistor at low frequencies. Therefore, the impedance of the sensor will be taken care of in the converter model by increasing R_c with R_1.

Buck converter with
a current controller
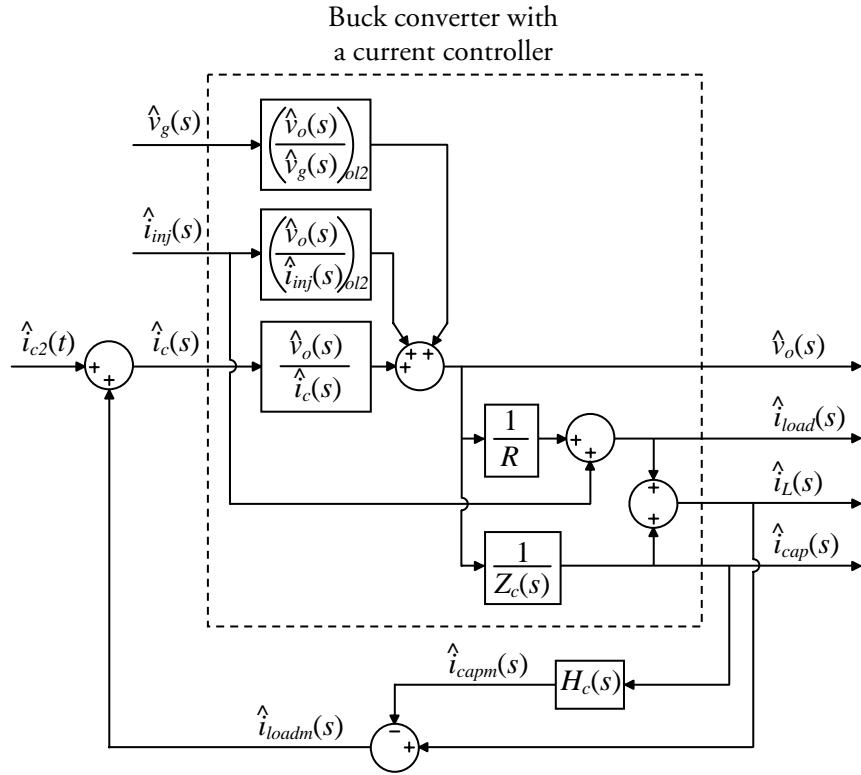
Figure 5.3: The system obtained when the transfer function for the capacitor-
current sensor, $H_c(s)$, is included.

In Section 5.2, it was shown that the capacitor-current sensor has another non-ideality. The sensor gain depends on the frequency. In Chapter 2 and Chapter 3, $H_i(s)$ was used as the transfer function for the load-current sensor. In the new converter model, $H_c(s)$ is used as the transfer function for the capacitor-current sensor.

General Expressions for the Transfer Functions

Figure 5.3 shows a modified version of Figure 2.41. $Z_c(s)$ is the impedance of the capacitor (and the sensor):

$$Z_c(s) = \frac{1}{sC} + R_c \; . \tag{5.8}$$

The transfer functions for the buck converter with a current controller are included in Figure 5.3 and they are derived with the assumption that the inductor current is measured with an ideal sensor. A measured version of the load current, $i_{loadm}(s)$, is calculated as the difference between the (measured) inductor current and the measured capacitor current. The following equations are obtained from Figure 5.3:

$$
\begin{aligned}
\hat{i}_c(s) &= \hat{i}_{c2}(s) + \hat{i}_{loadm}(s) = \hat{i}_{c2}(s) + \hat{i}_L(s) - H_c(s)\hat{i}_{cap}(s) = \\
&\hat{i}_{c2}(s) + \hat{i}_{load}(s) + \hat{i}_{cap}(s) - H_c(s)\hat{i}_{cap}(s) = \\
&\hat{i}_{c2}(s) + \frac{1}{R}\hat{v}_o(s) + \hat{i}_{inj}(s) + \left(1 - H_c(s)\right)\frac{1}{Z_c(s)}\hat{v}_o(s) = \\
&\hat{i}_{c2}(s) + \left(\frac{1}{R} + \frac{1 - H_c(s)}{Z_c(s)}\right)\hat{v}_o(s) + \hat{i}_{inj}(s) ,
\end{aligned}
\tag{5.9}
$$

$$
\begin{aligned}
\hat{v}_o(s) &= \frac{\hat{v}_o(s)}{\hat{i}_c(s)}\hat{i}_c(s) + \left(\frac{\hat{v}_o(s)}{\hat{i}_{inj}(s)}\right)_{ol2}\hat{i}_{inj}(s) + \left(\frac{\hat{v}_o(s)}{\hat{v}_g(s)}\right)_{ol2}\hat{v}_g(s) = \\
&\frac{\hat{v}_o(s)}{\hat{i}_c(s)}\left(\hat{i}_{c2}(s) + \left(\frac{1}{R} + \frac{1 - H_c(s)}{Z_c(s)}\right)\hat{v}_o(s) + \hat{i}_{inj}(s)\right) + \\
&\left(\frac{\hat{v}_o(s)}{\hat{i}_{inj}(s)}\right)_{ol2}\hat{i}_{inj}(s) + \left(\frac{\hat{v}_o(s)}{\hat{v}_g(s)}\right)_{ol2}\hat{v}_g(s) .
\end{aligned}
\tag{5.10}
$$

An expression for the output voltage is obtained from (5.10):

$$
\begin{aligned}
\hat{v}_o(s) &= \left(\frac{\hat{v}_o(s)}{\hat{i}_c(s)}\hat{i}_{c2}(s) + \left(\frac{\hat{v}_o(s)}{\hat{i}_c(s)} + \left(\frac{\hat{v}_o(s)}{\hat{i}_{inj}(s)}\right)_{ol2}\right)\hat{i}_{inj}(s) + \right. \\
&\left. \left(\frac{\hat{v}_o(s)}{\hat{v}_g(s)}\right)_{ol2}\hat{v}_g(s)\right)\left(1 - \frac{\hat{v}_o(s)}{\hat{i}_c(s)}\left(\frac{1}{R} + \frac{1 - H_c(s)}{Z_c(s)}\right)\right)^{-1} .
\end{aligned}
\tag{5.11}
$$

To obtain the control-to-output transfer function, the two input signals $\hat{v}_g(s)$ and $\hat{i}_{inj}(s)$ are set to zero in (5.11):

$$\frac{\hat{v}_o(s)}{\hat{i}_{c2}(s)} = \frac{\dfrac{\hat{v}_o(s)}{\hat{i}_c(s)}}{1 - \dfrac{\hat{v}_o(s)}{\hat{i}_c(s)}\left(\dfrac{1}{R} + \dfrac{1 - H_c(s)}{Z_c(s)}\right)}. \tag{5.12}$$

If $\hat{v}_g(s)$ and $\hat{i}_{c2}(s)$ are set to zero in (5.11), the output impedance is obtained:

$$Z_{out}(s) = -\frac{\hat{v}_o(s)}{\hat{i}_{inj}(s)} = -\frac{\dfrac{\hat{v}_o(s)}{\hat{i}_c(s)} + \left(\dfrac{\hat{v}_o(s)}{\hat{i}_{inj}(s)}\right)_{ol2}}{1 - \dfrac{\hat{v}_o(s)}{\hat{i}_c(s)}\left(\dfrac{1}{R} + \dfrac{1 - H_c(s)}{Z_c(s)}\right)}. \tag{5.13}$$

Finally, the audio susceptibility is obtained by setting the input signals $\hat{i}_{inj}(s)$ and $\hat{i}_{c2}(s)$ to zero in (5.11):

$$\frac{\hat{v}_o(s)}{\hat{v}_g(s)} = \frac{\left(\dfrac{\hat{v}_o(s)}{\hat{v}_g(s)}\right)_{ol2}}{1 - \dfrac{\hat{v}_o(s)}{\hat{i}_c(s)}\left(\dfrac{1}{R} + \dfrac{1 - H_c(s)}{Z_c(s)}\right)}. \tag{5.14}$$

Approximation of the Control-to Output Transfer Function

The control-to-output transfer function derived in the previous subsection is rewritten and approximated in this subsection.

(5.12) is rewritten by using (2.40):

$$\frac{\hat{v}_o(s)}{\hat{i}_{c2}(s)} = \frac{\dfrac{R(1+sR_cC)}{den(s)}}{1 - \dfrac{R(1+sR_cC)}{den(s)}\left(\dfrac{1}{R} + \dfrac{1-H_c(s)}{Z_c(s)}\right)} =$$

$$\frac{(1+sR_cC)\left(1+s\dfrac{L_M}{R_1}\right)}{\left(R^{-1}den(s) - R^{-1}(1+sR_cC)\left(1+R\dfrac{1-H_c(s)}{Z_c(s)}\right)\right)\left(1+s\dfrac{L_M}{R_1}\right)},$$

(5.15)

where $den(s)$ is defined in (2.43). The reason for using (2.40) instead of the approximate version (2.69) will be explained at the end of this section. The (last) denominator in (5.15) is rewritten by using (5.8):

$$\left(R^{-1}den(s) - R^{-1}(1+sR_cC)\left(1+R\frac{1-H_c(s)}{Z_c(s)}\right)\right)\left(1+s\frac{L_M}{R_1}\right) =$$

$$\left(R^{-1}den(s) - R^{-1}(1+sR_cC)\left(1+R\frac{sC(1-H_c(s))}{1+sR_cC}\right)\right)\left(1+s\frac{L_M}{R_1}\right) =$$

$$\left(R^{-1}den(s) - R^{-1}(1+sR_cC) - sC + sCH_c(s)\right)\left(1+s\frac{L_M}{R_1}\right) = \qquad (5.16)$$

$$R^{-1}(den(s) - (1+s(R+R_c)C))\left(1+s\frac{L_M}{R_1}\right) +$$

$$s^2C\frac{L_M}{R_1}\frac{(R_1/L_M+s)H_c(s)}{s}.$$

Hence, the denominator in (5.15) is a fourth order polynomial if $H_c(s)$ is according to (5.6). Therefore, there are four poles and two zeros in the control-to-output transfer function. Hence, one pole and one zero is added when the capacitor current is measured with a current transformer instead of a current shunt (compare (5.15) and (2.96)). The extra zero has a frequency equal to R_1/L_M, i.e. the corner frequency of $H_c(s)$. Assume that the corner frequency of $H_c(s)$ is low and $\hat{i}_{c2}(t)$ is a sinusoidal signal with high frequency. In this case, there are no low-frequency components in $\hat{i}_{cap}(t)$ and the current transformer gives a measurement signal that is almost the

same as the one a current shunt gives. Therefore, it is reasonable to assume that the positions of two of the poles in (5.15) are almost the same as the positions of the two high-frequency poles in (2.96) (which are approximately given by $F_h(s)$ when $H_i(s) = 1$) and that the two remaining poles in (5.15) are positioned much closer to the origin. With the assumption that there are two high-frequency poles and two low-frequency poles it is possible to approximate the denominator in (5.15). It is shown in the appendix (Section 5.6) that if $H_c(s)$ is according to (5.6) and the conditions

$$R_c \ll R ,\tag{5.17}$$

$$\frac{R_c T_s}{L}\left(m_c D'-0.5\right) \ll 1 ,\tag{5.18}$$

$$\frac{1}{\sqrt{LC}} \ll \omega_n ,\tag{5.19}$$

$$\frac{1}{\sqrt{LC}} \ll \omega_n Q ,\tag{5.20}$$

$$\frac{1}{RC} \ll \frac{\omega_n}{Q} ,\tag{5.21}$$

$$\frac{1}{RC} \ll \omega_n Q ,\tag{5.22}$$

$$\frac{R_1}{L_M} \ll \frac{\omega_n}{Q} ,\tag{5.23}$$

$$\frac{R_1}{L_M} \ll \omega_n Q ,\tag{5.24}$$

are fulfilled, then

$$\left(R^{-1}den(s) - R^{-1}\left(1 + sR_cC\right)\left(1 + R\frac{1 - H_c(s)}{Z_c(s)}\right)\right)\left(1 + s\frac{L_M}{R_1}\right) \approx$$

$$K_2^{-1}F_{l2ct}^{-1}(s)F_h^{-1}(s),$$

$$(5.25)$$

where

$$K_2 = \frac{1}{\dfrac{T_s}{L}\left(m_cD'-0.5\right)},$$

$$(5.26)$$

$$F_{l2ct}(s) = \frac{1}{1 + \dfrac{s}{\omega_{ct}Q_{ct}} + \dfrac{s^2}{\omega_{ct}^2}},$$

$$(5.27)$$

$$\omega_{ct} = \sqrt{\frac{T_s}{LC}\left(m_cD'-0.5\right)\frac{R_1}{L_M}},$$

$$(5.28)$$

$$Q_{ct} = \frac{1}{\left(R_cC + \dfrac{L}{R} + \dfrac{L_M}{R_1}\right)\omega_{ct}},$$

$$(5.29)$$

$F_h(s)$ is defined in (2.23), and Q is defined in (2.24). Hence, if $H_c(s)$ is according to (5.6) and the conditions (5.17)-(5.24) are fulfilled, an approximate version of the control-to-output transfer function is

$$\frac{\hat{v}_o(s)}{\hat{i}_{c2}(s)} = K_2 F_{l2ct}(s)F_{ESR}(s)F_{CT}(s)F_h(s),$$

$$(5.30)$$

where

$$F_{CT}(s) = 1 + s\frac{L_M}{R_1},$$

$$(5.31)$$

K_2 is defined in (5.26), $F_{l2ct}(s)$ is defined in (5.27), $F_{ESR}(s)$ is defined in (2.73), and $F_h(s)$ is defined in (2.23). The two low-frequency poles are given by $F_{l2ct}(s)$ and the two high-frequency poles are given by $F_h(s)$.

Approximation of the Audio Susceptibility

In previous chapters, the audio susceptibility was considered after the output impedance but here the order is reversed.

To rewrite (5.14), the non-approximated version of the improved Ridley model is used. According to this model, the audio susceptibility is given by (2.56) except that the denominator is replaced by $den(s)$ in (2.43). Furthermore, the control-to-output transfer function is given by (2.40). By using these two transfer functions, (5.14) is rewritten as follows:

$$\frac{\hat{v}_o(s)}{\hat{v}_g(s)} = \frac{\dfrac{RT_sL^{-1}D\big(m_cD'-F_f(s)\big)(1+sR_cC)}{den(s)}}{1-\dfrac{R(1+sR_cC)}{den(s)}\left(\dfrac{1}{R}+\dfrac{1-H_c(s)}{Z_c(s)}\right)} =$$

$$\frac{\dfrac{T_sD}{L}\big(m_cD'-F_f(s)\big)(1+sR_cC)\left(1+s\dfrac{L_M}{R_1}\right)}{\left(R^{-1}den(s)-R^{-1}(1+sR_cC)\left(1+R\dfrac{1-H_c(s)}{Z_c(s)}\right)\right)\left(1+s\dfrac{L_M}{R_1}\right)}, \qquad (5.32)$$

where $den(s)$ is defined in (2.43) and $F_f(s)$ is defined in (2.57). The denominator in (5.32) can be approximated by using (5.25). If $H_c(s)$ is according to (5.6) and the conditions (5.17)-(5.24) are fulfilled, an approximate version of the audio susceptibility is

$$\frac{\hat{v}_o(s)}{\hat{v}_g(s)} = \frac{T_sD}{L}\big(m_cD'-F_f(s)\big)K_2F_{l2ct}(s)F_{ESR}(s)F_{CT}(s)F_h(s), \qquad (5.33)$$

where $F_f(s)$ is a Taylor polynomial of degree 2 of $F_f(s)$ in (2.57), K_2 is defined in (5.26), $F_{l2ct}(s)$ is defined in (5.27), $F_{ESR}(s)$ is defined in (2.73), $F_{CT}(s)$ is defined in (5.31), and $F_h(s)$ is defined in (2.23).

Approximation of the Output Impedance

An approximate expression for the output impedance is presented in this subsection.

Since the stray resistances R_L, R_t, and R_d affect the output impedance significantly in the case where the capacitor current is measured with a current shunt, it is reasonable to assume that they do so also in the case where the capacitor current is measured with a current transformer. Therefore, the transfer functions derived in Chapter 3 are used as a starting point. (5.13) is rewritten by using (3.76) and (3.77):

$$
Z_{out}(s) = -\frac{\hat{v}_o(s)}{\hat{i}_{inj}(s)} = -\frac{\dfrac{R(1+sR_cC)}{den(s)} - \dfrac{R(1+sR_cC)\left(F_h^{-1}(s)+K_{sr}\right)}{den(s)}}{1 - \dfrac{R(1+sR_cC)}{den(s)}\left(\dfrac{1}{R} + \dfrac{1-H_c(s)}{Z_c(s)}\right)} =
$$

$$
\frac{\left(1-\left(F_h^{-1}(s)+K_{sr}\right)^{-1}\right)(1+sR_cC)\left(1+s\dfrac{L_M}{R_1}\right)}{\left(R^{-1}den(s) - R^{-1}(1+sR_cC)\left(1+R\dfrac{1-H_c(s)}{Z_c(s)}\right)\right)\dfrac{\left(1+s\dfrac{L_M}{R_1}\right)}{\left(F_h^{-1}(s)+K_{sr}\right)}}, \qquad (5.34)
$$

where $den(s)$ is defined in (3.79). If K_{sr} is zero, the denominator in (5.34) can be approximated with $K_2^{-1}F_{l2ct}^{-1}(s)$ according to (5.25). To check if it is reasonable to use this approximation also in the case where K_{sr} is not zero, the Bode plot for the denominator in (5.34) is compared with the Bode plot for $K_2^{-1}F_{l2ct}^{-1}(s)$. From Figure 5.4 it is seen that the approximation is good for the used parameter values, which are: $L_M = 2.81$ µH, $R_1 = 7.33$ mΩ, $R_c = 87.33$ mΩ, $R = 2$ Ω, and the rest are the same as the ones used in Chapter 4. Therefore, if $H_c(s)$ is according to (5.6) and the conditions (5.17)-(5.24) are fulfilled, a heuristic approximation of the output impedance in (5.34) is

$$
Z_{out}(s) = \left(1-\left(F_h^{-1}(s)+K_{sr}\right)^{-1}\right)K_2 F_{l2ct}(s) F_{ESR}(s) F_{CT}(s), \quad (5.35)
$$
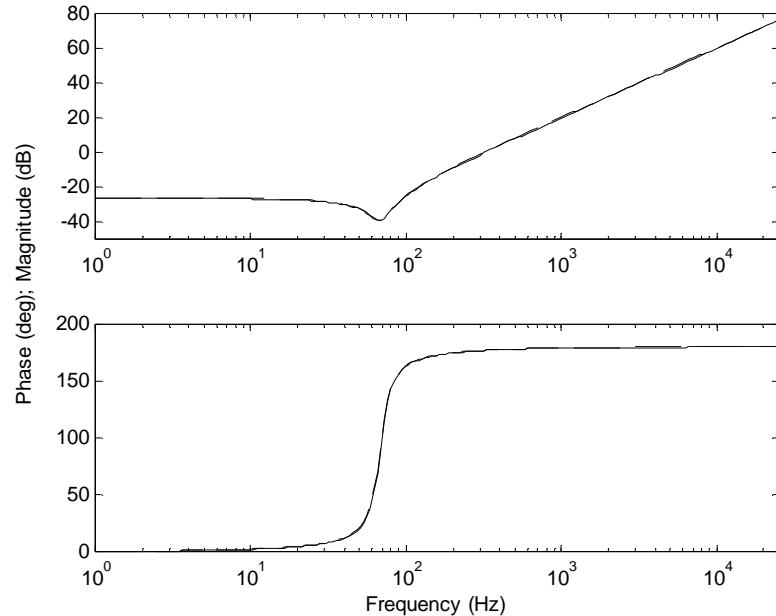
Figure 5.4: Comparing two Bode plots. Dashed line: denominator in (5.34). Solid line: $K_2^{-1} F_{l2ct}^{-1}(s)$. Note that the two lines almost coincide.

where $F_h(s)$ is defined in (2.23), K_{sr} is defined in (3.80), K_2 is defined in (5.26), $F_{l2ct}(s)$ is defined in (5.27), $F_{ESR}(s)$ is defined in (2.73), and $F_{CT}(s)$ is defined in (5.31).

Using Approximate Expressions in the Derivation

In this subsection, the consequences of using approximate expressions as a starting point in the derivation is discussed.

In the derivation of the control-to-output transfer function, (2.40) was used as a starting point instead of its approximate version (2.69). If the approximate version is used, it is found that the resulting transfer function makes bad predictions of simulation results near ω_{ct}. (A Bode plot that shows this is not included in this thesis.)

In the licentiate thesis, Johansson (2003), the approximate version is used as a starting point but it is mentioned that this may result in unreliable analysis. However, it is concluded that the resulting transfer function makes

good prediction of the value of the frequency function if $H_i(s)$ is equal to 1. It will now be shown that this may not be the case for other choices of $H_i(s)$.

In the case where the control-to-output transfer function (or the audio susceptibility) is analyzed, $i_{inj}(t)$ is considered to be zero. Therefore, (2.94) can be rewritten by using (2.95):

$$\hat{i}_c(s) = \hat{i}_{c2}(s) + H_i(s)\frac{\hat{v}_o(s)}{R}.$$
(5.36)

By combining (5.36) and (5.9), an expression for $H_i(s)$ is obtained:

$$\hat{i}_{c2}(s) + H_i(s)\frac{\hat{v}_o(s)}{R} = \hat{i}_{c2}(s) + \left(\frac{1}{R} + \frac{1 - H_c(s)}{Z_c(s)}\right)\hat{v}_o(s),$$
(5.37)

$$H_i(s) = 1 + R\frac{1 - H_c(s)}{Z_c(s)}.$$
(5.38)

Hence, the system in Figure 5.3 can be converted to the system in Figure 2.41 by using (5.38) if $i_{inj}(t)$ is zero. Furthermore, in the beginning of this subsection, it was mentioned that the control-to-output transfer function obtained by using approximate expressions in Figure 5.3 makes bad predictions of simulation results near ω_{ct}. The conclusion of all this is that (2.96) is not accurate in the case where $H_i(s)$ is according to (5.38) and $H_c(s)$ is according to (5.6).

5.4   Experimental Verification

The frequency functions predicted by the presented transfer functions and simulation model are compared with experimental results in this section. However, the conditions used to obtain the various results are first presented.

Conditions

The current transformer presented in Section 5.2 is used to measure the capacitor current. However, the current shunt is not removed, which means
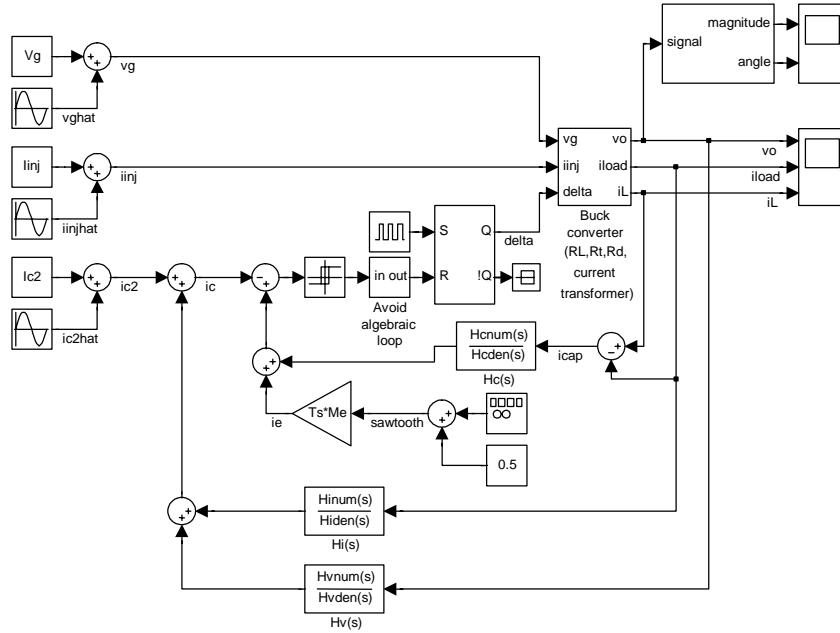
Figure 5.5: The simulation model where the capacitor current is calculated, filtered, and fed back.

that R_c is not changed so much between Chapter 4 and Chapter 5. The frequency functions are measured in the same way as in Section 4.2.

The simulation model in Figure 5.5 is used. The capacitor current is fed back in the inner loop instead of the inductor current (compare Figure 5.5 and Figure 3.6). The capacitor current is calculated from the inductor and load currents and then filtered using the transfer function for the (extended) current sensor (5.6). To model the impedance of the capacitor-current sensor, a resistor (*R1*) and an inductor (*LM*) are included in the buck converter subsystem as shown in Figure 5.6. The parameter values in Table 4.1 are used. Furthermore, L_M =2.81 µH, R_1 =7.33 mΩ, $H_i(s)$ =0, $H_v(s)$ =0, and I_{c2} is adjusted manually to obtain V_o equal to 12 V. Note that R_c is equal to 80 mΩ in the simulation model.

The parameter values in Table 4.1 are used also in the transfer functions except R_c, which is equal to 87.33 mΩ so that the impedance of the
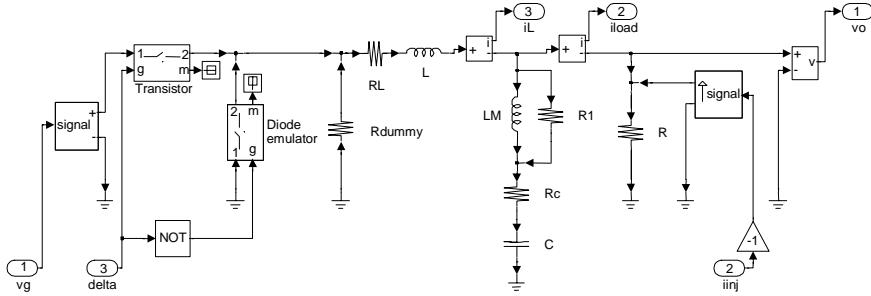
Figure 5.6: The buck converter subsystem where the impedance of the capacitor-current sensor is included.

capacitor-current sensor is taken care of. Furthermore, L_M =2.81 µH, R_1 =7.33 mΩ, D =0.5, and m_c is calculated according to (4.3).

Results

Figure 5.7 shows the Bode plot for the control-to-output transfer function in (5.30) when different loads are used. Simulation and experimental results are also shown in the figure for frequencies higher or equal to 10 Hz. From the figure it is seen that (5.30) is in good agreement with the simulation and experimental results. Compared to the case where a current shunt is used (Figure 4.3), a resonance is added at ω_{ct}, which is defined in (5.28). Note that ω_{ct} is the geometric mean of R_1/L_M, which is the corner frequency of the current transformer, and $T_s \left(m_c D'-0.5\right)/(LC)$, which approximately is the lowest corner frequency of the converter in the case where a current shunt is used (see (2.101)). Using (5.28), ω_{ct} is calculated to be 430 rad/s (68.4 Hz). Note that, contrary to previous Bode plots, simulation results for the frequency 66.6667 Hz ($\approx f_s/750$) are included to be able to verify the transfer function. According to (5.30), the control-to-output transfer function is almost independent of the load resistance, R. Only Q_{ct} in (5.29), which affects the height of the resonance peak, depends on R a little.

Figure 5.8 and Figure 5.9 show the corresponding results for the output impedance and audio susceptibility. The conclusions are the same. (5.35) and (5.33) are the used analytic models. As in Figure 4.9, the magnitude curves
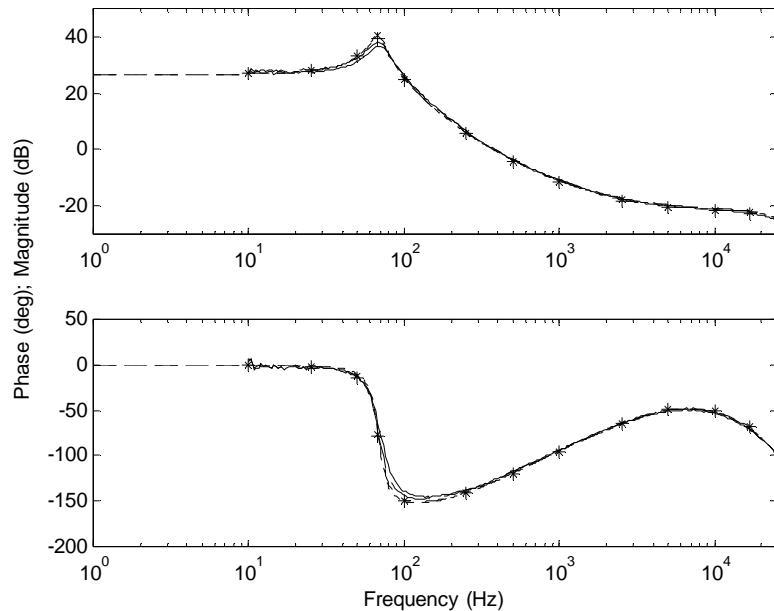
Figure 5.7: The control-to-output transfer function of the experimental buck converter when the capacitor current is measured with a current transformer and used for control. +: Simulation with $R = R_{min}$. Dash-dotted line: Analytic model with $R = R_{min}$. Solid line: Experiment with $R = R_{min}$. x: Simulation with $R = R_{max}$. Dotted line: Analytic model with $R = R_{max}$. Dashed line: Experiment with $R = R_{max}$. Note that the dash-dotted and dotted lines almost coincide.

from the experiments are shifted a little compared to the curves predicted by the simulation and analytic models for the audio susceptibility.

5.5   Summary and Concluding Remarks

A model for the capacitor-current sensor that uses a current transformer was first derived. We then derived a new model for the buck converter with feedback of the capacitor current, where the dynamics of a current sensor is
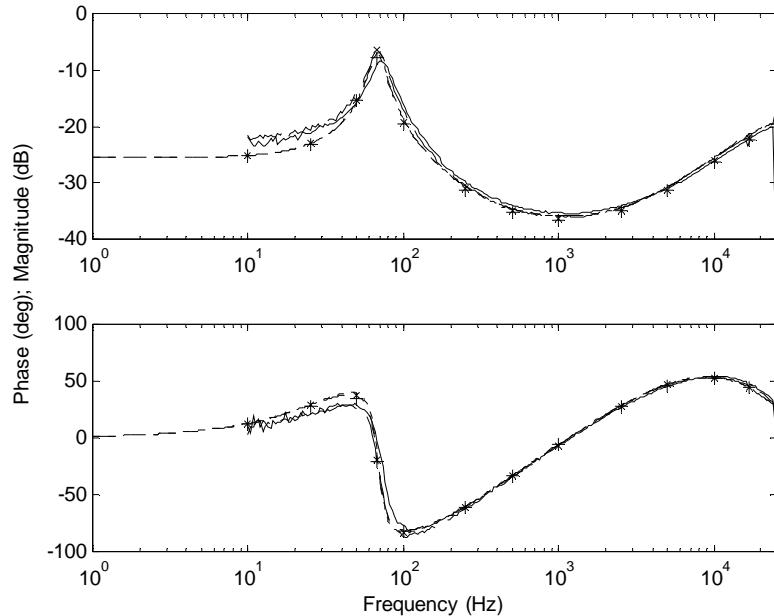
Figure 5.8: The output impedance of the experimental buck converter when the capacitor current is measured with a current transformer and used for control. +: Simulation with $R = R_{\min}$. Dash-dotted line: Analytic model with $R = R_{\min}$. Solid line: Experiment with $R = R_{\min}$. x: Simulation with $R = R_{\max}$. Dotted line: Analytic model with $R = R_{\max}$. Dashed line: Experiment with $R = R_{\max}$. Note that the dash-dotted and dotted lines almost coincide.

included. Approximate expressions for the control-to-output transfer function, audio susceptibility, and output impedance were also derived for the case where the sensor uses a current transformer. Finally, the approximate expressions were verified by means of experimental and simulation results.

One conclusion is that the high-pass-filter characteristics of the current transformer introduce a resonance in the converter at a low frequency. This frequency decreases if the corner frequency of the current transformer decreases. Another conclusion is that the analytic models are rather sensitive to approximations that are made in the middle of the derivation. Therefore, the (main) approximations are made at the end of the derivation.
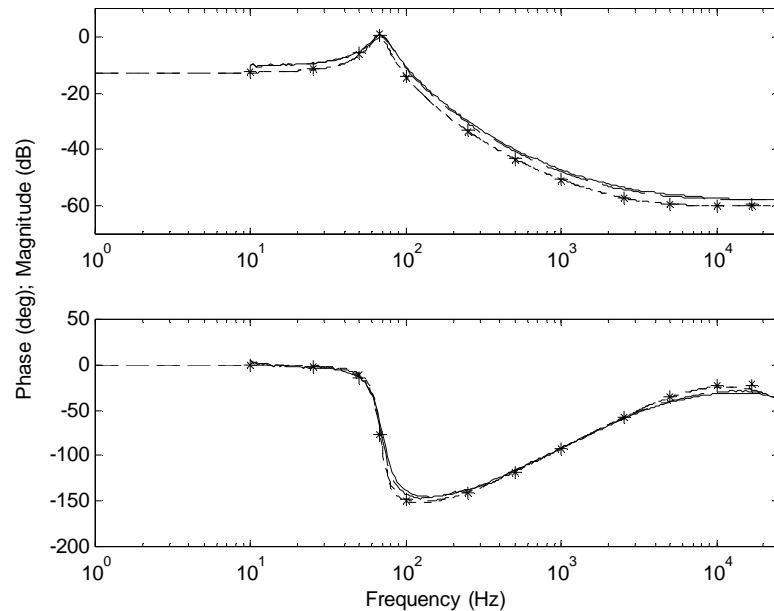
Figure 5.9: The audio susceptibility of the experimental buck converter when the capacitor current is measured with a current transformer and used for control. +: Simulation with $R = R_{min}$. Dash-dotted line: Analytic model with $R = R_{min}$. Solid line: Experiment with $R = R_{min}$. x: Simulation with $R = R_{max}$. Dotted line: Analytic model with $R = R_{max}$. Dashed line: Experiment with $R = R_{max}$. Note that the dash-dotted and dotted lines almost coincide.

5.6   Appendix

In Section 5.3, the denominators in the closed loop transfer functions were approximated using (5.25). In this section, (5.25) is derived. The left-hand-side expression in (5.25) is first approximated such that it consists of a product of three factors. To be able to do this approximation it is assumed that there are two high-frequency poles and two low-frequency poles. Next, two of the factors are approximated further to obtain the right-hand-side expression in (5.25). It is then shown that the conditions (5.17)-(5.24) ensure

that there are two high-frequency poles and two low-frequency poles. Finally, some remarks are presented.

Factorization

The expression to be approximated is denoted $den_{cl}(s)$ in this section:

$$den_{cl}(s) =$$
$$\left(R^{-1}den(s) - R^{-1}\left(1+sR_cC\right)\left(1+R\frac{1-H_c(s)}{Z_c(s)}\right)\right)\left(1+s\frac{L_M}{R_1}\right), \qquad (5.39)$$

where $den(s)$ is defined in (2.43). By using (5.16), (5.6), (2.43), and (2.23), $den_{cl}(s)$ is rewritten as follows:

$$den_{cl}(s) = R^{-1}\big(den(s) - (1 + s(R + R_c)C)\big)\left(1 + s\frac{L_M}{R_1}\right) + s^2 C\frac{L_M}{R_1} =$$

$$R^{-1}\left((1 + s(R + R_c)C)(F_h^{-1}(s) - 1) + \frac{RT_s}{L}(m_c D' - 0.5)(1 + sR_c C)\right) \bullet$$

$$\left(1 + s\frac{L_M}{R_1}\right) + s^2 C\frac{L_M}{R_1} =$$

$$\left((1 + s(R + R_c)C)\left(\frac{s}{R\omega_n Q} + \frac{s^2}{R\omega_n^2}\right) + \frac{T_s}{L}(m_c D' - 0.5)(1 + sR_c C)\right) \bullet$$

$$\left(1 + s\frac{L_M}{R_1}\right) + s^2 C\frac{L_M}{R_1} =$$

$$\frac{T_s}{L}(m_c D' - 0.5) +$$

$$\left(\frac{T_s}{L}(m_c D' - 0.5)R_c C + \frac{T_s}{L}(m_c D' - 0.5)\frac{L_M}{R_1} + \frac{1}{R\omega_n Q}\right)s +$$

$$\left(\frac{T_s}{L}(m_c D' - 0.5)R_c C\frac{L_M}{R_1} + C\frac{L_M}{R_1} + \frac{1}{R\omega_n^2} +\right.$$

$$\left.(R + R_c)C\frac{1}{R\omega_n Q} + \frac{1}{R\omega_n Q}\frac{L_M}{R_1}\right)s^2 +$$

$$\left((R + R_c)C\frac{1}{R\omega_n^2} + \frac{1}{R\omega_n^2}\frac{L_M}{R_1} + (R + R_c)C\frac{1}{R\omega_n Q}\frac{L_M}{R_1}\right)s^3 +$$

$$\left((R + R_c)C\frac{1}{R\omega_n^2}\frac{L_M}{R_1}\right)s^4 =$$

$$K_2^{-1}\big(1 + a_1 s + a_2 s^2 + a_3 s^3 + a_4 s^4\big) = K_2^{-1}P(s),$$

(5.40)

where K_2 is defined in (5.26),

$$P(s) = 1 + a_1 s + a_2 s^2 + a_3 s^3 + a_4 s^4, \tag{5.41}$$

$$a_1 = K_2 \left(\frac{T_s}{L} (m_c D' - 0.5) \left(R_c C + \frac{L_M}{R_1} \right) + \frac{1}{R\omega_n Q} \right), \qquad (5.42)$$

$$a_2 = K_2 \left(\frac{T_s}{L} (m_c D' - 0.5) R_c C \frac{L_M}{R_1} + C \frac{L_M}{R_1} + \frac{1}{R\omega_n^2} + \right.$$
$$\left. (R + R_c) C \frac{1}{R\omega_n Q} + \frac{1}{R\omega_n Q} \frac{L_M}{R_1} \right), \qquad (5.43)$$

$$a_3 = K_2 \left((R + R_c) C \frac{1}{R\omega_n^2} + \frac{1}{R\omega_n^2} \frac{L_M}{R_1} + (R + R_c) C \frac{1}{R\omega_n Q} \frac{L_M}{R_1} \right), \qquad (5.44)$$

$$a_4 = K_2 \left((R + R_c) C \frac{1}{R\omega_n^2} \frac{L_M}{R_1} \right). \qquad (5.45)$$

The following derivation is similar to the one made by Erickson and Maksimovic (2000, Section 8.1.8), Johansson (2003, Section 6.2), and Choi et al. (1999). The polynomial $P(s)$ in (5.41) is factored into

$$P(s) = \left(1 - p_1^{-1} s\right)\left(1 - p_2^{-1} s\right)\left(1 - p_3^{-1} s\right)\left(1 - p_4^{-1} s\right) =$$
$$\left(1 + \left(-p_1^{-1} - p_2^{-1}\right)s + p_1^{-1} p_2^{-1} s^2\right)\left(1 + \left(-p_3^{-1} - p_4^{-1}\right)s + p_3^{-1} p_4^{-1} s^2\right) =$$
$$1 + \left(-p_1^{-1} - p_2^{-1} - p_3^{-1} - p_4^{-1}\right)s +$$
$$\left(p_1^{-1} p_2^{-1} + p_1^{-1} p_3^{-1} + p_2^{-1} p_3^{-1} + p_1^{-1} p_4^{-1} + p_2^{-1} p_4^{-1} + p_3^{-1} p_4^{-1}\right)s^2 +$$
$$\left(-p_1^{-1} p_2^{-1} p_3^{-1} - p_1^{-1} p_2^{-1} p_4^{-1} - p_1^{-1} p_3^{-1} p_4^{-1} - p_2^{-1} p_3^{-1} p_4^{-1}\right)s^3 +$$
$$\left(p_1^{-1} p_2^{-1} p_3^{-1} p_4^{-1}\right)s^4, \qquad (5.46)$$

where p_1, p_2, p_3, and p_4 are the four poles. The coefficients a_1 and a_2 are identified by using (5.41) and (5.46):

$$a_1 = -p_1^{-1} - p_2^{-1} - p_3^{-1} - p_4^{-1}, \qquad (5.47)$$

$$a_2 = p_1^{-1} p_2^{-1} + p_1^{-1} p_3^{-1} + p_2^{-1} p_3^{-1} + p_1^{-1} p_4^{-1} + p_2^{-1} p_4^{-1} + p_3^{-1} p_4^{-1} \, . \qquad (5.48)$$

As mentioned in Section 5.3, the approximation is made with the assumption that there are two high-frequency poles and two low-frequency poles. This means that $|p_1| << |p_3|$, $|p_1| << |p_4|$, $|p_2| << |p_3|$, and $|p_2| << |p_4|$ if p_1 and p_2 are the two low-frequency poles. A consequence of this is that each of $|p_1 p_3|$, $|p_2 p_3|$, $|p_1 p_4|$, $|p_2 p_4|$, and $|p_3 p_4|$ is much larger than $|p_1 p_2|$. Therefore, a_1 and a_2 are approximated with

$$a_1 \approx -p_1^{-1} - p_2^{-1} \, , \qquad (5.49)$$

$$a_2 \approx p_1^{-1} p_2^{-1} \, . \qquad (5.50)$$

From the second row in (5.46) it is found that $P(s)$ can be approximated as follows by using (5.49) and (5.50):

$$\begin{aligned}
P(s) &\approx \left(1 + a_1 s + a_2 s^2\right)\left(1 + \left(-p_3^{-1} - p_4^{-1}\right)s + p_3^{-1} p_4^{-1} s^2\right) = \\
&\left(1 + a_1 s + a_2 s^2\right)\left(1 + b_1 s + b_2 s^2\right) = \\
&1 + \left(a_1 + b_1\right)s + \left(a_2 + a_1 b_1 + b_2\right)s^2 + \left(a_1 b_2 + a_2 b_1\right)s^3 + a_2 b_2 s^4 \, .
\end{aligned} \qquad (5.51)$$

The coefficients b_1 and b_2 are real since the poles p_3 and p_4 are either complex conjugated or real. The coefficients a_1 and a_2 are also real since the poles p_1 and p_2 are either complex conjugated or real. The first parenthesis in the second row in (5.51) represents the two low-frequency poles and the second parenthesis represents the two high-frequency poles. Approximate expressions for b_1 and b_2 are obtained by comparing (5.41) and (5.51):

$$b_2 \approx \frac{a_4}{a_2} \, , \qquad (5.52)$$

$$b_1 \approx \frac{a_3 - a_1 b_2}{a_2} \approx \frac{a_3 - a_1 \dfrac{a_4}{a_2}}{a_2} = \frac{a_3}{a_2} - \frac{a_1 a_4}{a_2^2} \, . \qquad (5.53)$$

(5.51) is rewritten by using (5.52) and (5.53):

$$P(s) \approx \left(1 + a_1 s + a_2 s^2\right)\left(1 + \left(\frac{a_3}{a_2} - \frac{a_1 a_4}{a_2^2}\right)s + \frac{a_4}{a_2}s^2\right). \tag{5.54}$$

By using (5.54), $den_{cl}(s)$ in (5.40) is approximated as follows:

$$den_{cl}(s) = K_2^{-1}P(s) \approx$$
$$K_2^{-1}\left(1 + a_1 s + a_2 s^2\right)\left(1 + \left(\frac{a_3}{a_2} - \frac{a_1 a_4}{a_2^2}\right)s + \frac{a_4}{a_2}s^2\right). \tag{5.55}$$

Further Approximations

In this subsection $den_{cl}(s)$ is approximated further. However, to do this some results are needed and they are first derived.

The following expression is rewritten by using (2.21) and (2.24):

$$\frac{1}{\omega_n Q} = \frac{1}{\dfrac{\pi}{T_s}\dfrac{1}{\pi(m_c D'-0.5)}} = T_s\left(m_c D'-0.5\right). \tag{5.56}$$

If $Q \geq 1$, (5.21) and (5.23) can be extended as follows:

$$\frac{1}{RC} << \frac{\omega_n}{Q} \leq \omega_n, \tag{5.57}$$

$$\frac{R_1}{L_M} << \frac{\omega_n}{Q} \leq \omega_n. \tag{5.58}$$

Similarly, (5.22) and (5.24) can be extended as follows if $Q < 1$:

$$\frac{1}{RC} << \omega_n Q < \omega_n, \tag{5.59}$$

$$\frac{R_1}{L_M} << \omega_n Q < \omega_n. \tag{5.60}$$

From (5.57) and (5.59), it is concluded that

$$\frac{1}{RC} << \omega_n \,,$$ (5.61)

and from (5.58) and (5.60), it is concluded that

$$\frac{R_1}{L_M} << \omega_n \,,$$ (5.62)

for all allowable values of Q .

The coefficient a_2 in (5.43) is approximated with

$$a_2 \approx K_2 C \frac{L_M}{R_1} \,.$$ (5.63)

To show that this is a valid approximation, the terms in the large parenthesis in (5.43) are compared with each other. The first term is compared with the second term by using (5.18):

$$\frac{T_s}{L}\left(m_c D'-0.5\right)R_c C \frac{L_M}{R_1} << C \frac{L_M}{R_1} \,.$$ (5.64)

The third term is compared with the second term by using (5.61) and (5.62):

$$\frac{1}{R\omega_n^2} = C \frac{1}{RC} \frac{1}{\omega_n^2} << C\omega_n \frac{1}{\omega_n^2} << C \frac{L_M}{R_1} \,.$$ (5.65)

Next, the fourth term is compared with the second term by using (5.17) and (5.24):

$$\left(R + R_c\right)C \frac{1}{R\omega_n Q} \approx C \frac{1}{\omega_n Q} << C \frac{L_M}{R_1} \,.$$ (5.66)

Finally, the fifth term is compared with the second term by using (5.22):

$$\frac{1}{R\omega_n Q}\frac{L_M}{R_1} = C\frac{1}{RC\omega_n Q}\frac{L_M}{R_1} << C\frac{L_M}{R_1}\,. \tag{5.67}$$

Form (5.64)-(5.67) it is concluded that a_2 in (5.43) can be approximated according to (5.63).

The approximation of the coefficient a_3 in (5.44) is now considered. The third term in the large parenthesis in (5.44) is approximated by using (5.17):

$$\left(R + R_c\right)C\frac{1}{R\omega_n Q}\frac{L_M}{R_1} \approx C\frac{1}{\omega_n Q}\frac{L_M}{R_1}\,. \tag{5.68}$$

By using (5.17) and (5.23), the first term in the large parenthesis in (5.44) is compared with (5.68):

$$\left(R + R_c\right)C\frac{1}{R\omega_n^2} \approx C\frac{1}{\omega_n^2} = C\frac{1}{\omega_n Q}\frac{Q}{\omega_n} << C\frac{1}{\omega_n Q}\frac{L_M}{R_1}\,. \tag{5.69}$$

Next, the second term in the large parenthesis in (5.44) is compared with (5.68) by using (5.21):

$$\frac{1}{R\omega_n^2}\frac{L_M}{R_1} = C\frac{1}{RC}\frac{1}{\omega_n^2}\frac{L_M}{R_1} << C\frac{\omega_n}{Q}\frac{1}{\omega_n^2}\frac{L_M}{R_1} = C\frac{1}{\omega_n Q}\frac{L_M}{R_1}\,. \tag{5.70}$$

Form (5.68)-(5.70) it is concluded that a_3 in (5.44) can be approximated with

$$a_3 \approx K_2 C\frac{1}{\omega_n Q}\frac{L_M}{R_1}\,. \tag{5.71}$$

The coefficient a_4 in (5.45) is approximated by using (5.17):

$$a_4 \approx K_2 C\frac{1}{\omega_n^2}\frac{L_M}{R_1}\,. \tag{5.72}$$

The first parenthesis in (5.55) is approximated and rewritten by using (5.42), (5.63), (5.26), (5.56), (5.28), (5.29), and (5.27):

$$1 + a_1 s + a_2 s^2 \approx$$

$$1 + K_2 \left(\frac{T_s}{L}(m_c D'{-}0.5)R_c C + \frac{T_s}{L}(m_c D'{-}0.5)\frac{L_M}{R_1} + \frac{1}{R\omega_n Q} \right)s +$$

$$K_2 C \frac{L_M}{R_1} s^2 =$$

$$1 + \left(R_c C + \frac{L_M}{R_1} + \frac{1}{\dfrac{T_s}{L}(m_c D'{-}0.5)} \frac{1}{R\omega_n Q} \right)s +$$

$$\frac{1}{\dfrac{T_s}{L}(m_c D'{-}0.5)} C \frac{L_M}{R_1} s^2 =$$

$$1 + \left(R_c C + \frac{L_M}{R_1} + \frac{L}{R} \right)s + \frac{s^2}{\dfrac{T_s}{LC}(m_c D'{-}0.5)\dfrac{R_1}{L_M}} =$$

$$1 + \frac{s}{\omega_{ct} Q_{ct}} + \frac{s^2}{\omega_{ct}^2} = F_{l2ct}^{-1}(s). \tag{5.73}$$

The second parenthesis in (5.55) is approximated by using (5.42), (5.63), (5.71), and (5.72):

$$1 + \left(\frac{a_3}{a_2} - \frac{a_1 a_4}{a_2^2}\right) s + \frac{a_4}{a_2} s^2 \approx 1 + \left(\frac{K_2 C \dfrac{1}{\omega_n Q} \dfrac{L_M}{R_1}}{K_2 C \dfrac{L_M}{R_1}} - \right.$$

$$\left. \frac{K_2 \left(\dfrac{T_s}{L}(m_c D'-0.5)\left(R_c C + \dfrac{L_M}{R_1}\right) + \dfrac{1}{R \omega_n Q}\right) K_2 C \dfrac{1}{\omega_n^2} \dfrac{L_M}{R_1}}{\left(K_2 C \dfrac{L_M}{R_1}\right)^2} \right) s +$$

$$\frac{K_2 C \dfrac{1}{\omega_n^2} \dfrac{L_M}{R_1}}{K_2 C \dfrac{L_M}{R_1}} s^2 = \tag{5.74}$$

$$1 + \left(\frac{1}{\omega_n Q} - \frac{R_c T_s}{L}(m_c D'-0.5)\frac{1}{\omega_n^2} \frac{R_1}{L_M} - \frac{T_s}{L}(m_c D'-0.5)\frac{1}{C \omega_n^2} - \right.$$

$$\left. \frac{1}{RC} \frac{1}{\omega_n Q} \frac{1}{\omega_n^2} \frac{R_1}{L_M} \right) s + \frac{1}{\omega_n^2} s^2 .$$

To approximate (5.74) further, the terms in the (last) parenthesis are compared with each other. The second term is compared with the first term by using (5.18) and (5.23):

$$\frac{R_c T_s}{L}(m_c D'-0.5)\frac{1}{\omega_n^2} \frac{R_1}{L_M} \ll \frac{1}{\omega_n^2} \frac{R_1}{L_M} \ll \frac{1}{\omega_n^2} \frac{\omega_n}{Q} = \frac{1}{\omega_n Q} . \tag{5.75}$$

Next, the third term is compared with the first term by using (5.56) and (5.19):

$$\frac{T_s}{L}(m_c D'-0.5)\frac{1}{C \omega_n^2} = \frac{1}{LC} \frac{1}{\omega_n Q} \frac{1}{\omega_n^2} \ll \omega_n^2 \frac{1}{\omega_n Q} \frac{1}{\omega_n^2} = \frac{1}{\omega_n Q} . \tag{5.76}$$

Finally, the fourth term is compared with the first term by using (5.61) and (5.62):

$$\frac{1}{RC}\frac{1}{\omega_n Q}\frac{1}{\omega_n^2}\frac{R_1}{L_M} << \omega_n \frac{1}{\omega_n Q}\frac{1}{\omega_n^2}\omega_n = \frac{1}{\omega_n Q}\,. \qquad (5.77)$$

(5.74) is approximated as follows by using (5.75)-(5.77):

$$1+\left(\frac{a_3}{a_2}-\frac{a_1 a_4}{a_2^2}\right)s+\frac{a_4}{a_2}s^2 \approx 1+\frac{1}{\omega_n Q}s+\frac{1}{\omega_n^2}s^2 = F_h^{-1}(s)\,, \qquad (5.78)$$

where $F_h(s)$ is defined in (2.23). By using (5.73) and (5.78), $den_{cl}(s)$ in (5.55) is approximated with

$$den_{cl}(s) \approx K_2^{-1}F_{l2ct}^{-1}(s)F_h^{-1}(s)\,, \qquad (5.79)$$

where K_2 is defined in (5.26), $F_{l2ct}(s)$ is defined in (5.27), and $F_h(s)$ is defined in (2.23).

Distances between Poles

In the derivation of the approximate $den_{cl}(s)$ it is assumed that there are two high-frequency poles and two low-frequency poles. In this subsection it is shown that the conditions (5.17)-(5.24) ensure that this assumption is fulfilled. For simplicity, the approximate $den_{cl}(s)$ in (5.79) is utilized to show this even if it is somewhat unsatisfactory to utilize the result of the approximation to show that the approximation is valid.

Assume that there are two high-frequency poles and two low-frequency poles. According to (5.79), the two low-frequency poles are given by $F_{l2ct}(s)$ and the two high-frequency poles are given by $F_h(s)$. The two low-frequency poles, p_1 and p_2, are obtain by solving the equation where the denominator in $F_{l2ct}(s)$ is set equal to zero:

$$p_1, p_2 = -\frac{\omega_{ct}}{2Q_{ct}} \pm \sqrt{\frac{\omega_{ct}^2}{4Q_{ct}^2}-\omega_{ct}^2} = -\frac{\omega_{ct}}{2Q_{ct}} \pm \sqrt{\omega_{ct}^2\left(\frac{1}{4Q_{ct}^2}-1\right)}\,. \qquad (5.80)$$

From (5.80) it is seen that p_1 and p_2 are complex conjugates if and only if $Q_{ct} > 0.5$. In this case, (5.80) can be rewritten as

$$p_1, p_2 = -\frac{\omega_{ct}}{2Q_{ct}} \pm j\sqrt{\omega_{ct}^2 - \frac{\omega_{ct}^2}{4Q_{ct}^2}} \qquad (5.81)$$

and the distance from each of p_1 and p_2 to the origin is

$$|p_{1,2}| = \sqrt{\left(-\frac{\omega_{ct}}{2Q_{ct}}\right)^2 + \left(\sqrt{\omega_{ct}^2 - \frac{\omega_{ct}^2}{4Q_{ct}^2}}\right)^2} = \omega_{ct} . \qquad (5.82)$$

If $Q_{ct} \leq 0.5$, p_1 and p_2 are real and

$$p_1 = -\frac{\omega_{ct}}{2Q_{ct}} + \sqrt{\frac{\omega_{ct}^2}{4Q_{ct}^2} - \omega_{ct}^2} , \qquad (5.83)$$

$$p_2 = -\frac{\omega_{ct}}{2Q_{ct}} - \sqrt{\frac{\omega_{ct}^2}{4Q_{ct}^2} - \omega_{ct}^2} . \qquad (5.84)$$

If Q_{ct} decreases from 0.5, p_1 moves from $-\omega_{ct}$ to the right along the real axis and p_2 moves from $-\omega_{ct}$ to the left along the real axis.

According to Erickson and Maksimovic (2000, Section 8.1.7), the poles can be approximated as follows if $Q_{ct} \ll 0.5$:

$$p_{1a} = -\omega_{ct}Q_{ct} \approx p_1 , \qquad (5.85)$$

$$p_{2a} = -\frac{\omega_{ct}}{Q_{ct}} \approx p_2 . \qquad (5.86)$$

Furthermore, if $Q_{ct} \leq 0.5$,

$$|p_{1a}| \leq |p_1| , \qquad (5.87)$$

$$|p_{2a}| \geq |p_2|. \tag{5.88}$$

Note that $p_{1a} = p_1/2$ and $p_{2a} = 2p_2$ if $Q_{ct} = 0.5$. Hence, the relative errors of p_{1a} and p_{2a} are large for this value of Q_{ct}.

We will now investigate how p_1 and p_2 depend on the corner frequency of the current transformer, R_1/L_M. The approximations in (5.85) and (5.86) are rewritten as follows by using (5.29) and (5.28):

$$p_{1a} = -\omega_{ct} Q_{ct} = -\frac{1}{R_c C + \dfrac{L}{R} + \dfrac{L_M}{R_1}}, \tag{5.89}$$

$$p_{2a} = -\frac{\omega_{ct}}{Q_{ct}} = -\frac{T_s}{LC}(m_c D' - 0.5)\frac{R_1}{L_M}\left(R_c C + \frac{L}{R} + \frac{L_M}{R_1}\right). \tag{5.90}$$

From the definitions of Q_{ct} and ω_{ct} in (5.29) and (5.28) it is concluded that Q_{ct} is low if R_1/L_M is low. Therefore, p_1 and p_2 can be approximated by using (5.89) and (5.90) in this case. Assume that R_1/L_M tends to zero. At the limit the following is obtained. p_1 is equal to zero and p_2 is equal to $-T_s(m_c D' - 0.5)/(LC)$, which approximately is the same as the low-frequency pole in the case where a current shunt is used to measure the capacitor current (see (2.101)). This is not a surprise since the gain of the current sensor is independent of the frequency if the corner frequency of the current transformer is zero. The pole p_1 is cancelled by the zero in $F_{CT}(s)$ since the zero also is positioned at the origin (see (5.31)).

If R_1/L_M increases from zero, p_1 moves from the origin to the left along the real axis. Hence, if $Q_{ct} \leq 0.5$, then $p_1 \leq 0$. p_2 is positioned to the left of p_1 (or they coincide) in this case. The conclusion is that $|p_2| \geq |p_1|$ if $Q_{ct} \leq 0.5$. By using (5.88), we obtain $|p_{2a}| \geq |p_2| \geq |p_1|$ if $Q_{ct} \leq 0.5$. According to (5.82), $|p_{1,2}| = \omega_{ct}$ if $Q_{ct} > 0.5$. Therefore, if it can be shown that $|p_3| \gg |p_{2a}|$, $|p_3| \gg \omega_{ct}$, $|p_4| \gg |p_{2a}|$, and $|p_4| \gg \omega_{ct}$, then there are two high-frequency poles and two low-frequency poles. To do this, the positions of the poles p_3 and p_4 are first considered. These two high-frequency poles are given by $F_h(s)$ in (2.23) according to (5.79). If $Q > 0.5$, p_3 and p_4 are complex conjugates and $|p_{3,4}| = \omega_n$. If $Q \leq 0.5$, p_3 and p_4 are real and can be approximated with

$$p_{3a} = -\omega_n Q \approx p_3 \,, \qquad\qquad (5.91)$$

$$p_{4a} = -\frac{\omega_n}{Q} \approx p_4 \,. \qquad\qquad (5.92)$$

Furthermore, $|p_4| \geq |p_3| \geq |p_{3a}|$ if $Q \leq 0.5$ (see (5.87)). If $0.5 < Q \leq 1$, $|p_{3,4}| = \omega_n$ and, therefore, $|p_{3,4}| \geq |p_{3a}|$. Hence, $|p_4| \geq |p_3| \geq |p_{3a}|$ if $Q \leq 1$. Therefore, if it can be shown that $|p_{3a}| \gg |p_{2a}|$ and $|p_{3a}| \gg \omega_{ct}$ when $Q \leq 1$ and that $\omega_n \gg |p_{2a}|$ and $\omega_n \gg \omega_{ct}$ when $Q > 1$, then there are two high-frequency poles and two low-frequency poles. The rest of this subsection is devoted to showing that this is the case.

First, consider the case where $Q \leq 1$. To show that $|p_{3a}| \gg |p_{2a}|$, each of the terms in p_{2a} is compared with $|p_{3a}|$. By using (5.18) and (5.24) we have

$$\frac{T_s}{LC}(m_c D'-0.5)\frac{R_1}{L_M}R_c C \ll \frac{R_1}{L_M} \ll \omega_n Q \,. \qquad (5.93)$$

The following is obtained by using (5.56), (5.22), and (5.24):

$$\frac{T_s}{LC}(m_c D'-0.5)\frac{R_1}{L_M}\frac{L}{R} = \frac{1}{RC}\frac{1}{\omega_n Q}\frac{R_1}{L_M} \ll \frac{R_1}{L_M} \ll \omega_n Q \,. \qquad (5.94)$$

Finally, by using (5.56) and (5.20) we obtain the following:

$$\frac{T_s}{LC}(m_c D'-0.5)\frac{R_1}{L_M}\frac{L_M}{R_1} = \frac{1}{\sqrt{LC}}\frac{1}{\sqrt{LC}}\frac{1}{\omega_n Q} \ll \frac{1}{\sqrt{LC}} \ll \omega_n Q \,. \qquad (5.95)$$

Since the operator $\ll$ occurs two times in each of (5.93), (5.94), and (5.95), it is reasonable to claim that

$$|p_{2a}| = \frac{T_s}{LC}(m_c D'-0.5)\frac{R_1}{L_M}\left(R_c C + \frac{L}{R} + \frac{L_M}{R_1}\right) \ll \omega_n Q = |p_{3a}| \,. \qquad (5.96)$$

To show that $|p_{3a}| \gg \omega_{ct}$, assume first that $T_s(m_c D'-0.5)/(LC) \leq R_1/L_M$. By using (5.28), (5.24), and (5.91) we have

$$\omega_{ct} = \sqrt{\frac{T_s}{LC}(m_c D'{-}0.5)\frac{R_1}{L_M}} \leq \sqrt{\frac{R_1}{L_M}\frac{R_1}{L_M}} << \omega_n Q = |p_{3a}|. \qquad (5.97)$$

Assume now that $T_s(m_c D'{-}0.5)/(LC) > R_1/L_M$. The following is obtained by using (5.28), (5.20), and (5.91):

$$\omega_{ct} = \sqrt{\frac{T_s}{LC}(m_c D'{-}0.5)\frac{R_1}{L_M}} < \sqrt{\left(\frac{T_s}{LC}(m_c D'{-}0.5)\right)^2} =$$
$$\frac{1}{LC}\frac{1}{\omega_n Q} << \omega_n Q = |p_{3a}|. \qquad (5.98)$$

From (5.97) and (5.98) it is concluded that $|p_{3a}| >> \omega_{ct}$.

Next, consider the case where $Q > 1$. This case is treated similarly as the case where $Q \leq 1$. To show that $\omega_n >> |p_{2a}|$, each of the terms in p_{2a} is compared with ω_n . By using (5.18) and (5.62) we have

$$\frac{T_s}{LC}(m_c D'{-}0.5)\frac{R_1}{L_M}R_c C << \frac{R_1}{L_M} << \omega_n . \qquad (5.99)$$

The following is obtained by using (5.56), (5.61), and (5.62):

$$\frac{T_s}{LC}(m_c D'{-}0.5)\frac{R_1}{L_M}\frac{L}{R} =$$
$$\frac{1}{RC}\frac{1}{\omega_n Q}\frac{R_1}{L_M} < \frac{1}{RC}\frac{1}{\omega_n}\frac{R_1}{L_M} << \frac{R_1}{L_M} << \omega_n . \qquad (5.100)$$

Finally, by using (5.56) and (5.19) we obtain the following:

$$\frac{T_s}{LC}(m_c D'{-}0.5)\frac{R_1}{L_M}\frac{L_M}{R_1} =$$
$$\frac{1}{\sqrt{LC}}\frac{1}{\sqrt{LC}}\frac{1}{\omega_n Q} < \frac{1}{\sqrt{LC}}\frac{1}{\sqrt{LC}}\frac{1}{\omega_n} << \frac{1}{\sqrt{LC}} << \omega_n . \qquad (5.101)$$

From (5.99)-(5.101) it is concluded that

$$\left| p_{2a} \right| = \frac{T_s}{LC}\left(m_c D'-0.5 \right)\frac{R_1}{L_M}\left(R_c C + \frac{L}{R} + \frac{L_M}{R_1} \right) << \omega_n . \qquad (5.102)$$

To show that $\omega_n >> \omega_{ct}$, assume first that $T_s\left(m_c D'-0.5 \right)/(LC) \le R_1/L_M$. By using (5.28) and (5.62) we have

$$\omega_{ct} = \sqrt{\frac{T_s}{LC}\left(m_c D'-0.5 \right)\frac{R_1}{L_M}} \le \sqrt{\frac{R_1}{L_M}\frac{R_1}{L_M}} << \omega_n . \qquad (5.103)$$

Assume now that $T_s\left(m_c D'-0.5 \right)/(LC) > R_1/L_M$. The following is obtained by using (5.28) and (5.19):

$$\omega_{ct} = \sqrt{\frac{T_s}{LC}\left(m_c D'-0.5 \right)\frac{R_1}{L_M}} < \sqrt{\left(\frac{T_s}{LC}\left(m_c D'-0.5 \right) \right)^2} =$$

$$\frac{1}{LC}\frac{1}{\omega_n Q} < \frac{1}{LC}\frac{1}{\omega_n} << \omega_n . \qquad (5.104)$$

From (5.103) and (5.104) it is concluded that $\omega_n >> \omega_{ct}$.

All the different cases are considered and the conclusion is that there are two high-frequency poles and two low-frequency poles if the conditions (5.17)-(5.24) are fulfilled.

Remarks

The conditions (5.21) and (5.23) set an upper limit for Q. If Q is very high, the two high-frequency poles are not according to $F_h(s)$ and the predictions made by the approximate expression is bad near ω_n. In Section 2.6, approximate versions of the expressions for the control-to-output transfer function, the output impedance, and the audio susceptibility obtained by applying the improved Ridley model to the buck converter were presented. This model assumes that only the inductor current is fed back. The approximate versions of the expressions are valid if the conditions (2.63)-(2.67) are fulfilled. Note that the conditions (2.63)-(2.67) do not set at an upper limit for Q. Therefore, in the case where (only) the inductor current is fed back the two high-frequency poles are according to $F_h(s)$ also when Q is very high.

The derivation of (5.25), made in this section, is not foolproof. The approximation in (5.25) is based on a sequence of approximations:

$$x_1 \approx x_2 \approx x_3 \approx \ldots \approx x_N . \qquad (5.105)$$

If N is large, x_N may be a bad approximation of x_1.

Chapter 6 Summary and Future Work

The work presented in this thesis is summarized in this chapter. Furthermore, suggestions for future work are presented.

6.1   Results

In the licentiate thesis, Johansson (2003), a number of analytic models for buck, boost and buck-boost converters were developed and analyzed in detail. To verify the models, the frequency functions predicted by them were compared with results from switched (large-signal) simulation models.

In this thesis, additional results have been presented for the buck converter. An experimental buck converter has been built. Experimental results obtained by means of a network analyzer are presented and compared with the frequency functions predicted by the developed analytic models and the simulation models. The experimental results have verified the control-to-output transfer functions and the audio susceptibility. However, the differences between the experimental result and the results predicted by the analytic and simulation models are significant for the output impedance at low frequencies in the case where the measured load current is utilized for control.

A new transfer function for the output impedance has been derived where the stray resistances in the inductor, transistor, and diode were considered. These stray resistances are also included in a new simulation model. We concluded that the frequency functions predicted by the new transfer function for the output impedance and the new simulation model are in good agreement with the experimental result.

The new transfer function shows that the output impedance is sensitive to the stray resistances if the load current is used for control as proposed by Redl

177

and Sokal (1986). The measured inductor and load currents are in this control technique only used to calculate the difference, i.e. the capacitor current. Hence, the capacitor current is controlled. Since the inductor current is not controlled, the output impedance is sensitive to the stray resistances. If current-mode control is used and the load current is not used for control, the inductor current is controlled and the indictor acts as a current source. Therefore, the output impedance is insensitive to the stray resistances, which are connected in series with the inductor.

Since the capacitor current is controlled in the control proposed by Redl and Sokal (1986), cascade control is obtained when an outer voltage controller is added. If a gain-scheduling controller is designed in such a way that the measurements of the inductor and load currents are used only to calculate the difference, i.e. the capacitor current, the obtained gain scheduling controller will simply act as a cascade controller.

In this thesis, an analytic model and a simulation model were developed for the case where the capacitor current is measured by means of a current transformer instead of a current shunt and they were verified by means of experimental results. Low-frequency resonance is introduced in the frequency functions predicted by the three major transfer functions in this case due to the high-pass-filter characteristics of the current transformer. The resonance frequency decreases if the corner frequency of the current transformer decreases.

6.2   Implications of the Results

The results of this and the licentiate thesis were summarized in Section 6.1 and Chapter 2, respectively. The practical importance of some of the results was discussed in Section 1.4. We concluded that the result that is the most interesting to use in practice is probably the model for the case where the load current is measured (indirectly) by means of a current transformer and used for control since the resonance may affect the design of the (outer) voltage controller.

Other results may not in practice affect the design of converters but can still be valuable knowledge for a designer of dc-dc converters. A designer can obtain increased understanding of the properties of the converters and the reasons for differences between some models and experimental results.

The results that are of little practical interest can be of academic interest since it is easier to draw conclusions from an analysis if it is known that the error in the model that is used as a starting point is small.

6.3   Future Work

Suggestions for future work are summarized here.

- The novel model for the audio susceptibility derived in the licentiate thesis is sensitive to errors (Johansson, 2003, Section 4.4) and the model should be modified in order to reduce this sensitivity.
- The improved Ridley model includes in some cases unstable feedforward transfer functions (Johansson, 2003, Sections 5.3 and 5.4) and the improvement should be made such that they are stable. An idea of how to do this was presented in Johansson (2003, Section 5.5).
- Models for the case where measured load current is used for control were derived in Johansson (2003, Sections 7.4-7.6) by using approximate expressions presented in Johansson (2003, Chapter 6) as a starting point. The non-approximate expressions should be used as a starting point and the approximations should be made at the end of the derivation (see Johansson (2003, Section 7.7)).
- Suitable methods to identify more complex loads should be found. How to use the identification result in an adaptive controller should be investigated. (See Section 1.2.)

Chapter 7 References

Al-Mothafar, M. R. D., Hammad, K. A. (1999), Small-signal modelling of peak current-mode controlled buck-derived circuits, *IEE Proceedings - Electric Power Applications*, vol. 146, no. 6, pp. 607-619, 1999.

Carrasco, J. M., Tombs, J., Torralba, A., Ridao, F. P., Franquelo, L.G. (1995), An analog fuzzy logic controller for power converters, *IEEE International Conference on Industrial Electronics, Control, and Instrumentation (IECON 95)*, vol. 2, pp. 1490-1495, 1995.

Chen, C. –T. (1999), *Linear system theory and design*, Third edition, Oxford University Press, ISBN 0-19-511777-8.

Cho, B. H., Lee, F. C. (1984), Measurement of loop gain with the digital modulator, *IEEE Power Electronics Specialists Conference Record*, pp. 363-373, 1984.

Choi, B., Cho, B. H., Hong, S. –S. (1999), Dynamics and control of DC-to-DC converters driving other converters downstream, *IEEE Transactions on Circuits and System-I: Fundamental Theory and Applications*, vol. 46, no. 10, pp. 1240-1248, 1999.

Choi, B., Kim, J., Cho, B. H., Choi, S., Wildrick, C. M. (2002), Designing control loop for DC-to-DC converters loaded with unknown AC dynamics, *IEEE Transactions on Industrial Electronics*, vol. 49, no. 4, pp. 925-932, 2002.

Clique, M., Fossard, A. J. (1977), A general model for switching converters, *IEEE Transactions on Aerospace and Electronic Systems*, vol. AES-13, no. 4, pp. 397-400, 1977.

Erickson, R. W., Maksimovic, D. (2000), *Fundamentals of power electronics*, Second edition, Kluwer Academic Publishers, ISBN 0-7923-7270-0.

Feng, X., Liu, J., Lee, F. C. (2002), Impedance specifications for stable DC distributed power systems, *IEEE Transactions on Power Electronics*, vol. 17, no. 2, pp. 157-162, 2002.

Goodwin, G. C., Graebe, S. F., Salgado, M. E. (2001), *Control System Design*, Prentice-Hall, ISBN 0-13-958653-9.

Hiti, S., Borojevic, D. (1993), Robust nonlinear control for boost converter, *IEEE Power Electronics Specialists Conference Record*, pp. 191-196, 1993.

Ioannidis, G., Kandianis, A., Manias, S. N. (1998), Novel control design for the buck converter, *IEE Proceedings - Electric Power Applications*, vol. 145, no. 1, pp. 39-47, 1998.

Ioannidis, G. C., Manias, S. N. (1999), H_∞ loop-shaping control schemes for the buck converter and their evaluation using μ-analysis, *IEE Proceedings - Electric Power Applications*, vol. 146, no. 2, pp. 237-246, 1999.

Johansson, B., Lenells, M. (2000), Possibilities of obtaining small-signal models of DC-to-DC power converters by means of system identification, *IEEE International Telecommunications Energy Conference*, pp. 65-75, 2000.

Johansson, B. (2002a), Analysis of DC-DC converters with current-mode control and resistive load when using load current measurements for control, *IEEE Power Electronics Specialists Conference*, vol. 1, pp. 165-172, 2002.

Johansson, B. (2002b), A comparison and an improvement of two continuous-time models for current-mode control, *IEEE International Telecommunications Energy Conference*, pp. 552-559, 2002.

Johansson, B. (2003), *Improved models for DC-DC converters*, Licentiate thesis, Department of Industrial Electrical Engineering and Automation, Lund University, Lund, Sweden, ISBN 91-88934-29-2.

Kanemaru, S., Nabeshima, T., Nakano, T. (2001), Transient response in a DC-DC converter employing load-current feedforward control, *Electronics and Communications in Japan*, part 1, vol. 84, no. 8, pp. 14-22, 2001.

Kislovski, A. S., Redl, R., Sokal, N. O. (1991), *Dynamic analysis of switching-mode dc/dc converters*, Van Nostrand Reinhold, ISBN 0-442-23916-5.

Ljung, L. (1999), *System identification: theory for the user*, Second edition, Prentice-Hall, ISBN 0-13-656695-2.

Lo, Y. –W., King, R. J. (1999), Sampled-data modeling of the average-input current-mode-controlled buck converter, *IEEE Transactions on Power Electronics*, vol. 14, no. 5, pp. 918-927, 1999.

Mayer, E. A., King, R. J. (2001), An improved sampled-data current-mode-control model which explains the effects of control delay, *IEEE Transactions on Power Electronics*, vol. 16, no. 3, pp. 369-374, 2001.

Middlebrook, R. D., Cuk, S. (1976), A general unified approach to modeling switching converter power stages, *IEEE Power Electronics Specialists Conference Record*, pp. 18-34, 1976.

Mitchell, D. M. (1988), *Switching regulator analysis*, McGraw-Hill, ISBN 0-07-042597-3.

Poon, F. N. K., Tse, C. K., Liu, J. C. P. (1999), Very fast transient voltage regulators based on load correction, *IEEE Power Electronics Specialists Conference*, vol. 1, pp. 66-71, 1999.

Redl, R., Sokal, N. O. (1986), Near-optimum dynamic regulation of dc-dc converters using feedforward and current-mode control, *IEEE Transactions on Power Electronics*, vol. 1, no. 3, pp. 181-192, 1986.

Ridley, R. B. (1990a), A new, continuous-time model for current-mode control with constant frequency, constant on-time, and constant off-time, in CCM and DCM, *IEEE Power Electronics Specialists Conference Record*, pp. 382-389, 1990.

Ridley, R. B. (1990b), A new small-signal model for current-mode control, Ph.D. dissertation, Virginia Polytechnic Institute and State University, Blacksburg, 1990.

Ridley, R. B. (1991), A new, continuous-time model for current-mode control, *IEEE Transactions on Power Electronics*, vol. 6, no. 2, pp. 271-280, 1991.

Schoneman, G. K., Mitchell, D. M. (1989), Output impedance considerations for switching regulators with current-injected control, *IEEE Transactions on Power Electronics*, vol. 4, no. 1, pp. 25-35, 1989.

Sudhoff, S. D., Glover, S. F., Lamm, P. T., Schmucker, D. H., Delisle, D. E. (2000), Admittance space stability analysis of power electronic systems, *IEEE Transactions on Aerospace and Electronic Systems*, vol. 36, no. 3, pp. 965-973, 2000.

Sun, J., Mitchell, D. M., Greuel, M. F., Krein, P. T., Bass, R. M. (2001), Averaged modeling of PWM converters operating in discontinuous conduction mode, *IEEE Transactions on Power Electronics*, vol. 16, no. 4, pp. 482-492, 2001.

Suntio, T., Kostov, K., Tepsa, T., Kyyrä, J. (2003), Effect of output current feedback on converter dynamics, *European Conference on Power Electronics and Applications (EPE 2003)*, CD-ROM pages 10, 2003.

Tan, F. D., Middlebrook, R. D. (1995), A unified model for current-programmed converters, *IEEE Transactions on Power Electronics*, vol. 10, no. 4, pp. 397-408, 1995.

Tymerski, R. (1991), Frequency analysis of time-interval-modulated switched networks, *IEEE Transactions on Power Electronics*, vol. 6, no. 2, pp. 287-295, 1991.

Tymerski, R., Li, D. (1993), State-space models for current programmed pulsewidth-modulated converters, *IEEE Transactions on Power Electronics*, vol. 8, no. 3, pp. 271-278, 1993.

Tymerski, R. (1994), Application of the time-varying transfer function for exact small-signal analysis, *IEEE Transactions on Power Electronics*, vol. 9, no. 2, pp. 196-205, 1994.

Varga, L. D., Losic, N. A. (1989), Synthesis of load-independent switch-mode power converters, *IEEE Industry Applications Society Annual Meeting*, vol. 1, pp. 1128-1134, 1989.

Varga, L. D., Losic, N. A. (1992), Synthesis of zero-impedance converter, *IEEE Transactions on Power Electronics*, vol. 7, no. 1, pp. 152-170, 1992.

Vorperian, V. (1990), Simplified analysis of PWM converters using model of PWM switch: Part I and II, *IEEE Transactions on Aerospace and Electronic Systems*, vol. 26, no. 3, pp. 490-505, 1990.

Wester, G. W., Middlebrook, R. D. (1973), Low-frequency characterization of switched dc-dc converters, *IEEE Transactions on Aerospace and Electronic Systems*, vol. AES-9, no. 3, pp. 376-385, 1977.

Zhang, X., Yao, G., Huang, A. Q. (2004), A novel VRM control with direct load current feedback, *IEEE Applied Power Electronics Conference and Exposition*, vol. 1, pp. 267-271, 2004.

Åström, K. J., Hägglund, T. (1995), *PID controllers; theory, design, and tuning*, Second edition, Instrument Society of America, ISBN 1-55617-516-7.

Åström, K. J., Wittenmark, B. (1995), *Adaptive control*, Second edition, Addison-Wesley, ISBN 0-201-55866-1.